AIAA
G-065-1999

Guide

# Guide to Global Aerosol Models (GAM)

AIAA standards are copyrighted by the American Institute of Aeronautics and Astronautics (AIAA), 1801 Alexander Bell Drive, Reston, VA 20191-4344 USA. All rights reserved.

AIAA grants you a license as follows: The right to download an electronic file of this AIAA standard for temporary storage on one computer for purposes of viewing, and/or printing one copy of the AIAA standard for individual use. Neither the electronic file nor the hard copy print may be reproduced in any way. In addition, the electronic file may not be distributed elsewhere over computer networks or otherwise. The hard copy print may only be distributed to other employees for their internal use within your organization.

**AIAA**
**G-065-1999**

# Guide to Global Aerosol Models

Sponsor

**American Institute of Aeronautics and Astronautics**

## Abstract

This Guide defines a set of existing reference global aerosol models. It includes tables, plots, and other information describing the optical and mechanical properties of atmospheric aerosols, both natural and man-made. Intended for use by the aerospace and meteorological communities, the emphasis is on the physical and chemical characteristics, size distributions, sources, locations, and sinks. Urban, rural, maritime, desert, and polar locations; combustion and volcanic sources; and geographic variations are all treated.

Guide to global aerosol models/sponsor, American Institute of
Aeronautics and Astronautics.
p. cm.
“AIAA G-065-1999"
Includes bibliographical references.
ISBN 1-56347-348-8 (softcover), 1-56347-369-0 (electronic)
1. I. American Institute of Aeronautics and
Astronautics.
QC882.42.G85 1999
551.51’ 13—dc21 99-36696
CIP

Published by
**American Institute of Aeronautics and Astronautics**
**1801 Alexander Bell Drive, Reston, VA 22091**

Copyright © 1999 American Institute of Aeronautics and Astronautics
All rights reserved

No part of this publication may be reproduced in any form, in an electronic
retrieval system or otherwise, without prior written permission of the publisher.

Printed in the United States of America

# Contents

## List of Figures

## List of Figures (continued)

## List of Tables

## Foreword

This *Guide to Global Aerosol Models* has been sponsored by the American Institute of Aeronautics and Astronautics (AIAA) as part of its Standards Program.

The purpose of this Guide is to provide, in convenient form, a set of reference global aerosol models (GAM) for use by the aerospace community. Information is provided on aerosol physical and chemical characteristics, size distribution, physical state, and mass concentration, as well as on their basic optical properties.

The scope of the effort is confined to aerosols commonly found in the atmosphere, particularly those arising from natural causes; somewhat less emphasis is placed on aerosols produced by human development and industry. The aim has been to provide a general survey of aerosol types and characteristics, rather than detailed physical and chemical properties. Derived quantities, such as atmospheric radiative characteristics, have similarly been omitted.

The information provided in the form of tables and graphs is taken from published sources. No attempt has been made to create new data or new models. In this effort, assistance was sought from a worldwide community of aerosol scientists. A draft outline of the guide was prepared and distributed to over 40 atmospheric aerosol scientists around the world. The following individuals, who responded by sending and/or suggesting relevant literature, tables, and models, comprise the AIAA Global Aerosol Model Working Group. They are

A. Deepak, Chairman (Science and Technology Corporation, USA)
A. D. Clarke (University of Hawaii, USA);
D. A. Gillette (National Oceanic and Atmospheric Administration (NOAA), USA);
G. Hänel (Johann Wolfgang Goethe-Universität, Germany);
P. V. Hobbs (University of Washington, USA);
R. Jaenicke (Johannes Gutenberg-Universität, Germany);
J. Lenoble (Université des Sciences et Technologies de Lille, France);
G. S. Kent (Science and Technology Corporation, USA)
F. Parungo (Science and Technology Corporation, USA);
J. Podzimek (University of Missouri-Rolla, USA);
E. P. Shettle (Naval Research Laboratory, USA);
K. S. Shifrin (Oregon State University–Corvallie, USA);
L. L. Stowe (NOAA, USA).

Their assistance in this effort is gratefully acknowledged.

To facilitate convenient access to aerosol characteristics and models, this guide is structured so that the early sections provide general information on aerosol properties and classification, as well as on the nomenclature used to describe them. The latter sections contain more detailed models and data relating to aerosol normally occurring in specific atmospheric regions and environments.

It is a pleasure to acknowledge the assistance of STC staff, especially M. D. (Sue) Crotts, Linda Schofield, and Hope Tarr, in the preparation of the camera-ready copy of this guide. It is hoped this volume will be a valuable contribution to the international standards on global aerosol models for the aerospace community, and will act as a useful reference point for future updates.

The AIAA Standards Procedures provide that all approved Standards, Recommended Practices, and Guides are advisory only. Their use by anyone engaged in industry or trade is entirely voluntary. There is no agreement to adhere to any AIAA standards publication and no commitment to conform to or be guided by any standards report. In formulating, revising, and approving standards publications, the Committees on Standards will not consider patents which may apply to the subject matter. Prospective users of the publications are responsible for protecting themselves against liability for infringement of patents or copyrights, or both.

The AIAA Atmospheric & Space Environments Committee on Standards (Shu T. Lai, Chairman) approved the document in .January 2000.

The members of this consensus body at the time of voting on the document are:

Dana A. Brewer (NASA Headquarters)
Herbert C Carlson (Air Force Office of Scientific Research)
Adarsh Deepak (Science & Technology Corp.)
Gerald Dittberner (NOAA/NEDIS)
L. J. Ehernberger (NASA Ames-Dryden Facility)
Jeffrey M. Forbes (University of Colorado)
Henry B. Garrett (Jet Propulsion Lab.)
G. Barry Hillard (NASA Lewis Research Center)
Stuart L. Huston (Boeing Space & Defense)
JoAnn Joselyn (NOAA Space Environment Lab.)
Neil D. Kelley (National Renewable Energy Lab.)
O. Kenneth Moe (USAF Space & Missile Systems Center)
Jerry Owens (NASA Marshall Space Flight Center)
Robert Sears (Jamieson Science & Engineering)
Robert A. Skrivanek (Visidyne Inc.)
Guy F. Spitale (Jet Propulsion Laboratory)
Walther Spjeldvik (Weber State University)
Robert M. Suggs (NASA Marshall Space Flight Center)
Gopal D. Tejwani (Lockheed Martin Space Operations.)
Alfred Vampola (Consultant)
William W. Vaughan (UAH Research Center)

The AIAA Standards Executive Council accepted the document for publication in January 2000

# 1 Introduction

## 1.1 Scope

The purpose of this work is to describe, in a convenient form, a standard Global Atmospheric Model which is composed of a set of existing reference aerosol models. This guide contains tables, plots, and other information describing the properties of atmospheric aerosols, both natural and man-made. These are intended for use by the aerospace community and the emphasis is on the physical and chemical characteristics, size distributions, sources, locations, and sinks. Somewhat less emphasis is placed upon aerosol optical properties, which are discussed in Section 2.5.

Information provided is based on published sources, particularly models and summary data. No attempt has been made to create new models or tables directly from measured data.

## 1.2 Aerosol Background

An “aerosol” is a suspension of finely divided matter (liquid or solid) dispersed in a gaseous medium such as air. The suspended particles are called “aerosol particles” or “aerosols.”

Aerosol particles which occur naturally in the atmosphere are called “atmospheric aerosols;” those which are produced in the laboratory or field space by man-made chemical, thermal, or mechanical means are called “artificial aerosols.” In this work, the term atmospheric aerosols will cover aerosols derived from both natural and anthropogenic sources, the latter being those generated as by-products of human activity, such as burning of fossil fuels and are often referred to as “anthropogenic aerosols.”

Atmospheric aerosols may be formed as the result of wind action at the earth’s surface (land or ocean) or formed *in situ* by condensation from the gaseous phase. Gaseous precursors may, in turn, be formed by the action of sunlight and chemical action on other naturally or anthropogenically-produced gases. Aerosols are subject to changes in size and composition by processes of condensation, evaporation, and coagulation. Water soluble aerosols may also change size in response to changes in atmospheric humidity. Aerosols, particularly those in the troposphere, are often mixtures of different chemical components. Such mixtures may be external, in which different particles within the same air mass have differing compositions, or “internal,” in which individual particles are of mixed composition. An example of a relatively simple homogeneous aerosol is that found in the stratosphere which, except just after a volcanic eruption, consists of a solution of sulfuric acid in water that is in equilibrium with its surroundings. The marine boundary layer aerosol is an example of an external mixture, in which aerosols of different compositions (sea salt and sulfates) occupy different parts of the size distribution spectrum. Internal mixtures are often formed within the atmosphere, as for example, when a solid desert aerosol passes through an industrial plume and the individual particles acquire a layer of sulfuric acid. Atmospheric aerosols are also subject to modification by cloud processes, where aerosols becomes integrated into the cloud droplets and may be later regenerated, often in modified form, as a result of evaporation. Cloud processes are also responsible for the removal of much of the aerosol from the atmosphere within rain or snow.

Aerosol concentrations and compositions depend on location relative to source regions, production and removal rates, transport, and altitude. It is possible to classify aerosols according to their sources and to describe their approximate chemical composition and size distribution. The most significant sources for atmospheric aerosols lie within the planetary boundary layer, and it is here that the largest concentrations are normally to be found. Sources are not only localized but may also vary in time. These variations may be seasonal, such as in the formation of desert dust plumes by spring-time surface wind erosion or in the annual cycle of biomass burning and smoke production in tropical countries. Examples of sporadic aerosol production are those formed as a result of volcanic activity or forest fires.

## 1.3 Sources for Raw Data

Numerous data sources exist for model development. Data may be obtained by *in situ* or remote techniques. Measurements of size distributions, chemical composition, and the characteristics of individual particles normally require *in situ* instruments. Most commonly, these instruments will be located at the earth’s surface but airborne and, somewhat less commonly, balloon-borne measurements are also made. The flexibility of airborne measurements lies not only in the ability to sample different altitudes, but also in its capability to reach remote locations.

Bulk aerosol properties may be measured by both *in situ* and remote techniques. Remote methods are typically optical and include lidar and satellite techniques, the latter giving global coverage but requiring careful validation

and interpretation for proper understanding of the data. *In situ* measurements are also often, but not uniquely, optical. Particle collection, plus mass measurement and chemical analysis play an important role. A list of commonly used techniques for measuring the characteristics and behavior of atmospheric aerosols is given in Table 1 and is taken from Stowe et al.

**Table 1. Commonly Used Techniques for Measuring Aerosol Characteristics from Space, Airborne, and Ground-Based Platforms**

| Remote Sensors | | In situ Sensors |
|---|---|---|
| Lidars | (s,a,g) | Optical Spectrometers |
| Transmissometers | (g) | Impactors |
| Photometers (λ) | (a,g) | Electric Mobility Analyzers |
| Radiometers (λ) | (s,a,g) | Diffusion Mobility Analyzers |
| Multi-Spectral | (s,a,g) | Filter Samplers |
| Shadowband | (g) | Condensation Nuclei Counters |
| Solar Occultation | (s) | Ice Nuclei Counters |
| Limb Scattering | (s) | Mass Spectrometers |
| Surface Radiance | (s) | |

Legend: s–space-borne; a–airborne; g–ground-based

## 1.4 History

Many publications exist that list aerosol models and characteristics. Most of these are specific in nature but several form important reference works that summarize a wide range of aerosol types and characteristics. A short list of these is given in Table 2. They supply much background information to the tables given in the present monograph and in some cases have supplied the tables reproduced here. There is also much overlapping and duplicated information between these sources.

**Table 2. Important General References on Aerosol Models and Characteristics**

| Authors | References | Notes |
|---|---|---|
| World Meteorological Organization (WMO) | *Aerosols and Climate: Report of the Meeting of Experts on Aerosols and Climate*. Geneva, 27–31 October 1980. World Meteorological Organization, WCP-12 | Reviews the role of aerosols in climate, aerosol models, measurements, present state of knowledge. |
| A. Deepak, H.E. Gerber | Report of Experts Meeting on Aerosols and Their Climatic Effects. Williamsburg, VA., 28-30 March 1983, World Meteorological Organization, WCP-55. | Summarizes aerosol physical properties, effects on climate, available data and recommended improvements. |
| R. Jaenicke | Aerosol Physics and Chemistry in Landolt-Borstein *Numerical Data and Functional Relationships in Science and Technology*. V, 4b (Meteorology), 1988. | Numerous tables and graphs covering physical, chemical, and optical properties of aerosols. Instrumentation and sampling also described. |
| R. Jaenicke | *Tropospheric Aerosols in Aerosol-Cloud-Climate Interactions*. Ed. P.V. Hobbs. Academic Press, 1993. | A review of tropospheric aerosols, types, sources, and behavior. Source of some of the tables used in present monograph. |
| D'Almeida, P. Koepke, and E.P. Shettle | *Atmospheric Aerosols, Global Climatology, and Radiative Characteristics*. A. Deepak Publishing, Hampton, VA, 1991. | Aerosol types, sources, characteristics, size distributions, and composition. Emphasis on radiative characteristics. |
| J. Prospero, R.J. Charlson, V. Mohnen, R. Jaenicke, A.C. Delany, J. Moyers, W. Zoller, and K. Ruhn | The Atmospheric Aerosol System: An Overview. Rev. Geophys. and Space Physics, 21, 1607–1629, 1983. | General article on aerosols and their interactions with the environment. |

## 1.5 Structure of the Guide

This guide consists of three sections. Sections 1 and 2 contain introductory and background material. Section 3 contains the models for individual regions of the atmosphere included in the GAM. Further information on these is given at the beginning of Section 3. Section 2 of this guide gives an overview of global atmosphere aerosol characteristics. In Section 2, we discuss and list aerosol sources, size distributions, and associated analytical models, classification by type, and the component structure that makes up these aerosol types. An overview is also presented of the vertical aerosol structure in the atmosphere, aerosol variations in time and space, modification and removal processes, and dependence upon humidity. Subsections of this section also include descriptions of aerosol optical properties, and how these are characterized, as well as aerosol mechanical properties. Some of the information given in Section 2 may be needed as background for the appreciation of the detailed models given in Section 3.

# 2 Global Aerosol Characteristics

## 2.1 Sources, Production Rates, and Vertical Distribution

Atmospheric aerosol sources may be divided into two general classes natural and anthropogenic. Inside these classes, it is possible to make a further subdivision into direct particle production at the earth's surface and formation within the atmosphere from gas to particle conversion and cloud evaporation. Estimates for the annual production rates of atmospheric particles from the various sources are shown in Table 3. These estimates are in order of magnitude only and different authors may give quite different numbers. There are three large natural sources, all producing of the order of $10^9$ metric tons of aerosol per year. Salt particles are produced at the oceans' surface as a result of wind action. These have a wide range of sizes, the largest of which are not transported very far. Wind action similarly produces aerosols from the earth's deserts and other arid regions. These may be transported considerable distances away from the source regions. The third important natural source consists of aerosols formed by nucleation and condensation of naturally produced precursor gases. These gases form aerosols containing sulphate and nitrates, as well as organic materials. Less significant natural sources include volcanic debris, natural biologic particles, soot from wild fires, and extraterrestrial dust. A further source of natural aerosols, not included in Table 3 are those produced by evaporation of cloud [*Jaenicke, 1993*].

**Table 3. Source Strength of Atmospheric Aerosol Particles in Tg/yr for Radii Smaller than 100 μm** (Data taken from *D'Almeida et al. [1991]* with modifications from *Jaenicke [1993]*)

| Aerosol Component | Source Strength | |
|---|---|---|
| ***Natural Aerosol Sources*** | | |
| Extraterrestrial dust | 10 - | 18 |
| Sea–salt | 1,000 - | 10,000 |
| Desert dust | 500 - | 2,000 |
| Volcanic debris | 15 - | 250 |
| Biogenic/biologic | | 80 |
| Gas to Particle Conversion (sulfate, organics, nitrate) | 345 - | 1,300 |
| Subtotal | 1925 – | 13,648 |
| ***Man-Made Aerosol Sources*** | | |
| Direct particulate emission | 10 - | 90 |
| Gas to Particle Conversion (carbonaceous substances, organics, sulfate, nitrate) | 175 - | 325 |
| Forest fires and slash–burning debris* | 3 - | 150 |
| Subtotal | 188 - | 565 |
| **TOTAL** | **2,673 -** | **14,213** |

* Includes unknown amount of indirect natural contributions.

The mass of aerosol produced by man-made activities is considerably less than that produced naturally. As much of this is produced within the atmosphere by gas-to-particle conversion and has a considerable residence time, its regional impact may be out of proportion to its mass. In addition to particles formed from gaseous anthropogenic emissions, others are produced mechanically and as the result of combustion (power production, agricultural burning, and road traffic).

Figure 1 shows a simple schematic of the general character of atmospheric aerosols from the earth's surface to 200-km altitude. Above an altitude of about 30 km, most aerosols are likely to be of extra-terrestrial origin and to exist in low concentrations. A particular phenomenon is the occurrences of noctilucent clouds in certain latitudes at an altitude of about 80 km. Between the tropopause and 30 km, stratospheric aerosols consist of sulfuric acid and are mainly of volcanic origin, formed by oxidation and hydrolysis of $SO_2$ injected directly into the atmosphere. At

times of low volcanic activity, transformation of stable surface derived gases, such as OCS, into sulphuric acid may be the dominant mechanism in this region. The upper troposphere within a few kilometers of the tropopause represents an overlapping region in which aerosols may be lifted from below or derived from the stratosphere by sedimentation and dynamical processes. In the two lowest regions, aerosols are derived from surface sources. The structure, depth, and aerosol content in the boundary layer is determined by the local sources and meteorological conditions (such as the height of the inversion layer), with aerosol concentration normally decreasing with altitude. Above the boundary layer, surface-derived aerosols have lower concentrations, often exhibit a layered structure and show evidence of considerable horizontal transport.

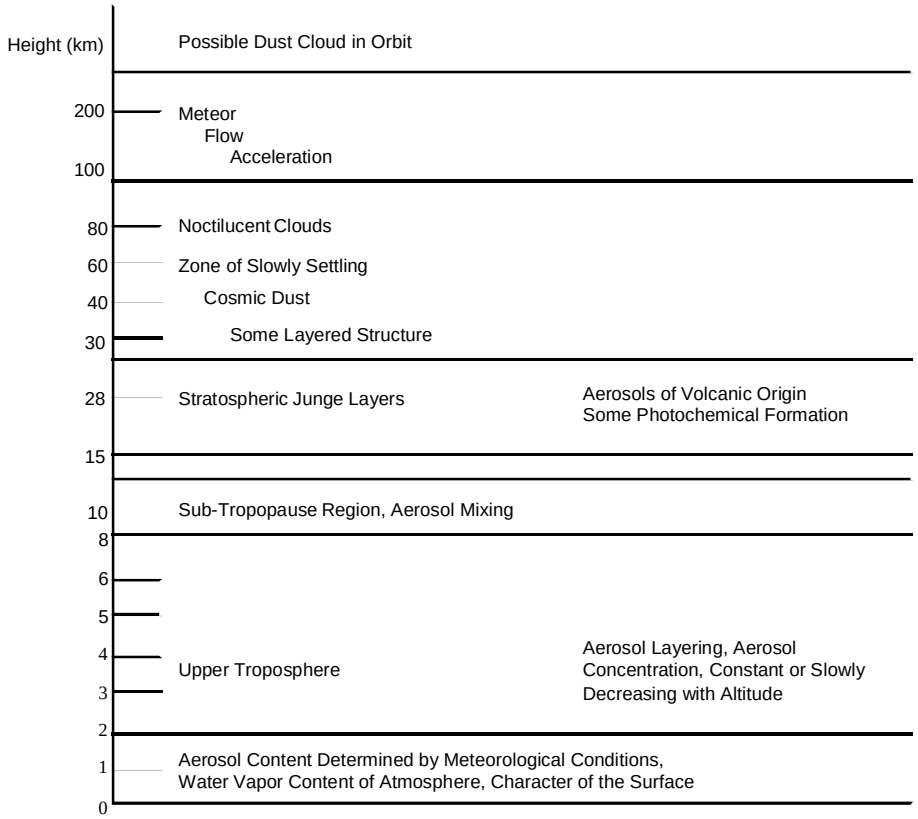


**Figure 1. Characteristics of the atmospheric aerosols as a function of altitude.** [Modified from *Shettle, 1989*.]

## 2.2 Aerosol Size Distribution

### 2.2.1 Characterization of Atmospheric Aerosols

Aerosols are characterized by their physical and chemical properties, namely, size, shape, and material composition. The properties of atmospheric aerosols not only vary within a unit volume of the atmosphere, but also vary considerably over the global atmosphere. Of these, traditionally the most commonly used aerosol property is the particle size. It is assumed that the shape of atmospheric aerosols is spherical, which is a valid assumption for most applications of interest, so that the size can be represented by the parameter, $r$, for the particle radius. (The non-sphericity of atmospheric particles becomes important in dealing with snowflakes, ice crystals, rain drops, volcanic ash, etc.)

When neither the shape, size, nor the constitution of the aerosol particles is uniform, it is referred to as *polydisperse aerosol* (a term ethnologically [Deirmendjian, 1969] derived from the classical concept of light dispersion by a prism). However, if a polydisperse suspension has particles that are uniform in physical constitution and shape but *vary in number concentration depending on the size only*, it is referred to as a "*polydispersion;*" and, if all particles have the same size or a very narrow range of sizes, then the aerosol is referred to as "monodisperse aerosol" or "*monodispersion*."

### 2.2.2 Aerosol Size Distribution Functions

It is convenient to characterize the polydispersity of atmospheric aerosols by a distribution function, called the *size distribution*, which gives the variation of the particle size in terms of either number concentration or surface area, or volume, with size being represented by either radius $(r)$ or logarithm (natural or to the base 10) of the radius. Before

discussing the relative merits and applications of these three representations, it is in good order to present the definition of size distribution in terms of the number concentration.

2.2.2.1 Number Size Distribution and Cumulative Number Size Distribution

The nomenclature used to represent the particle size distribution and the cumulative size distribution in the literature on the subject varies somewhat. Therefore, in order to avoid confusion, we define below the symbols, terms, and concepts that we will use and how they relate to concepts used by others to characterize these two distributions as well as altitude-size distributions.

The particle size distribution is frequently represented by [Green, A.E.S., A. Deepak, and B.J. Lipofsky, Interpretation of the Sun's Aureole Based on Atmospheric Aerosol Models, *Applied Optics, 10* (1970), 1263–79]:

i. The *number-radius distribution, n(r)* [$m^{-3}\mu m^{-1}$], which is defined as the number of particles per unit volume within a unit radius range at $r$, where $r$ is the particle radius in micrometers (μm). This quantity may be defined by the expression:

$$n(r) = dN_u(r)/dr, \ [m^{-3}\,\mu m^{-1}] \qquad [1]$$

where $N_u(r)$ is the *cumulative undersize distribution*[5]. The cumulative distribution function represents the total number of particles per cubic centimeter that have radii less (greater) than $r$ and is represented by $N_u(r)[N(r)]$ and is called the cumulative undersize (oversize)[5] distribution function. In essence

$$N_u(r) = \int_0^r n(r)dr \ [m^{-3}] \qquad [2]$$

$$N(r) = \int_r^\infty n(r)dr \ [m^{-3}] \qquad [3]$$

Unless stated otherwise, the cumulative oversize distribution, $N(r)$, is considered in this work, and definitions of other quantities is based on it. Also, the number-radius distribution, $n(r)$, will be referred to as the size distribution. Note that $N(0)$ would then be the total density of the particles. Note also that

$$n(r) = - dN(r)/dr, \ [m^{-3}\,\mu m^{-1}] \qquad [4]$$

so that size distribution $n(r)$ is sometimes referred to as the *differential particle number distribution*.

ii. The *log number-radius distribution*, $N_L(r)[cm^{-3}]$, that is given by

$$N_L(r) = dN_u(r)/d(\log_{10} r), [\,m^{-3}\,] \qquad [5]$$

This nomenclature was introduced by Junge, who preferred the use of the logarithmic scales because of the wide range of particle sizes and concentrations involved in representing the polydispersity of the atmospheric aerosols. It is simple to show that

$$N_L(r) = 2.306r\ n(r) \qquad [6]$$

Various derived parameters are also frequently quoted; these include

1. the total particle number, $N_o$, e.g., $N(0)$ for $r = 0$ from Eq. [3]
2. the mean radius $\bar{r} = \int_o^\infty rn(r)dr \int_o^\infty n(r)dr$
3. the effective radius $r_{eff} = \int_o^\infty r^3 n(r)dr \int_o^\infty r^2 n(r)dr$
4. mode radii, values of $r$ where $dN/dr = 0$
5. Particle diameter $D = 2r$.

2.2.2.2 Commonly Used Analytical Size Distribution Models

Atmospheric aerosols typically have sizes in the range 0.01–10 μm, and their number distribution across this range may be very variable. For purposes of representation and intercomparison, it is common to represent these size distributions by suitable approximating mathematical functions. Three commonly used functions are shown in Table

4. A set of eight such mathematical functions are described in *Deepak and G.P. Box [1979]*. Real distributions are often represented by a combination of one or more of these functions. The form in which these functions are presented may also differ from one author to another. In Table 4, the distributions are expressed in terms of the variation with particle radius, r, of the cumulative particle number N (i.e., the total number of particles with radii greater than r per unit volume).

**Table 4. Commonly Used Size Distribution Functions** (Formula Taken From *Rosen and Ivanov [1993]*)

| Type | Function | Adjustable Parameters |
|---|---|---|
| 1. Junge Power Law | $\frac{dN}{dr} = Ar^{-p}$ | A, p constants |
| 2. Log Normal | $\frac{dN}{dr} = ar^{\alpha}\exp(-br^{\gamma})$ | A, constant<br>$r_g$, mode radius<br>$\sigma_g$, geometrical standard duration |
| 3. Modified Gamma | $\frac{dN}{dr} = \frac{A}{r\ln(\sigma_g)}\exp\left\{\frac{-\ln^2(r/r_g)}{2\left(\ln^2\sigma_g\right)}\right\}$ | a, b, $\alpha$, $\gamma$, constants |

Legend: N is the cumulative particle number distribution for particles with radius greater than r.

The simplest function in Table 4 is that due to *Junge [1952, 1958]*, which has only two adjustable parameters. The exponent p is normally positive, particle number thus increases with decreasing particle radius. Use of a single positive value of p would result in an infinite total number of particles. In practice, the law may be used in a segmented form in which different values of p are used over different radius intervals, p being zero for the smallest particle (e.g., *Gras and Michael, 1979*).

The Junge power law, in its basic form, has no maximum, except at r = 0. Atmospheric size distributions frequently show modal structure and may be better represented by a log normal distribution or a combination of such distributions and this is probably the distribution in most common use *[D'Almeido et al., 1991; Jaenicke, 1993]*. The distribution has three constants: A, which relates to the total particle number, $r_g$ the mode radius, and $\sigma_g$ which determines the width of the size distribution. The third distribution shown is the modified gamma distribution proposed by *Deirmendjian [1963, 1964]*. This has four adjustable constants and is frequently applied to particle size distributions in haze and clouds *[McCartney, 1976]*.

2.2.2.3 Surface and Volume Size Distributions

Each of the three representations of aerosol size is convenient or suitable for understanding and/or describing different aerosol properties on interactions. It is not always convenient nor suitable to present aerosol size information in terms of the number distribution. For applications to chemical interaction, surface area is more suitable, and for the discussion of mass loading and conservation, the volume distribution is the most suitable. Optical properties relate more closely to both the area and volume distributions than to the number distribution. Figure 2 shows the number, surface, and volume distributions for a typical urban aerosol distribution *[Whitby, 1975]*. The number distribution is clearly uni-model with a peak near to a particle diameter of 0.01 μm. The distribution is not symmetric but has a tail extending to larger particle sizes. As we proceed to the area and volume distribution, new modes emerge from this tail, which are not evident in the number distribution.

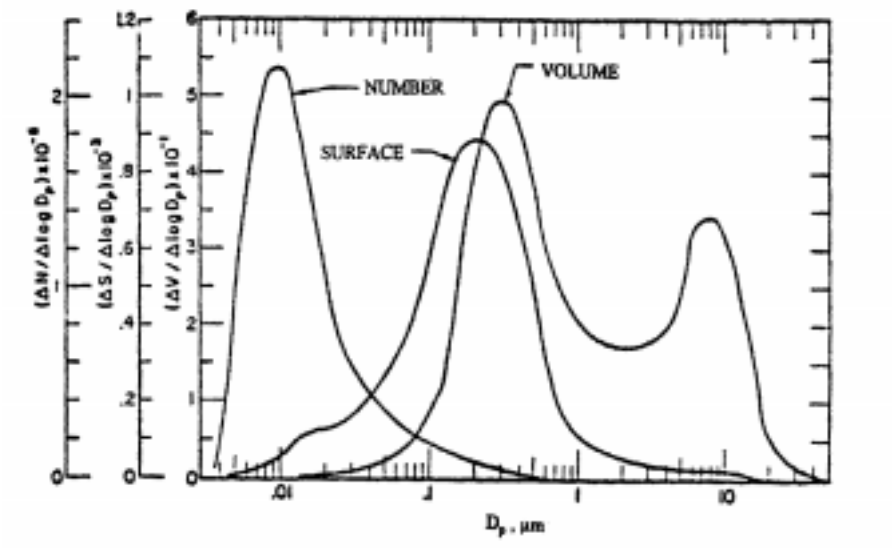


**Figure 2. Normalized frequency plots of the number, surface, and volume distributions as a function of particle size for the grand average 1969 Pasadena smog aerosol.** (From *Prospero et al., 1983; Whitby, 1975.]*

Real aerosol size distributions frequently show a trimodal structure as evidenced in Figure 2 *[Prospero et al., 1983; Johnson, 1993]*. This is also shown schematically in Figure 3 which depicts the principal mechanisms responsible for each of these modes. The mode with the smallest radius, namely, the nucleation mode (also referred to as Aitken or transient nuclei), represents particles that are formed by condensation and coagulation from the gaseous phase. Particles in this mode tend to grow by coagulation to form large particles in the so-called accumulation mode. The largest group of particles shown in Figure 3 (coarse particle mode) are directly produced from the land surface, the ocean, and as volcanic ash. Figure 3 also shows the primary removal mechanisms for particles in these modes. Those in the nucleation mode evolve into the accumulation mode, where (in the troposphere) they are removed by cloud and rain processes. Larger particles tend to disappear by sedimentation, as do accumulation mode particles in the stratosphere.

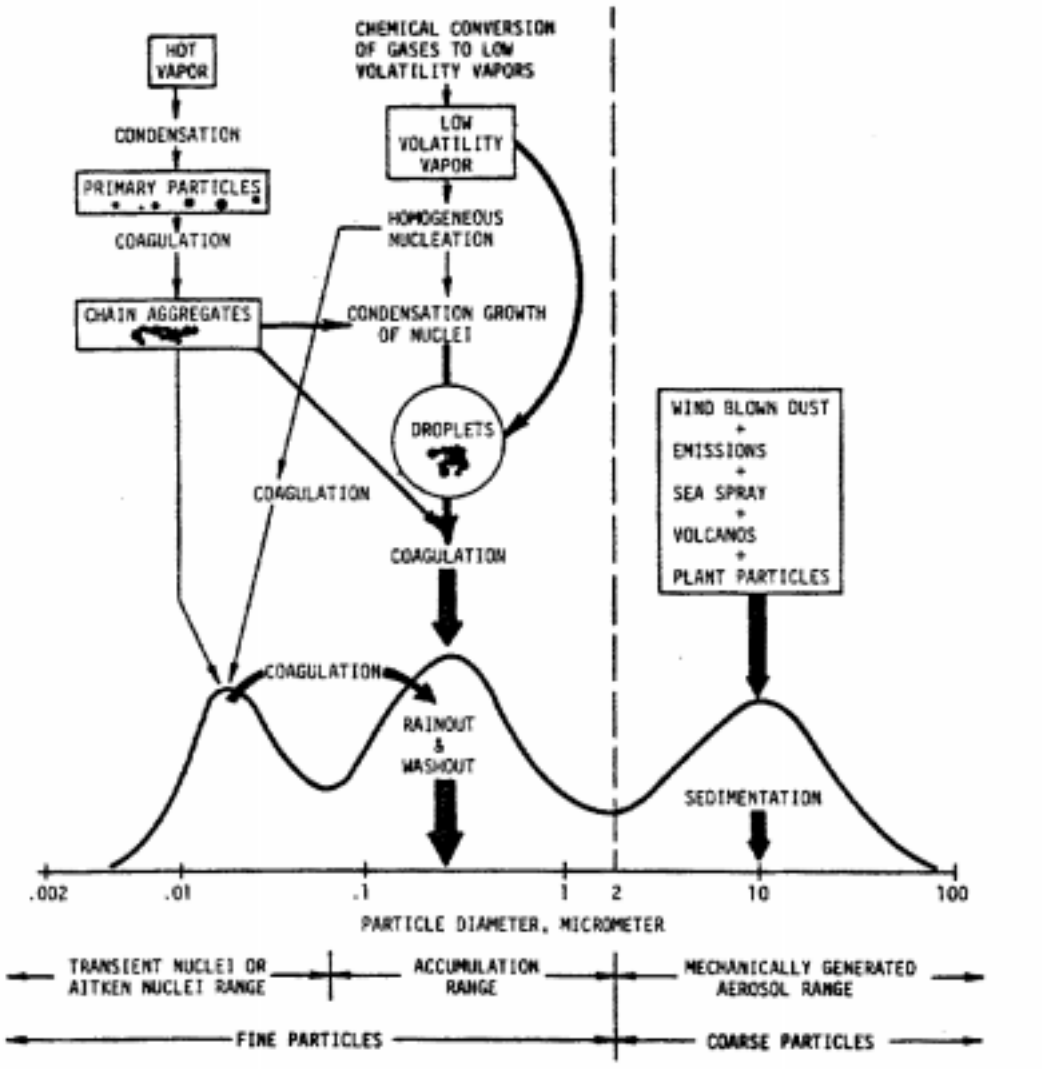


**Figure 3. Atmospheric aerosol surface area distribution showing the principal modes, the main source of mass in each mode, and the principal removal mechanisms** [From *Prospero et al., 1983; Whitby and Cantrell, 1976].*

## 2.3 Aerosol Types

It is conventional to divide aerosols into a number of types dependent upon the regions of the earth's surface or atmosphere in which they are to be found. The number of types and sub-types may vary somewhat between authors, but the main categories have general acceptance. Table 5 shows a list of such aerosol types generated by *Jaenicke [1993]* for the tropopause, to which has been added four more types for the upper atmosphere. This table also contains a brief summary of the regions of the earth or atmosphere in which these types most commonly occur and the conditions under which they are formed.

**Table 5. Aerosol Types** (Adapted from *Jaenicke, 1993*)

| Type | Characteristics |
|---|---|
| A. TROPOSPHERIC | |
| Polar | Aerosols close to the surface in the Arctic and Antarctic regions. Aerosols are well-aged. Hemispheric differences exist. |
| Background | Typical of mid-tropospheric conditions, seen near surface is subsiding air masses or at mountain sites. |
| Maritime | Found at lower altitudes over the oceans. In remote locations (e.g., southern hemispheric oceans) composed of background aerosol plus sea salt. May also contain mineral dust and continental pollution in other regions. |
| Remote Continental | Aerosols close to surface in areas away from human development, e.g., that near forest. May contain biogenic material. |
| Desert Dust | Naturally occurring aerosols, wind derived from desert surfaces. Often have high mass concentrations depends upon wind speed. |
| Rural | Continental aerosols with moderate anthropogenic impact. |
| Urban | Dominated by anthrogenic emissions from industry, homes, and traffic. |
| B. STRATOSPHERIC | |
| Background | Aerosols found under non-volcanic conditions. Data from 1979 frequently cited as an example of background conditions. |
| Volcanic | Aerosols found in the stratosphere when perturbed by fresh volcanic injection. Consists of larger sulfuric acid droplet and ash (for very recent eruptions). |
| Polar Stratospheric Clouds | Found in winter at high latitudes, composed of solid nitric acid and ice. |
| C. MESOSPHERIC | |
| Noctilucent Clouds | Ice particle at high latitude summer mesopause. |

Seven tropospheric aerosol types are shown in Table 5. Four of these (Polar, Maritime, Remote Continental, Desert Dust) relate to the main divisions of the earth's surface where there is little or no anthropogenic influence. Northern hemisphere Polar does not fit well into the category as there may be considerable transport of pollution into this region. Two (Urban and Rural) have respectively, major and minor anthropogenic components, and one (Background) relates to the mid-troposphere and is usually seen at the surface only at mountain locations. Two stratospheric types are shown respectively describing the stratosphere under conditions of volcanic perturbation by direct injection and under quiescent background conditions. A third stratospheric type describes polar stratospheric clouds (PSCs), which are formed in the wintertime Arctic and Antarctic regions at very low temperatures. The final type is for much higher altitude clouds forming near the mesopause and seen from the earth's surface as noctilucent clouds.

The classifications just discussed are formed in terms of global aerosol distributions and sources and, to some extent, they also reflect aerosol composition. Nevertheless, most aerosols are mixtures of components with different chemical compositions and it is necessary also to classify these aerosol components. Such a list, derived in somewhat simplified form from a list given by *D'Almeida et al. [1991]*, is shown in Table 6(a). While a few of them, such as soot and sulfuric acid, reflect fairly basic chemical compositions, most of these components consist of very complex and somewhat variable chemical mixtures which, nevertheless, have been identified as major fractions of the common aerosol types. Despite the variable nature of these components, average physical and optical characteristics have been measured and commonly are used in the modeling of aerosols. Tables of these characteristics will be presented later. Table 6(b) shows the components which make up each aerosol type listed in Table 5. Where possible, approximate component amounts have been specified and two of the aerosol types (Polar

and Maritime) have been further subdivided to reflect different amounts of aerosol transported from outside into the regions where the aerosol types exist.

**Table 6. Aerosol Components and Contribution to Aerosol Types** [From *D'Almeida et al., 1991; Jaenicke, 1993*]

| **(a) Aerosol Components** | | |
|---|---|---|
| 1. Dust-like | | |
| 2. Water-soluble | | |
| 3. Soot | | |
| 4. Sea-salt | | |
| 5. Mineral | | |
| 6. Sulfuric Acid | | |
| 7. Volcanic ash | | |
| 8. Meteoric | | |
| 9. Sulfate | | |
| 10.Biogenic | | |
| **(b) Component Structure of Aerosol Types shown in Table 5** | | |
| *A. Tropospheric* | | |
| Polar | –Antarctic | .99 (6) + 0.005 (4) + 0.005 (5) |
| | – Arctic | var. (3) + var. (4) + var. (5) + var. (9) [var. ≡ variable] |
| Background | | var. (6) + var. (9) |
| Maritime | -Clean | 0.6 (4) + 0.4 (9) |
| | – Mineral | var. (4) + var. (5) + var. (9) |
| | – Polluted | 0.6 (2) + 0.4 (3) + trace (4) |
| Remote Continental | | var. (1) + var. (2) + var. (10) |
| Desert Dust | | (5) |
| Rural | | 0.94 (2) + 0.06 (3) + trace (1) |
| Urban | | 0.6 (2) + 0.4 (3) + trace (1) |
| *B. Stratospheric* | | |
| Background | | (6) |
| Volcanic | | var. (6) + var. (7) |
| Polar Stratospheric Clouds | | var. Nitric Acid Trihydrate + var. Ice + trace (6) |
| *C. Mesospheric* | | |
| var. (8) + Ice | | |

As the names of the various aerosol types imply, they are often confined to specific regions of the globe. Actual distributions of specific aerosol types are difficult to measure on a global scale although there may be much regional documentation. In order to estimate the global distribution, models incorporating source strengths, transport and loss mechanisms and, where appropriate, chemical transformation, nucleation, and coagulation have been developed. The predictions of one such model for desert aerosols is shown in Figure 4. This figure (after *Jaenicke, 1993*) is based on a model described by *Zimmermann et al. [1989]*. This distribution was obtained *[Wefers, 1990]* by adapting a three-dimensional climatological transport model for the desert aerosols. The aerosols in that model are followed in 10 size ranges between 0.1 and 100 μm radius. The activities of the sources are calculated from wind velocities. The sinks include only the settling velocity of the aerosols. Thus, the model is more realistic in dry than in wet geographical regions. The highly non-homogeneous distribution is very evident, major

concentrations occur over the deserts themselves, but there is evidence (supported by direct measurements) for long-distance transport over the oceans. Similar distributions are shown by *Tegen and Fung [1994]*, where the aerosols have been classified by size. Similar regional scale models have been developed for the more complex case of pollution derived aerosols. It is important to note that long-range distributions are strongly dependent upon not only the sources and wind direction, but also upon the atmospheric removal processes, particularly those associated with clouds and precipitation.

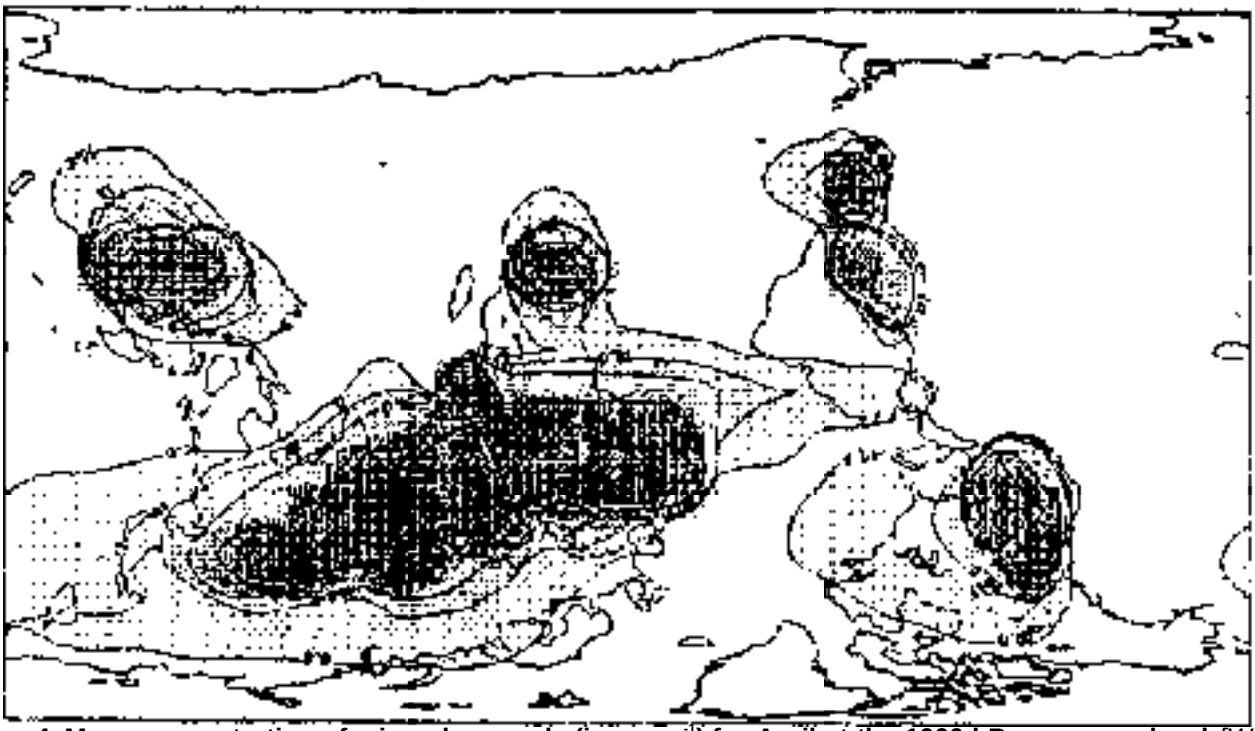

**Figure 4. Mass concentration of mineral aerosols (in μm $m^{-1}$) for April at the 1000 hPa pressure level** *[Wefers and Jaenicke, 1990].*

## 2.4 Aerosol Variations

The concentration and distribution of aerosols in the atmosphere is extremely variable. Even after aerosol formation has taken place, further modification can occur, particularly, as a result of cloud processes which are also responsible for much of the removal of aerosol from the atmosphere. Figure 5, taken from *Prospero et al. [1983]*, depicts the atmospheric processes of aerosol modification and removal. This figure emphasizes the role of clouds in aerosol conversion and removal processes. Box 5 is subdivided into 5a and 5b to denote those aerosol species that are effective as cloud condensation and ice nuclei. Note that super-cooled droplets (6a) will be converted to ice crystals (7) if they make contact with a freezing nucleus (5b). The surface area of cloud droplets (6) and ice crystals (7) in a typical cloud is tremendous; consequently, the sorptive removal of gases (1 and 2) is facilitated. Because most clouds dissipate through evaporation (i.e., the reverse of arrows 5a-6 and 5b-7), a modified aerosol population will be injected back into the atmospheric aerosol system (box 5). Rain (8) and snow (9) can also evaporate in the atmosphere, but this process is not nearly as common as cloud evaporation. Aerosols can also be deposited directly to the earth's surface by diffusion, impaction, and sedimentation; however, precipitation is responsible for the removal of about 80-90% of the submicron mass from the atmosphere. Some dry removal of aerosol occurs but the bulk of removal is by precipitation. *Jaenicke [1993]* estimates that aerosol pass through clouds about five times before precipitation occurs. This absorption and re- evaporation may produce considerable change in the aerosol physical characteristics. Jaenicke estimates that 3000 Tg per year of aerosol is "produced" from evaporating clouds, a figure comparable to those shown for other sources in Table 3.

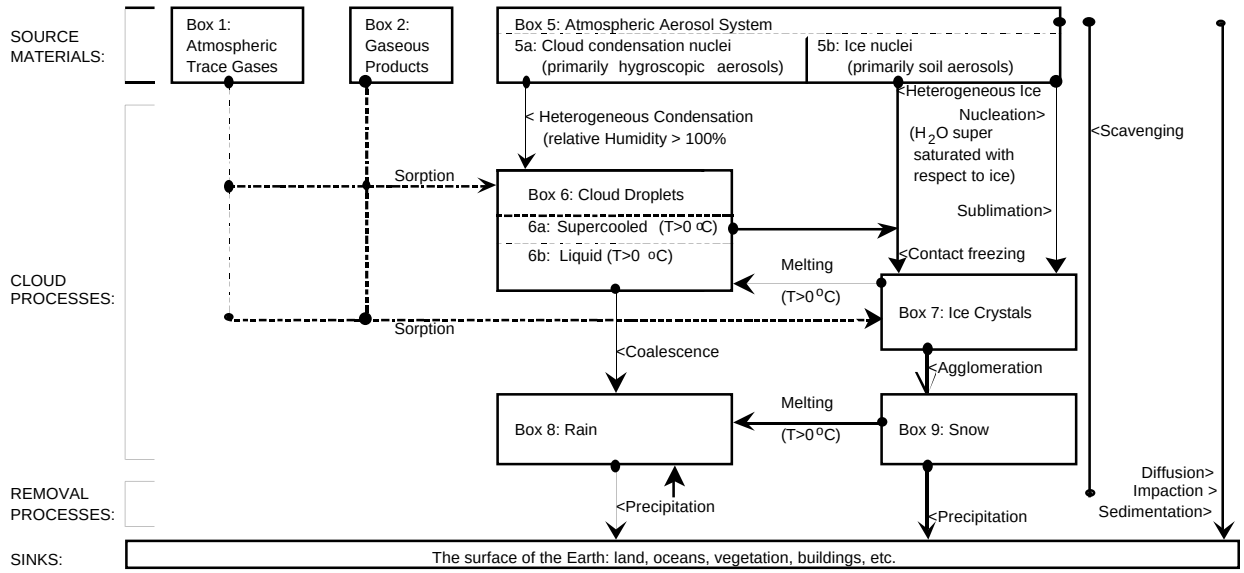


**Figure 5. Aerosol modification and removal processes.** [From *Prospero et al., 1983.*]

Residence times for aerosols in the atmosphere is dependent upon their size and altitude. This is shown by Figure 6 (after *Prospero et al., 1983*). The figure also shows recent estimates of the residence times of specific classes of aerosol particles (hatching *[Hofmann and Rosen, 1981]* and arrow *[Pruppacher and Klett, 1978]*). The larger particles disappear by sedimentation, the smaller particles by coagulation, resulting in the formation of longer-lived particles of intermediate size. *Jaenicke [1988]* has proposed the formula

$$\frac{1}{\tau} = \frac{1}{K}\left(\frac{r}{R}\right) + \frac{1}{K}\left(\frac{r}{R}\right)^{-2} + \frac{1}{\tau_{wet}} \qquad [7]$$

to describe the mean residence time, $\tau$. In this expression, K is a constant ($1.28 \times 10^8$ s); R is the radius of the particles with the maximum residence time (R = 0.3 μm); and $\tau_{wet}$ is a measure of the influence of wet removal ($\tau_{wet}$ = 8 days, in the lower troposphere; and, $\tau_{wet}$ = 3 weeks, in the middle to upper troposphere). This yields a maximum residence time in the lower troposphere of about a week, increasing to several weeks in the upper troposphere. In the stratosphere, residence times are typically of the order of 12 months for volcanic aerosols.

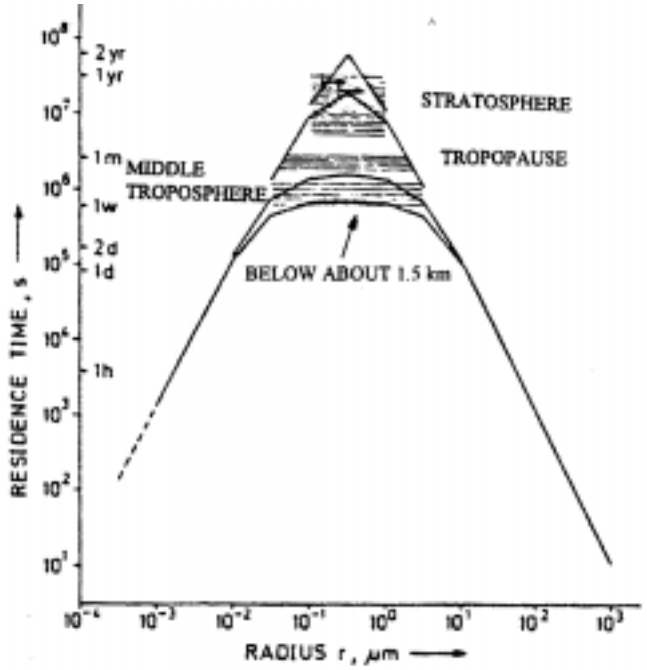


**Figure 6. Aerosol residence time of individual particles as a function of particle size and altitude in the atmosphere** *[Prospero et al., 1983; Jaenicke, 1980].*

Water soluble aerosols change their radius in response to changes in atmospheric humidity. *Hänel and Bullrich [1978]* and *Hänel and Lehmann [1981]* discuss these variations and present compilations of radii versus relative humidity for different aerosol compositions. A rough approximation for the equilibrium radius versus relative humidity can be obtained using:

$$\ln f = \frac{(A/r_o)}{(r/r_o)} - \frac{B}{(r/r_o)^3 - 1} \qquad [8]$$

f = relative humidity as pressure ratio (actual to value when saturated)

r = equilibrium radius of the wet particle

$r_o$ = radius of the dry particle

A and B are constants

Values for f and $r/r_o$ are tabulated for four different classes of aerosols by Hänel and Bullrich (*1978*). An example of one of the tables for continental background aerosol is reproduced as Table 7. Note the difference in values when f is decreasing and increasing and the small radius change for values of less than about 0.6.

Aerosol concentrations also change in response to episodic events. These include desert storms, fires, and volcanic eruptions. Desert dust storms and fires related to burning for agricultural purposes show regular seasonal cycles, and statistical predictions can be made about their likely impact on the troposphere. Volcanic eruptions are random in magnitude and time and, as a result, stratospheric aerosol concentrations are unpredictable, even though, under background conditions, there are regular seasonal changes. Other episodic events, such as naturally occurring fires (forest, oil, etc.), industrial catastrophes, etc., all produce nonpredictable changes in aerosol concentrations. Climate changes, either natural or associated with human activity, can also be expected to cause long-term regional changes in aerosol amounts.

**Table 7. Aerosol Equivalent Volume Radius at Different Relative Humidities** (From *(Hänel and Bullrich, 1978)*—Continental Background

| Model D : $\rho_0$ = 1.85 g/cm3 | | | | | | | | |
|---|---|---|---|---|---|---|---|---|
| | **$r_0$ (cm)** | **$10^{-6}$** | **$3x10^{-6}$** | **$10^{-5}$** | **$3x10^{-5}$** | **$10^{-4}$** | **$3x10^{-4}$** | **$10^{-3}$** |
| | **f** | **$r/r_0$** | | | | | | |
| **Increasing Humigity** | 0.2 | 1.004 | 1.004 | 1.004 | 1.004 | 1.004 | 1.004 | 1.004 |
| | 0.4 | 1.011 | 1.011 | 1.011 | 1.011 | 1.011 | 1.011 | 1.011 |
| | 0.6 | 1.036 | 1.036 | 1.036 | 1.036 | 1.036 | 1.036 | 1.036 |
| | 0.65 | 1.047 | 1.047 | 1.047 | 1.047 | 1.047 | 1.047 | 1.047 |
| | 0.7 | 1.061 | 1.067 | 6.067 | 1.067 | 1.067 | 1.067 | 1.067 |
| | 0.75 | 1.081 | 1.114 | 1.129 | 1.132 | 1.135 | 1.135 | 1.135 |
| | 0.8 | 1.114 | 1.210 | 1.246 | 1.257 | 1.261 | 1.264 | 1.264 |
| | 0.9 | 1.332 | 1.441 | 1.482 | 1.493 | 1.497 | 1.500 | 1.500 |
| | 0.95 | 1.444 | 1.582 | 1.644 | 1.664 | 1.671 | 1.674 | 1.674 |
| | 0.975 | 1.511 | 1.716 | 1.934 | 2.014 | 2.044 | 2.053 | 2.056 |
| | 0.99 | 1.560 | 1.985 | 2.480 | 2.695 | 2.781 | 2.807 | 2.816 |
| | 0.995 | 1.578 | 2.157 | 2.968 | 3.356 | 3.521 | 3.571 | 3.589 |
| | - | - | - | - | - | - | - | - |
| **Decreasing Humidity** | 0.2 | 1.012 | 1.012 | 1.012 | 1.012 | 1.012 | 1.012 | 1.012 |
| | 0.4 | 1.026 | 1.026 | 1.026 | 1.026 | 1.026 | 1.026 | 1.026 |
| | 0.6 | 1.058 | 1.958 | 1.058 | 1.058 | 1.058 | 1.058 | 1.058 |
| | 0.65 | 1.075 | 1.075 | 1.075 | 1.075 | 1.075 | 1.075 | 1.075 |
| | 0.7 | 1.098 | 1.109 | 1.109 | 1.109 | 1.109 | 1.109 | 1.109 |
| | 0.75 | 1.136 | 1.244 | 1.244 | 1.244 | 1.244 | 1.244 | 1.244 |
| | 0.8 | 1.181 | 1.248 | 1.281 | 1.293 | 1.298 | 1.301 | 1.301 |
| | 0.85 | 1.262 | 1.422 | 1.430 | 1.434 | 1.436 | 1.436 | 1.436 |

## 2.5 Aerosol Optical Properties

Whenever electromagnetic radiation passes through a medium composed of particles and molecules, its intensity always decreases during transit. The loss of intensity is due to either scattering or absorption or both by the medium constituents. In the absorption process, the light radiation actually disappears (the energy being converted into the heat motion of the particles). During the scattering process, some of the incident radiation is re-radiated in all directions at different rates, with a change in its state of polarization but with no change in wavelength ($\lambda$). The sum of lost contributions due to "scattering" and "absorption" is called "extinction." The medium in which both "scattering" and "absorption" processes are present is often called a "turbid" medium. The angular scattering and polarization change, absorption, and extinction are generically called the "optical" properties of aerosols, independently of the wavelength of radiation. These aerosol optical properties are dependent on variations in particle size, shape, and refractive index. For this work, it is assumed that the particle shape is spherical, the size is represented by the radius ($r$), and the refractive index by a complex function $m$ (= $m_1$ - $im_2$), where $i = \sqrt{-1}$, and $m_1$ and $m_2$ are the respective real and imaginary parts of the refractive index corresponding to the "scattering" and "absorption" processes. One can, therefore, take advantage of this knowledge to devise appropriate "optical" techniques to remotely and non-intrusively measure the particle size distribution, $n(r)$, of polydisperse aerosols.

Some of the terms, definitions, and notations used for depicting atmospheric aerosol optical properties and their effects are presented as follows.

### 2.5.1 Optical Properties of a Single Particle

The exact solution of scattering of a plane wave of wavelength $\lambda$ by a spherical particle of radius $r$, where $r \sim \lambda$, was given by Gustaw Mie [*Mie, G. Ann. Physik, 1908, 25, 377*], hence the name Mie Scattering, and the scatterers are often called "Mie particles." However, since Lorenz had solved the problem in 1886, of which Mie was unaware, it is sometimes referred to as Lorenz-Mie scattering. The details of the derivation of the Mie scattering theory are deferred to Van de Hulst [*1957*], Deirmendjian [*1969*], and Lenoble [*1994*].

As illustrated in Figure 7, if a plane electromagnetic wave of wavelength, $\lambda$, of irradiance $I_o(\lambda)$ (watts/cm$^2$–$\mu$m) is incident on a single spherical particle (P) of radius $r$ and complex refractive index $m = m_1\text{-}im_2$, then the intensity $I_s(\theta)$ of the scattered radiation at distance $R$ along a direction given by the scattering angle, $\theta$, measured from the direction of the incident beam, is given by the Mie theory as

$$I_s(\theta, x, m) = I_o(\lambda) f(\theta, x, m)/R^2 \qquad [9]$$

where $f(\theta, x, m)$ is referred to as the "differential scattering cross-section" or "single-particle scattering function" with units ($m^2 sr^{-1}$), given by the following expression:

$$I_s(\theta, x, m) = I_o(\lambda) f(\theta, x, m)/R^2 \qquad [10]$$

where $k = 2\pi/\lambda$, $x = 2\pi r/\lambda$ is the dimensionless "size parameter," $i^1$ and $i^2$ are Mie intensity functions from Mie theory results, and sr is the unit for steradian. The "differential cross-section" is defined as the energy/$m^2$ scattered within a unit solid angle about the direction $\theta$ with respect to the direct beam and at a unit distance from the particle on which a beam of unit irradiance is incident.

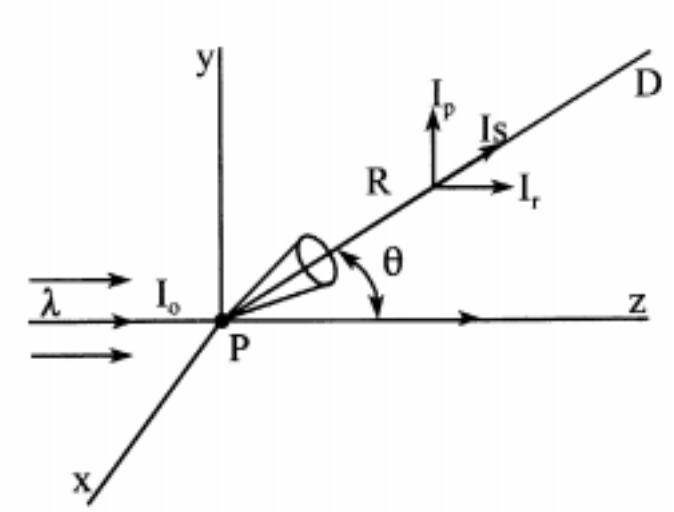


**Figure 7. Scattering by a single particle at p.**

The total scattering cross-section of the single particle, $\sigma(x,m)$, is obtained by integrating $f(\theta, x, m)$ over all solid angles (i.e., over $4\pi$)

$$I_s(\theta, x, m) = I_o(\lambda) f(\theta, x, m)/R^2 \qquad [11]$$

The total extinction cross-section, $\sigma_e$, from conservation of energy, is given by $\sigma_e = \sigma_s + \sigma_a [m^2]$, where subscripts *e, s,* and *a* represent extinction, scattering, and absorption processes. For non-absorbing particles, $\sigma_e = \sigma_s$.

The efficiency factor, $Q(x, m)$. The efficiency factor is a dimensionless parameter, obtained by dividing the respective "optical" cross-sections by the particle "geometrical" cross-section, $G (= \pi r^2)$, i.e.,

$$Q_e = \sigma_e / G, Q_s = \sigma_s / G, \text{ and } Q_a = \sigma_a / G \quad [12]$$

The Mie scattering diagram (also called in literature the "phase diagram" *[Chandrasekhar, S. Radiative Transfer, Oxford Clarendon Press, London, 1950]* or the "indicatrix," shown in Figure 8, illustrates the angular distribution of irradiance of the two components of polarization $I_p$ (solid line) and $I_r$ (dashed line) of the scattered radiation, around a particle of radius $r$ at P. The most characteristic scattering property of the Mie particles (i.e., those particles whose sizes are comparable to, or greater than, the wavelength of incident light) is their strong forward scattering. The larger the size parameter $x$ of the particle, the stronger is the scattered intensity in the forward direction, i.e., the forward lobe, that contains approximately 84% of scattered energy, becomes longer and narrower.

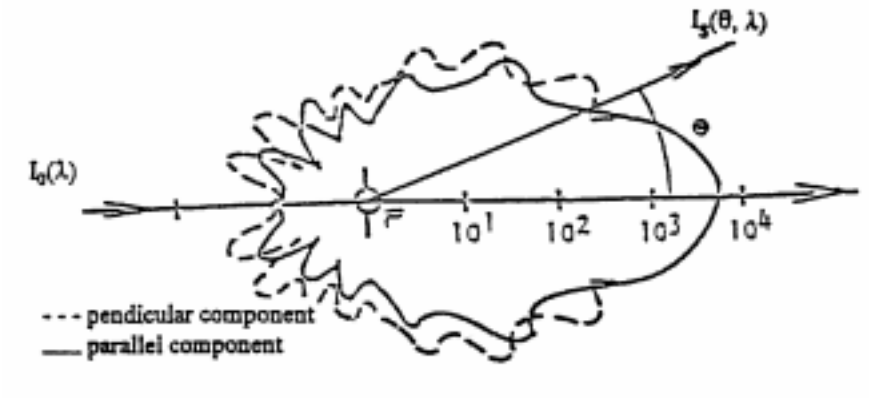


**Figure 8. Mie scattering diagram**

Also, for the forward scattered light, the two components of polarization, $I_r$ and $I_p$, have nearly the same magnitude, where $I_r$ and $I_p$ represent states of polarization perpendicular and parallel to the scattering plane, as shown by the dashed and solid scattering diagrams, respectively, in Figure 8.

Further, the plot of $Q(x, m)$ versus size parameter $x$ (Figure 9) for given values of $m_1$ and $m_2$, illustrates that the total loss of radiation from the direct beam is greatest for particles with size parameters $x \sim 4.0$ (i.e., the efficiency factor $Q$ is maximum), and for large particles, $Q$ attains a value of approximately 2.0. In other words, for particles with $r \sim \lambda$, the scattering cross-section is maximum, and for very large particles the scattering cross-section becomes twice the geometrical cross-section.

### 2.5.2 Optical Properties of a Cloud of Particles

If monochromatic electromagnetic radiation of wavelength, $\lambda$, and irradiance, $I_o(\lambda)$ [watts/cm$^2$–μm], is incident on a turbid medium, containing a cloud of polydisperse aerosols of size distribution $n(r)$ and refractive index $m = m_1 – im_2$, the irradiance $I_s(\lambda)$ of scattered radiation reaching the detector (D) from all scatterers in the particle cloud (Figure 10), can be computed from the previous relations (Eqs. [9]–[12]) and Mie theory by assuming that the single scattering (SS) theory which should really be called SS approximation. The SS theory is valid.

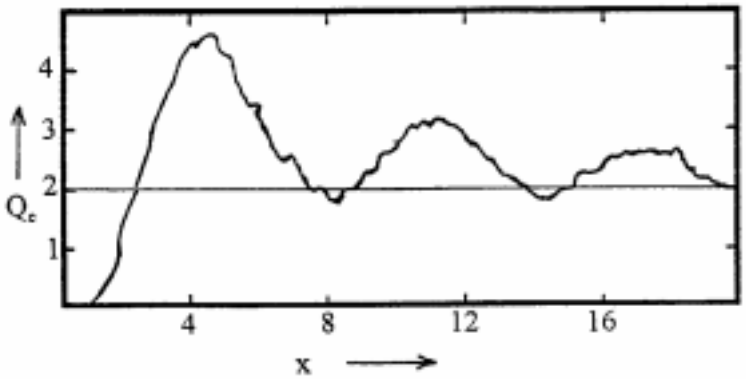


**Figure 9. Dependence of the efficiency factor $Q_e$ on the size parameter.**

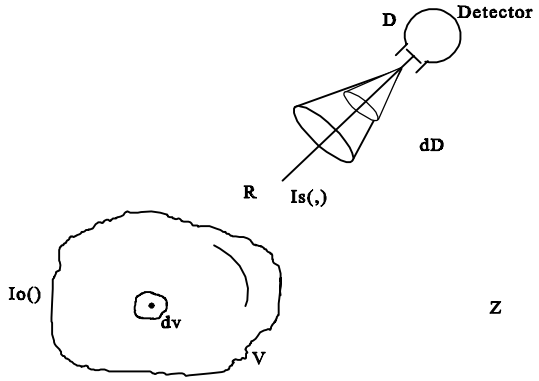


**Figure 10. Scattering by an element dV of the aerosol medium of total volume V.**

In the SS theory [References [60, 8, 30, 33], it is assumed that: (1) scattered light has the same wavelength as the incident light, and (2) the scattering is independent. The latter assumption requires that the particles are: (a) well-defined and separate (unlike those in a high polymer solution), (b) in random motion (so that no phase effects are permissible), and (c) sufficiently apart (a mutual distance of about three times the radius is a sufficient condition, according to Van de Hulst [1957]). For instance, even a dense fog, in which light can penetrate only about 10 meters, has about one droplet per $cm^3$, giving a mutual distance of about 20 times the radius. In most applications of our study of atmospheric aerosols, all these assumptions and requirements are valid.

2.5.2.1 The Volume Scattering Function, $F_s(\theta,\lambda)$, and the Volume Scattering Coefficient, $\beta_s(\lambda)$.

The scattering and transmission properties of a unit volume of the particles, are characterized by the volume scattering function, $F_s(\theta, \lambda, m_1)$, with units $[m^{-1}sr^{-1}]$, and the volume scattering coefficient, $\beta_s(\lambda,m)$, with units $[m^{-1}]$, defined as follows:

$$F_s(\theta,\lambda,m_1) = \int_{r_1}^{r_2} f(\theta,r,\lambda,m_1)n(r)dr, \ [m^{-1}sr^{-1}] \qquad [13(a)]$$

$$= \frac{\lambda^2}{4\pi^2}\int_{r1}^{r2}\left(\frac{i_1+i_2}{2}\right)n(r)dr, \ [m^{-1}sr^{-1}] \qquad [13(b)]$$

$$\beta_s(\lambda) = \int_{4\pi} F_s(\theta, \chi, m\Omega, \ [m^{-1}] \qquad [14]$$

$$= \int_{r1}^{r2}\sigma_s(r,\lambda)n(r)\,dr, \ [m^{-1}]$$

Thus, by conservation, the volume extinction coefficient, $\beta_e = \beta_s + \beta_a$, where $\beta_a$ is the volume absorption coefficient.

2.5.2.2 The Phase function, $P(\theta, \lambda)$

The phase function, $P(\theta, \lambda)$, is a useful concept (introduced by Chandrasekhar [1928]) is defined by:

$$P(\theta, \lambda) = F_e(\theta, \lambda)/\beta_e(\lambda), \ [sr^{-1}] \qquad [15]$$

If only scattering is present, $\beta_e(\lambda) = \beta_s(\lambda)$ and $P(\theta, \lambda) = F_s(\theta, \lambda)/\beta_s(\lambda)$ such that

$$\int_{4\pi} P(\theta)d\Omega = 1 \qquad [16]$$

2.5.2.3 The Scattered Radiation.

If radiation with irradiance $I_o(\lambda)$ [watts/$cm_2$-μm] is incident on a volume element dV of the medium, then radiance $B_S(\lambda)$ (i.e., watts/$cm_2$-sr-μm) of scattered radiation received by the detector with a view cone of solid angle $d\Omega_D$ at distance R from dV is given by

$$B_s(\theta,\lambda) = I_o(\lambda)\frac{F(\theta)dV}{R^2}\quad\frac{1}{dQ_D} \qquad [17]$$

2.5.2.4 The Transmitted Radiation.

If $I_o(\lambda)$ is the irradiance of a parallel, monochromatic beam of radiation incident on a layer of a turbid (i.e., scattering and absorbing) medium (Figure 11), $I(\lambda)$ its irradiance at a distance $l$, and $dI(\lambda)$ is the amount of irradiance by which the beam is diminished after passage through an elemental layer of thickness $dl$, then for an "optically thin" medium *[Bauer, E., Applied Optics, 3, 197 (1964)*, i.e., a medium in which only "single" scattering prevails, is given by the Beer-Bouger law, namely:

$$dI(\lambda) \propto -I(\lambda)dl \qquad [18a]$$

or

$$dI(\lambda) = -\beta_e I(\lambda)dl \qquad [18b]$$

where $\beta_e$ is the volume extinction coefficient. After traversing a length $L$ of the medium, the beam intensity is obtained by integrating Eq. [18], the transmission or Beer-Bouger law is given by

$$I(\lambda,L) = I_o(\lambda)e^{-\tau(\lambda,L)} \qquad [19]$$

$$\tau(\lambda,L) = \int_o^L \beta_e dl$$

where $\tau(\lambda,L) = \int_o^L \beta_e dl$ is referred to as the "optical thickness" of the medium of thickness $L$.

### 2.5.3 Aerosol Refractive Indices

Refractive indices for common aerosol components (see Table 6) are listed in Table 8 for wavelengths between 0.35 and 10.0 μm. Graphical representations and detailed informationon the radiation characteristics are given D'Almeida, et al [1991.

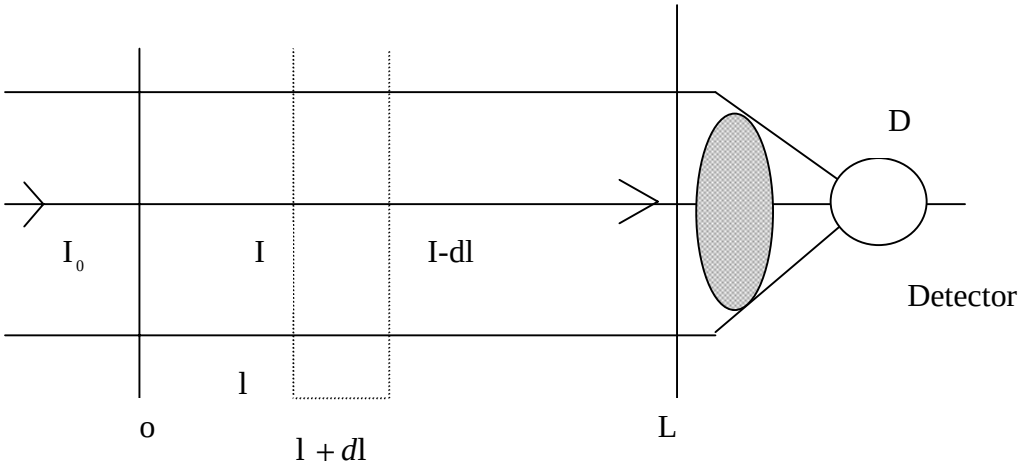


**Figure 11. Transmission law for ana erosol medium of length $L$.**

.

**Table 8. Complex Refractive Index (mr + imi) of Various Aerosol Components and Water** (D'Almeida et al, 1991; Palmer, 1975)o

| Wave-length | Dust-like | | Water-soluble | | Soot | | Oceanic* | | Sulfate | | Mineral | | Water | | 75% Sulfuric Acid | |
|---|---|---|---|---|---|---|---|---|---|---|---|---|---|---|---|---|
| (μm) | mr | mi | mr | mi | mr | mr | mi | mr | mr | mi | mr | mi | mr | mi | mr | mi |
| .350 | 1.530 | 8.00E-3 | 1.530 | 5.00E-3 | 1.750 | .465 | 1.390 | 1.20E-7 | 1.452 | 1.00E-8 | 1.530 | 1.70E-2 | 1.343 | 6.50E-9 | 1.452 | - |
| .400 | 1.530 | 8.00E-3 | 1.530 | 4.00E-3 | 1.750 | .460 | 1.385 | 9.90E-9 | 1.440 | 1.00E-8 | 1.530 | 1.30E-2 | 1.339 | 1.86E-9 | 1.440 | - |
| .450 | 1.530 | 8.00E-3 | 1.530 | 5.00E-3 | 1.750 | .455 | 1.383 | 9.90E-9 | 1.432 | 1.00E-8 | 1.530 | 8.50E-3 | 1.337 | 1.02E-9 | 1.432 | - |
| .500 | 1.530 | 8.00E-3 | 1.530 | 1.30E-2 | 1.750 | .450 | 1.382 | 6.41E-9 | 1.431 | 1.00E-8 | 1.530 | 7.80E-3 | 1.335 | 1.00E-9 | 1.431 | - |
| .550 | 1.530 | 8.00E-3 | 1.530 | 1.20E-2 | 1.750 | .440 | 1.381 | 3.70E-9 | 1.430 | 1.00E-8 | 1.530 | 5.50E-3 | 1.333 | 1.96E-9 | 1.432 | - |
| .600 | 1.530 | 8.00E-3 | 1.530 | 1.80E-2 | 1.750 | .435 | 1.379 | 4.26E-9 | 1.429 | 1.47E-8 | 1.530 | 4.50E-3 | 1.332 | 1.09E-8 | 1.430 | - |
| .650 | 1.530 | 8.00E-3 | 1.530 | 2.30E-2 | 1.750 | .435 | 1.377 | 1.62E-8 | 1.429 | 1.47E-8 | 1.530 | 4.50E-3 | 1.331 | 1.64E-8 | 1.429 | - |
| .700 | 1.530 | 8.00E-3 | 1.530 | 2.70E-2 | 1.750 | .430 | 1.376 | 5.04E-8 | 1.428 | 1.99E-8 | 1.530 | 4.00E-3 | 1.331 | 3.35E-8 | 1.428 | 2.1E-9 |
| .750 | 1.530 | 8.00E-3 | 1.530 | 3.39E-2 | 1.750 | .430 | 1.375 | 1.09E-6 | 1.427 | 1.89E-8 | 1.530 | 4.00E-3 | 1.330 | 1.56E-7 | 1.427 | 7.1E-8 |
| .800 | 1.520 | 8.00E-3 | 1.520 | 7.00E-2 | 1.750 | .430 | 1.374 | 6.01E-5 | 1.426 | 1.70E-7 | 1.530 | 1.20E-3 | 1.329 | 1.25E-7 | 1.427 | 8.6E-8 |
| .900 | 1.520 | 8.00E-3 | 1.520 | 6.50E-2 | 1.750 | .435 | 1.373 | 1.41E-5 | 1.425 | 1.79E-7 | 1.530 | 1.20E-3 | 1.328 | 4.86E-7 | 1.425 | 2.5E-8 |
| 1.000 | 1.520 | 8.00E-3 | 1.520 | 1.00E-1 | 2.130 | .440 | 1.370 | 2.43E-5 | 1.423 | 1.50E-6 | 1.530 | 1.00E-3 | 1.327 | 2.86E-6 | 1.422 | 1.5E-8 |
| 1.250 | 1.460 | 8.00E-3 | 1.510 | 2.15E-1 | 2.150 | .450 | 1.365 | 3.11E-4 | 1.410 | 1.00E-5 | 1.530 | 1.30E-3 | 1.323 | 4.69E-5 | 1.413 | 6.9E-6 |
| 1.500 | 1.410 | 8.00E-3 | 1.420 | 2.90E-1 | 2.160 | .460 | 1.360 | 1.07E-3 | 1.403 | 1.34E-4 | 1.420 | 1.40E-3 | 1.321 | 1.12E-4 | 1.404 | 1.2E-4 |
| 1.750 | 1.340 | 8.00E-3 | 1.420 | 3.70E-1 | 2.170 | .480 | 1.352 | 8.50E-4 | 1.390 | 5.50E-4 | 1.370 | 1.80E-3 | 1.212 | 1.00E-4 | 1.394 | 4.2E-4 |
| 2.000 | 1.260 | 8.00E-3 | 1.420 | 4.20E-1 | 2.180 | .490 | 1.347 | 2.39E-3 | 1.384 | 1.26E-3 | 1.267 | 2.00E-3 | 1.306 | 1.10E-3 | 1.384 | 1.3E-3 |
| 2.500 | 1.180 | 9.00E-3 | 1.420 | 1.60E-1 | 2.190 | .510 | 1.309 | 1.56E-2 | 1.344 | 3.76E-3 | 1.180 | 3.40E-3 | 1.261 | 1.74E-3 | 1.344 | 3.8E-3 |
| 3.000 | 1.160 | 1.20E-2 | 1.420 | 9.50E-2 | 2.200 | .540 | 1.439 | 1.97E-1 | 1.293 | 9.55E-2 | 1.160 | 1.20E-2 | 1.371 | 2.72E-1 | 1.293 | 0.095 |
| 3.200 | 1.220 | 1.00E-2 | 1.430 | 9.00E-2 | 2.210 | .540 | 1.481 | 6.69E-2 | 1.311 | 3.35E-1 | 1.220 | 1.00E-2 | 1.478 | 9.24E-2 | 1.307 | 0.132 |
| 3.392 | 1.260 | 1.30E-2 | 1.430 | 7.00E-3 | 1.870 | .550 | 1.439 | 1.51E-2 | 1.352 | 1.59E-1 | 1.260 | 1.30E-2 | 1.422 | 2.04E-2 | 1.352 | 0.159 |

**Table 8. Complex Refractive Index (mr+imi) of Various Aerosol Components and Water** [D'Almeida et al., 1991; Palmer and Williams, 1975].

| Wave-length | Dust-like | | Water-soluble | | Soot | | Oceanic* | | Sulfate | | Mineral | | Water | | 75% Sulfuric Acid | |
|---|---|---|---|---|---|---|---|---|---|---|---|---|---|---|---|---|
| (μm) | mr | mi | mr | mi | mr | mr | mi | mr | mr | mi | mr | mi | mr | mi | mr | mi |
| 3.500 | 1.280 | 1.10E-2 | 1.450 | 5.00E-3 | 1.880 | .560 | 1.423 | 7.17E-3 | 1.376 | 1.58E-1 | 1.280 | 1.10E-2 | 1.400 | 9.40E-2 | 1.370 | 0.160 |
| 3.750 | 1.270 | 1.10E-2 | 1.452 | 4.00E-3 | 1.900 | .570 | 1.398 | 2.90E-3 | 1.396 | 1.31E-1 | 1.270 | 1.10E-2 | 1.369 | 3.50E-3 | 1.396 | 0.130 |
| 4.000 | 1.260 | 1.20E-2 | 1.455 | 5.00E-3 | 1.920 | .580 | 1.388 | 3.69E-3 | 1.398 | 1.36E-1 | 1.260 | 1.20E-2 | 1.351 | 4.60E-3 | 1.398 | 0.126 |
| 4.500 | 1.260 | 1.40E-2 | 1.460 | 1.30E-2 | 1.940 | .590 | 1.377 | 9.97E-3 | 1.385 | 1.20E-1 | 1.260 | 1.40E-2 | 1.332 | 1.34E-2 | 1.384 | 0.119 |
| 5.000 | 1.250 | 1.60E-2 | 1.450 | 1.20E-2 | 1.970 | .600 | 1.366 | 9.57E-3 | 1.360 | 1.21E-1 | 1.250 | 1.60E-2 | 1.321 | 1.24E-2 | 1.362 | 0.121 |
| 5.500 | 1.220 | 2.10E-2 | 1.440 | 1.80E-2 | 1.990 | .610 | 1.333 | 9.31E-3 | 1.337 | 1.83E-1 | 1.220 | 2.10E-2 | 1.298 | 1.16E-2 | 1.337 | 0.182 |
| 6.000 | 1.150 | 3.70E-2 | 1.410 | 2.30E-2 | 2.020 | .620 | 1.306 | 7.96E-2 | 1.425 | 1.95E-1 | 1.220 | 2.10E-2 | 1.265 | 1.07E-2 | 1.425 | 0.195 |
| 6.200 | 1.140 | 3.90E-2 | 1.430 | 2.70E-2 | 2.030 | .625 | 1.431 | 6.91E-2 | 1.424 | 1.65E-1 | 1.140 | 3.90E-2 | 1.363 | 8.80E-2 | 1.423 | 0.146 |
| 6.500 | 1.130 | 4.20E-2 | 1.460 | 3.39E-2 | 2.040 | .630 | 1.374 | 2.94E-2 | 1.370 | 1.28E-1 | 1.130 | 4.20E-2 | 1.339 | 3.92E-2 | 1.367 | 0.123 |
| 7.200 | 1.400 | 5.50E-2 | 1.400 | 7.00E-2 | 2.060 | .650 | 1.343 | 2.49E-2 | 1.210 | 1.76E-1 | 1.400 | 5.50E-2 | 1.312 | 3.21E-2 | 1.222 | 0.173 |
| 7.900 | 1.150 | 4.00E-2 | 1.200 | 6.50E-2 | 2.120 | .670 | 1.324 | 2.79E-2 | 1.140 | 4.88E-1 | 1.150 | 4.00E-2 | 1.294 | 3.39E-2 | 1.146 | 0.46 |
| 8.200 | 1.130 | 7.42E-2 | 1.010 | 1.00E-1 | 2.130 | .680 | 1.324 | 3.08E-2 | 1.200 | 6.45E-1 | 1.130 | 7.42E-2 | 1.286 | 3.51E-2 | 1.210 | 0.63 |
| 8.500 | 1.300 | 9.00E-2 | 1.300 | 2.15E-1 | 2.150 | .690 | 1.336 | 3.36E-2 | 1.370 | 7.55E-1 | 1.300 | 9.00E-2 | 1.278 | 3.67E-2 | 1.488 | 0.75 |
| 8.700 | 1.400 | 1.00E-1 | 2.400 | 2.90E-1 | 2.160 | .690 | 1.366 | 3.56E-2 | 1.530 | 7.72E-1 | 1.400 | 1.00E-1 | 1.272 | 2.79E-2 | 1.545 | 0.76 |
| 9.000 | 1.700 | 1.40E-1 | 2.560 | 3.70E-1 | 2.170 | .700 | 1.373 | 3.65E-2 | 1.650 | 6.33E-1 | 1.400 | 1.40E-1 | 1.262 | 3.99E-2 | 1.669 | 0.59 |
| 9.200 | 1.720 | 1.50E-1 | 2.200 | 4.20E-1 | 2.180 | .700 | 1.356 | 3.71E-2 | 1.600 | 5.86E-1 | 1.720 | 1.50E-1 | 1.255 | 4.15E-2 | 1.614 | 0.70 |
| 9.500 | 1.730 | 1.62E-1 | 1.950 | 1.60E-1 | 2.190 | .710 | 1.339 | 3.68E-2 | 1.670 | 7.50E-1 | 1.730 | 1.62E-1 | 1.243 | 4.44E-2 | 1.684 | 0.70 |
| 9.800 | 1.740 | 1.62E-1 | 1.870 | 9.50E-2 | 2.200 | .715 | 1.324 | 3.88E-2 | 1.910 | 6.80E-1 | 1.740 | 1.62E-1 | 1.229 | 4.79E-2 | 1.944 | 0.54 |
| 10.000 | 1.750 | 1.62E-1 | 1.820 | 9.00E-2 | 2.210 | .720 | 1.310 | 4.06E-2 | 1.890 | 4.55E-1 | 1.750 | 1.62E-1 | 1.218 | 5.08E-2 | 1.915 | 0.40 |

*Oceanic is 70% water + 30% sea-salt.

## 2.6 Aerosol Mechanical Characteristics

The impact of an aerosol can cause abrasion. The effect of the impact depends upon the nature of the surface impacted, the aerosol velocity, the angle of impact, and the hardness of the particle. The hardness of a particle may be compared using Moh's scale of hardness, which is reproduced in Table 9(a). A listing of the hardness of other materials is given in Table 9(b) *[Johnson, 1993]*. The most abrasive aerosols encountered are likely to be sand (quartz) and volcanic ash both with hardness values of 6–7. Minerals found in clay and dust (Kaolinite, Gypsum) and sea-salt (Halite), have consistently lower hardness values. Soot and organic materials have low hardness values.

**Table 9(a). Moh's Scale-of-hardness for Minerals**

| Moh's Relative Hardness | Mineral |
|---|---|
| 1 | Talc |
| 2 | Gypsum |
| 3 | Calcite |
| 4 | Fluorite |
| 5 | Apatite |
| 6 | Orthoclase |
| 7 | Quartz |
| 8 | Topaz |
| 9 | Carborundum |
| 10 | Diamond |

**Table 9(b). Moh's Hardness Values for Some Other Minerals**

| Material | Hardness |
|---|---|
| Lead | 1.5 |
| Aluminum | 2–2.5 |
| Halite (sea-salt) | 2–2.5 |
| Kaolinite | 2–2.5 |
| Zinc | 2.5 |
| Copper | 2.5–3 |
| Gold | 2.5–3 |
| Brass | 3–4 |
| Iron | 4–5 |
| Platinum | 4.3 |
| Glass | 4.5–6.5 |
| Steel | 5–8.5 |
| Volcanic Ash | 6–7 |

# 3 Global Aerosol Models

The following sections present aerosol models for three altitude-separated regions of the atmosphere. The information is more detailed and specific than that given in the previous sections, to which reference may be made as necessary.

Information is provided in one of the following three forms:

1. Parameters of fitted analytic models and equations, e.g., the parameters for log normal models fitted to measured aerosol size distributions.
2. Numerical tables of measured quantities, e.g., stratospheric aerosol optical depth.
3. Graphical representations of the variation of useful physical characteristics, e.g., humidity effects on aerosol size in the maritime boundary layer. These graphs may show measured data or fitted models.

Figure 12 shows schematically the relationship between the various regions of the globe, the altitude subdivisions, and the models used to describe these. The figure is intended to be used as an aid to the quick accessing of these models.

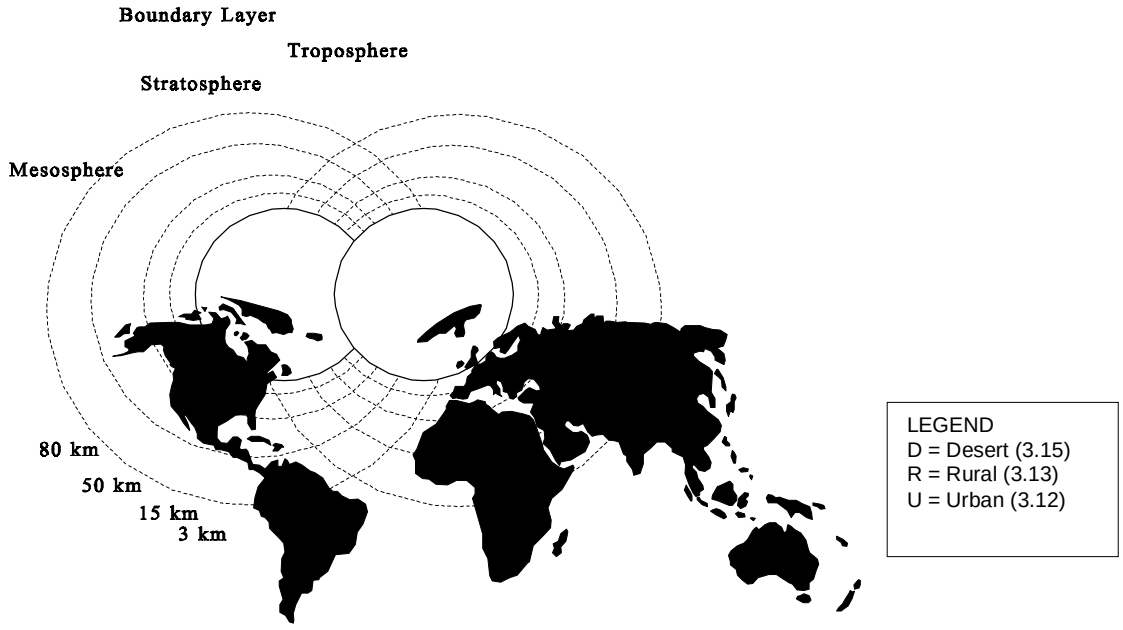


**Figure 12. Schematic showing the various geographical and altitude regions used in defining aerosol models.**

## 3.1 Boundary Layer

### 3.1.1 General Models

Section 2.3 described the general types of aerosols to be found in the Earth's atmosphere. Seven tropospheric aerosol types were listed in Table 5, and their approximate composition were given in Table 6. Here, we supply the corresponding size distributions, which are listed in Table 10 (taken from *Jaenicke, 1993*). Each size distribution is shown as the sum of three log normal functions for which the parameters are supplied. Plots of particle numbers as a function of particle radius are shown in Figure 13.

**Table 10. Parameters for Models of Aerosol Size Distributions Described by the Sum of Three Log Normal Functions** (from *Jaenicke [1993]*)

| Aerosol | Range | i | $n_i$($cm^{-1}$) | $R_i$(μm) | log $\sigma_i$ |
|---|---|---|---|---|---|
| Polar | I | 1 | $2.17 \times 10^{1}$ | 0.0689 | 0.245 |
| | II | 2 | $1.86 \times 10^{-1}$ | 0.375 | 0.300 |
| | III | 3 | $3.04 \times 10^{-2}$ | 4.29 | 0.291 |
| Background | I | 1 | $1.29 \times 10^{2}$ | 0.0036 | 0.645 |
| | II | 2 | $5.97 \times 10^{1}$ | 0.127 | 0.253 |
| | III | 3 | $6.35 \times 10^{1}$ | 0.259 | 0.425 |
| Maritime | I | 1 | $1.33 \times 10^{2}$ | 0.0039 | 0.657 |
| | II | 2 | $6.66 \times 10^{1}$ | 0.133 | 0.210 |
| | III | 3 | $3.06 \times 10^{0}$ | 0.29 | 0.396 |
| Remote Continental | I | 1 | $3.20 \times 10^{3}$ | 0.01 | 0.161 |
| | II | 2 | $2.90 \times 10^{3}$ | 0.058 | 0.217 |
| | III | 3 | $3.00 \times 10^{-1}$ | 0.9 | 0.380 |
| Desert Dust Storm | I | 1 | $7.26 \times 10^{2}$ | 0.001 | 0.247 |
| | II | 2 | $1.14 \times 10^{3}$ | 0.0188 | 0.770 |
| | III | 3 | $1.78 \times 10^{-1}$ | 10.8 | 0.438 |
| Rural | I | 1 | $6.65 \times 10^{3}$ | 0.00739 | 0.225 |
| | II | 2 | $1.47 \times 10^{2}$ | 0.0269 | 0.557 |
| | III | 3 | $1.99 \times 10^{3}$ | 0.0419 | 0.266 |
| Urban | I | 1 | $9.93 \times 10^{4}$ | 0.00651 | 0.245 |
| | II | 2 | $1.11 \times 10^{3}$ | 0.00714 | 0.666 |
| | III | 3 | $3.64 \times 10^{4}$ | 0.0248 | 0.337 |

Legend: Range I: $R_1$ is the Aitken or nucleation particle mode ($0.001 < R_1 < 0.1$ μm); Range II: $R_2$ is in the large or accumulation particles mode ($0.1 < R_2 < 1$ μm); and Range III: $R_3$ is in the giant or coarse particles mode ($R_3 > 1$ μm). For other explanations, see Table 4 and Table 6.

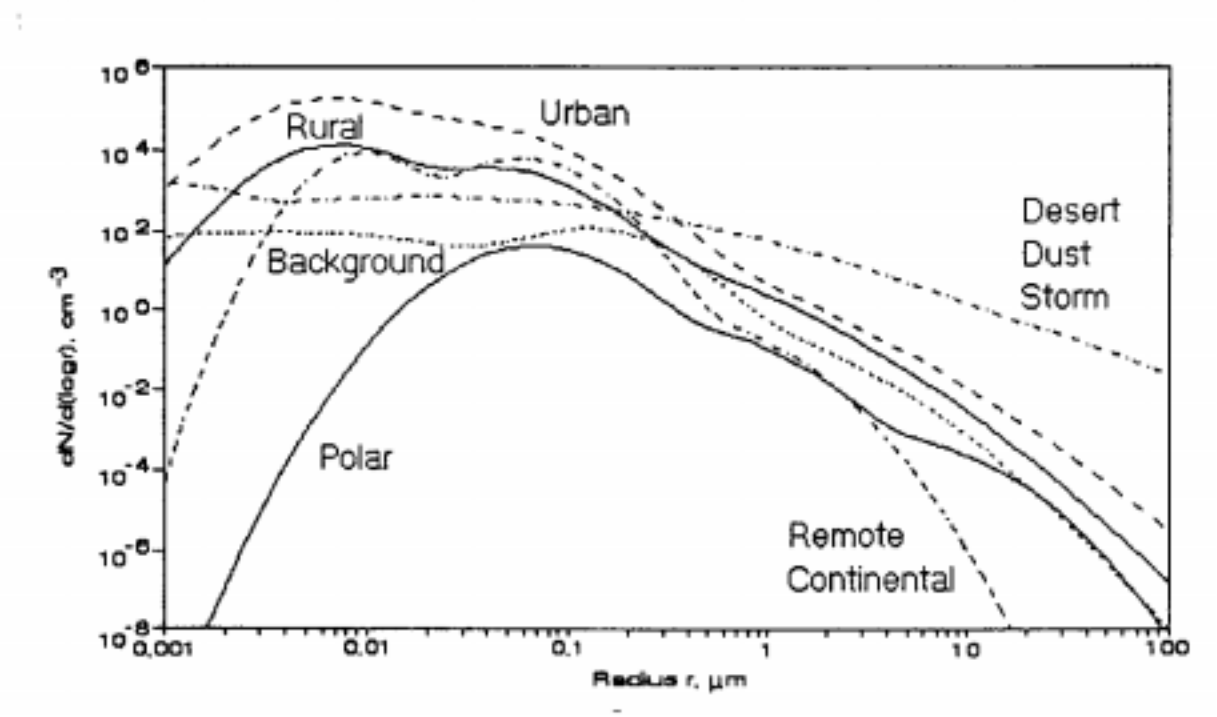


**Figure 13. Model size distributions of selected atmospheric aerosols according to Table 10.**

### 3.1.2 Urban Boundary Layer

See Table 10 (from Jaenicke, 1993).

### 3.1.3 Rural Boundary Layer

See Table 10 (from Jaenicke, 1993).

### 3.1.4 Maritime Boundary Layer

The remote marine boundary layer aerosol consists typically of a mixture of approximately 75% sea salt (sodium chloride) and 25% sulfate aerosol (sulfuric acid and ammonium sulfate [Porter and Clarke, 1997]). Size distributions show two main modes, the sulfate aerosol occupies the accumulation mode, and the sea salt is the coarse particle mode (see Section 2.2 and Figure 2). Coarse particle mode size distributions depend strongly upon surface wind velocity. Size distributions for dry sea salt are shown in Figure 14 as a function of wind velocity. The curves in Figure 14a correspond to wind speeds of 0.4 to 10.7 m/s, while Figure 14b corresponds to wind speeds from 10.8 to 33.5 m/s. The parameters for these area distributions are given in Table 11 as bimodal, log-normal, number distributions

Figure 15 shows the effect of humidity on both coarse and accumulation mode components of the marine aerosol.

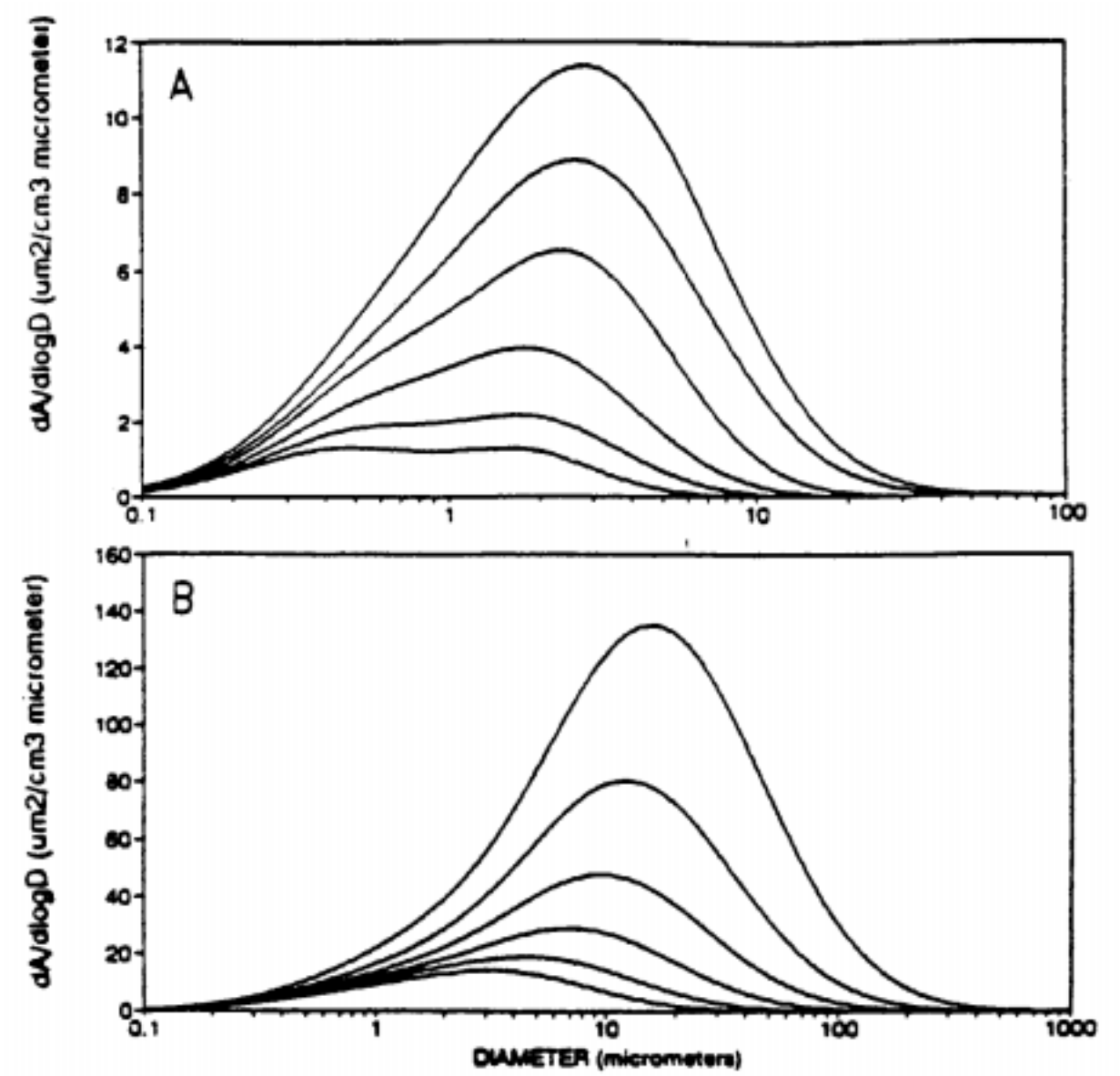


**Figure 14. Model dry sale aerosol distributions (shown as area) developed from the combination of OPC and Woodcock size distributions.** *[Porter and Clarke, 1997.]*

**Table 11. Log Normal Parameters for Sea Salt Aerosol Number Size Distributions (dN/dlogD)** *[Porter and Clarke, 1997]*

| **Wind** m/s | **Volume** $\mu g/m^3$ | **Number** $cm^3$ | **Curve1** GMD | **Curve1** STD σ | **Curve1** Multiplier | **Curve2** GMD | **Curve2** STD σ | **Curve2** Multiplier |
|---|---|---|---|---|---|---|---|---|
| 0.4 – 1.5 | 0.307 | 4.143 | 1.366 | 1.7 | 0.2911 | 0.275 | 2.00 | 2.01 |
| 1.6 –3.3 | 0.654 | 5.011 | 1.407 | 1.85 | 0.5277 | 0.3 | 2.05 | 2.57 |
| 3.4 – 5.4 | 1.50 | 6.003 | 1.41 | 2 | 1.104 | 0.308 | 2.1 | 3 |
| 5.5 – 7.9 | 2.74 | 7.325 | 1.5 | 2.1 | 1.55 | 0.338 | 2.23 | 3.8 |
| 8.0 – 10.7 | 5.47 | 8.98 | 1.51 | 2.3 | 2.39 | 0.349 | 2.30 | 4.55 |
| 10.8 – 13.8 | 8.32 | 9.9 | 1.773 | 2.30 | 2.53 | 0.397 | 2.45 | 6.07 |
| 13.9 - 17.1 | 11.8 | 11.52 | 2.05 | 2.30 | 2.607 | 0.442 | 2.55 | 7.06 |
| 17.2 - 20.7 | 25.1 | 13.4 | 2.807 | 2.4 | 2.617 | 0.4935 | 2.7 | 8.9 |
| 20.8 - 24.4 | 58.6 | 15.46 | 3.38 | 2.55 | 3.743 | 0.5 | 2.8 | 10 |
| 24.5 - 28.4 | 129 | 17.89 | 4.1 | 2.64 | 5.319 | 0.517 | 2.88 | 11.6 |
| 28.5 - 33.5 | 270 | 20.77 | 4.72 | 2.74 | 7.96 | 0.544 | 2.95 | 13.7 |
| >33.5 | 556 | 25 | 5.57 | 2.85 | 11.4 | 0.6 | 3.00 | 17.8 |

These distributions are shown as area distributions in Figure 14. The final distribution is the sum of two log normal curves (see equation). The geometric mean diameter (GMD) (μm), standard deviation (STD), and curve multiplier are given for both curves 1 and 2. Also shown are the integrated volume and integrated number for the total distribution. The first column shows the wind speed based on Woodcock *[1953].*

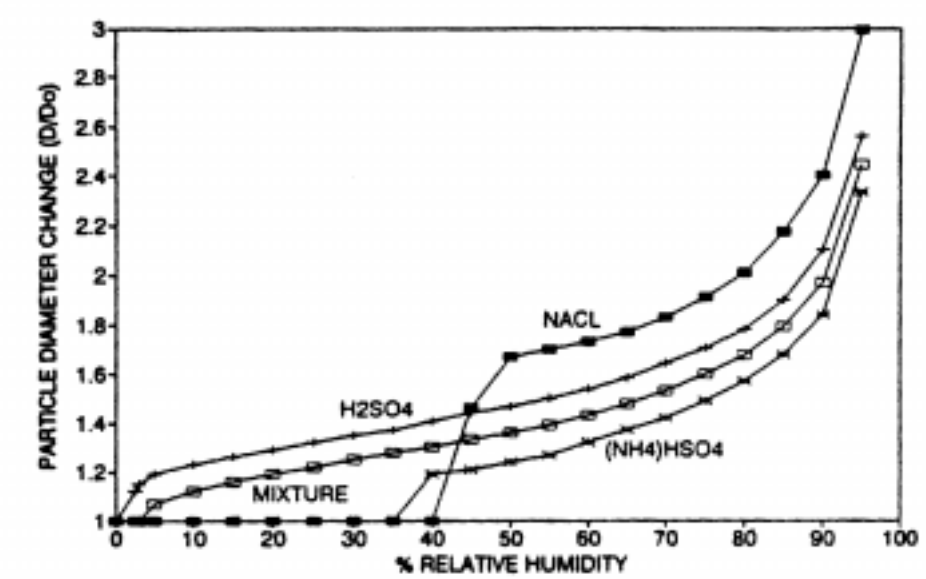


**Figure 15. Equilibrium aerosol diameters as a function of relative humidity for various aerosol compositions. The values for NaCl, $H_2SO_4$ and $(NH_4)HSO_4$ are based on work of Tang et al. [1977]; Tang and Munkelwitz [1977]; and Tang [1980]. The line shown for the mixture is based on our laboratory experiments with various molar ratios of $(NH_4/SO_4)$ ranging from 0 to 1** [*Porter and Clarke, 1997*].

### 3.1.5 Desert Boundary Layer

Aerosols in the desert boundary layer are multi-modal, but even at low wind speeds, the mass loading is dominated by sand. Background carbonaceous and water soluble aerosols occupy the accumulation mode while wind-blown sand forms the coarse particle mode. The latter is very dependent upon wind speed. Table 12, Figure 16(a), and Figure 16(b) present this variation.

The mass loading equation of *Jaenicke [1988]* is the basis for the wind-speed dependence:

$$c = 52.77\ exp\ (0.30\ u) \qquad [20]$$

where $c$ is the mass concentration in $\mu g\ m^{-3}$ of air and $u$ is the wind speed in $ms^{-1}$ at a height of 10 meters. The models shown in Figure 16 assume the background (carbonaceous and water soluble) components of the aerosol to remain constant. Actual measured size spectra for different regions and wind conditions are shown in Figure 17 *[Sviridenkov et al., 1993].*

**Table 12. Wind Speed Dependence of the Desert Aerosol Size Distribution Parameters** [After *Longtin et al., 1988*]

| **Aerosol Component** | **Wind Speed** ($ms^{-1}$) | **Size Distribution Parameters** | | |
|---|---|---|---|---|
| | | $\mathbf{R_i}(\mu m)$ | **Log** ($\sigma_i$) | **Comments** |
| Carbonaceous | 0 – 30 | 0.0118 | 0.301 | WMO[2] |
| Water Soluble | 0 – 30 | 0.0285 | 0.350 | WMO[2] |
| Sand | 0 | 6.24 | 0.277 | Coarse Mode of the Remote Continental Model of Jaenicke[33] |
| | 10 | 7.76 | 0.331 | Linear Interpolation of the Values at 0 and 30 m/s |
| | 20 | 9.28 | 0.384 | |
| | 30 | 10.80 | 0.438 | Coarse Mode of the Dust Storm Model of Jaenicke[33] |

Legend: $r_1 \equiv r_g$ ; $\sigma_1 \equiv \sigma_g$

### 3.1.6 Polar Boundary Layer

See Table 10.

### 3.1.7 Combustion Products and Their Transport

Measurements have been made on the aerosols produced by the Kuwait oil fires in May 1991 *[Parungo et al., 1992]*. A typical size distribution and compositions for the aerosol is shown in Figure 18(a), collected at an altitude of 3.7 km, 160 km downwind from the fires. Dominant particles consisted of soot coated with sulfuric acid. Size distributions and compositions change with distance from the fire, the concentration of small particles increasing with distance [Figure 18(b)].

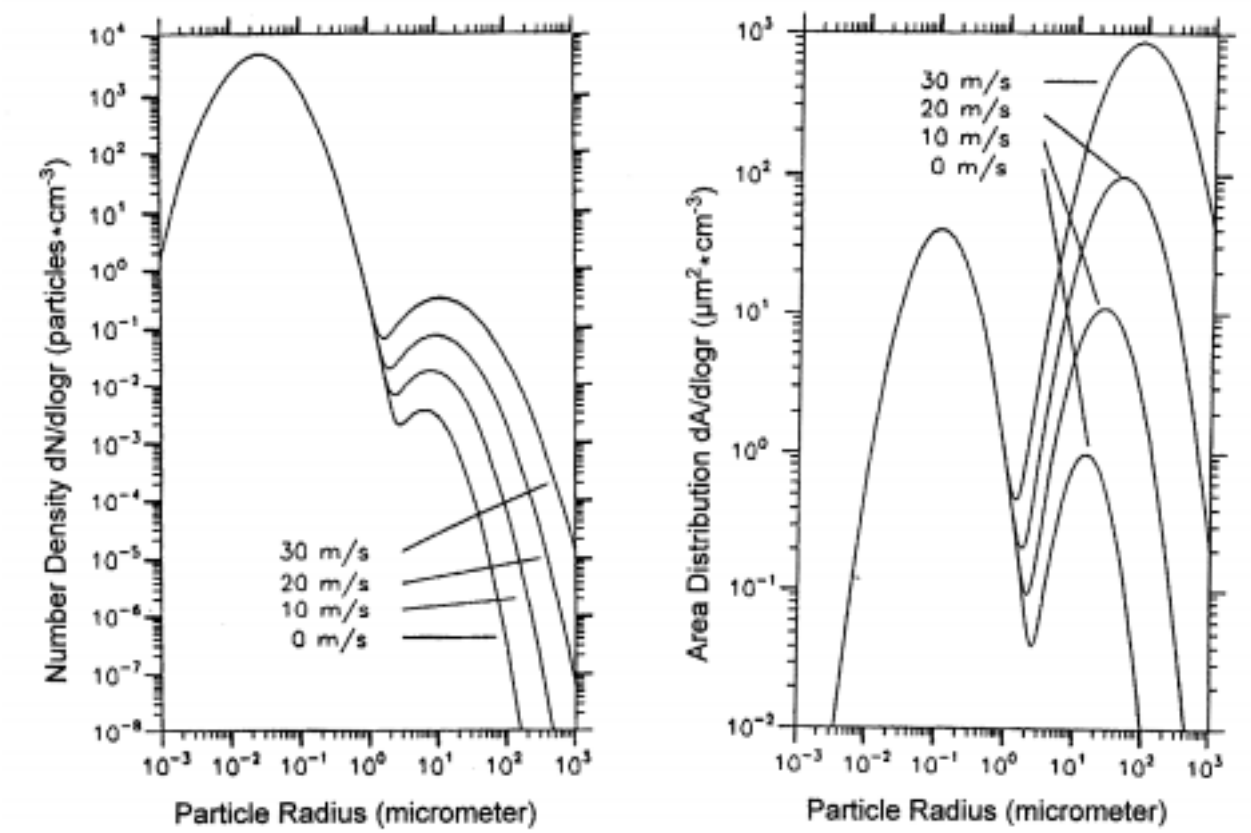


**Figure 16. Variation of (a) desert aerosol particle number density and (b) surface area with wind velocity** (from *Longtin et al., 1988*).

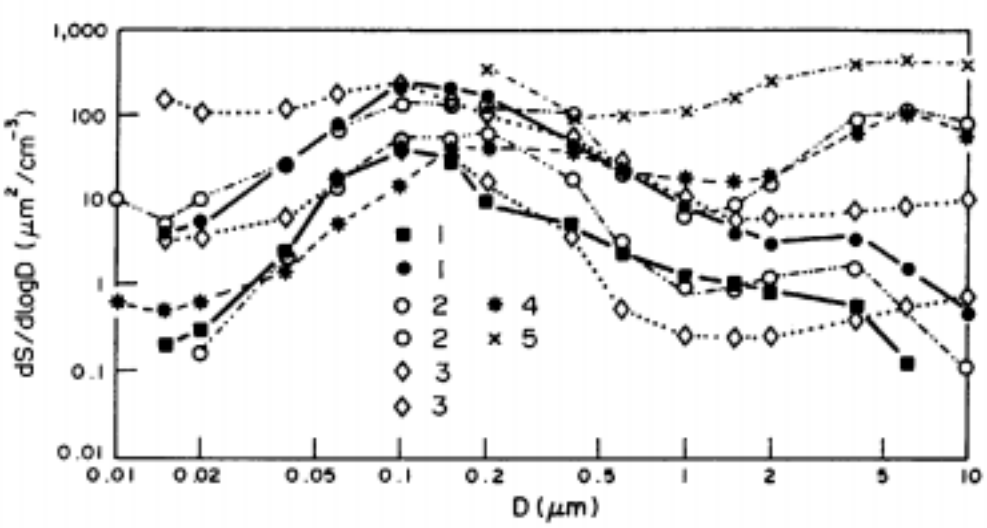


**Figure 17. The differential spectra of the areas of continental aerosol particles:** 1—rural regions in the European Soviet Territory (EST) center; 2—non-industrial town in the EST center; 3—Great Plains, U.S.A.; 4—semi-desert in the Shaartuz region, a day after the end of the dust storm; 5—same as region 4 but 3 hours after the end of the dust storm. The two 1, 2, and 3s give the range of the values for the measurements taken in the above mentioned regions. Curves 4 and 5 represent one time each [From *Sviridenkov et al., 1993*].

Carbonaceous aerosols are also observed over the oceans as a result of industrial activity and long distance transport. Such concentrations decrease with distance from the shore as is shown in Figure 19. The fitted relationship between the black carbon concentration (C) and distance (X) is:

$$\ln C = k_1 X/U + b_1 = k_1 T + b_2 \qquad [21]$$

where $k_1$ is $-0.2 \times 10^{-5}$, giving a half-life for black carbon in the atmosphere of less than one day. Beyond 2000 km, the carbon concentration no longer fits this model, and the residence time is of the order of five days.

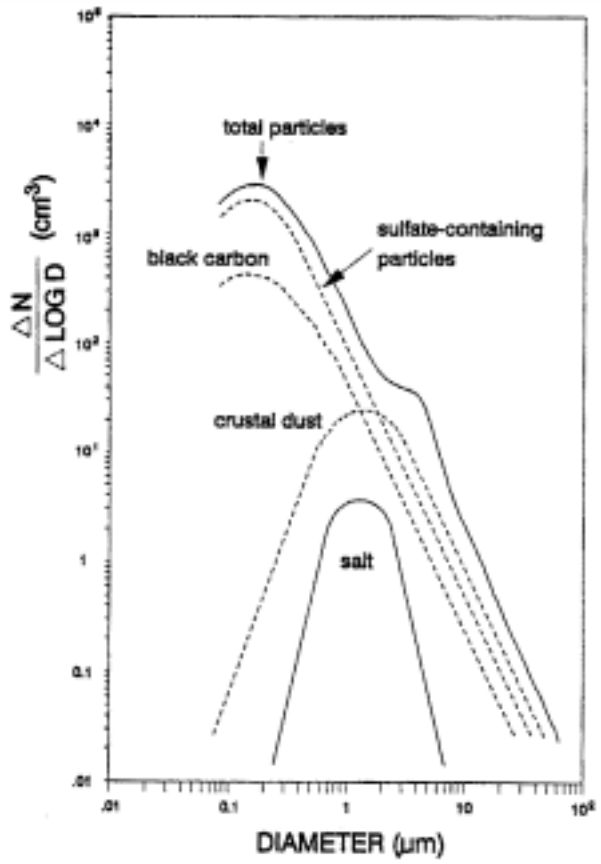


**Figure 18(a). Size distributions of various kinds of particles collected following the Kuwait oil fires** [From *Parungo et al., 1992*].

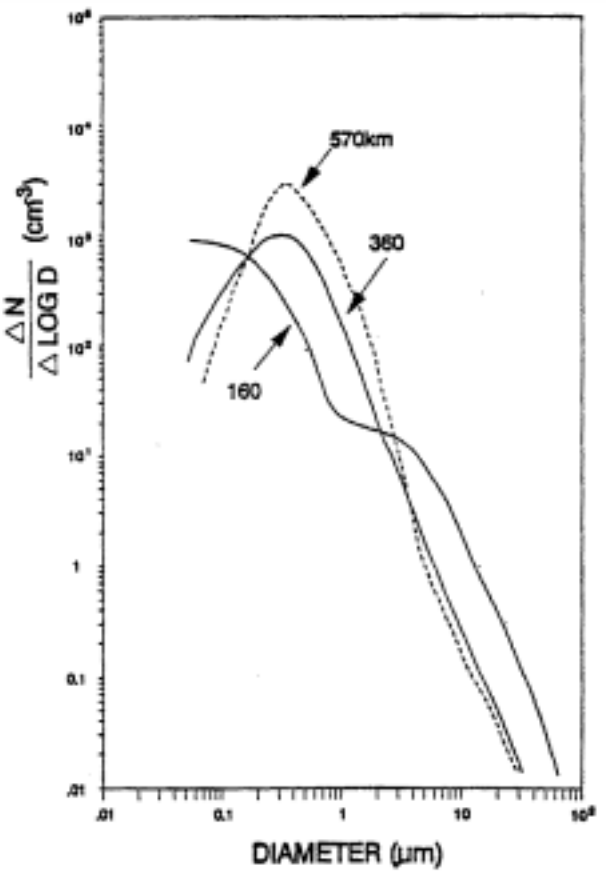


**Figure 18(b). Size distributions of aerosol samples collected at various distances from the fire but at similar altitudes (1-2 km)** [From *Parungo et al., 1992*].

### 3.1.8 Optical Characteristics

The oceans form a sufficiently dark background for the measurement of aerosol optical depth to be possible from space. No height discrimination is possible, and the product is strongly weighted toward the boundary layer. Figure 20 and Figure 21 show values for the optical depth (at a wavelength of 0.5 μm) measured with the AVHRR satellite *[Husar and Stowe, 1994]*. Figure 20 shows, in particular, areas of pollution (north Atlantic Ocean in March–May, June–August), desert dust (sub-tropical Atlantic Ocean, both sides of the Equator, Arabian Sea), biomass burning (south sub-tropical Atlantic Ocean, Indonesia, September–November). The strong seasonal variation observed are shown in Figure 21 for selected regions of the earth. We may note the haziest region of the earth to be the Arabian sea in June–August.

Measurements have been made over Europe of the extinction and absorption coefficient in various air masses. The range of values observed are shown in Figure 22 *[Hänel, 1994]*.

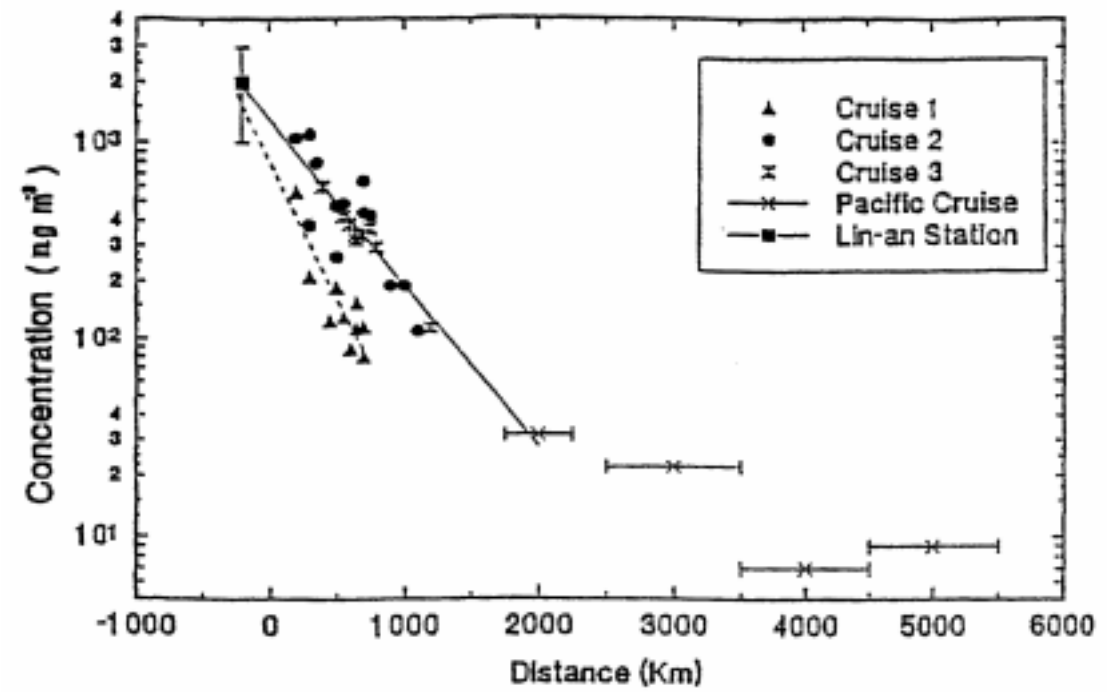


**Figure 19. Relationship between black carbon concentrations and distance from China shore** [*From Parungo et al., 1994*].

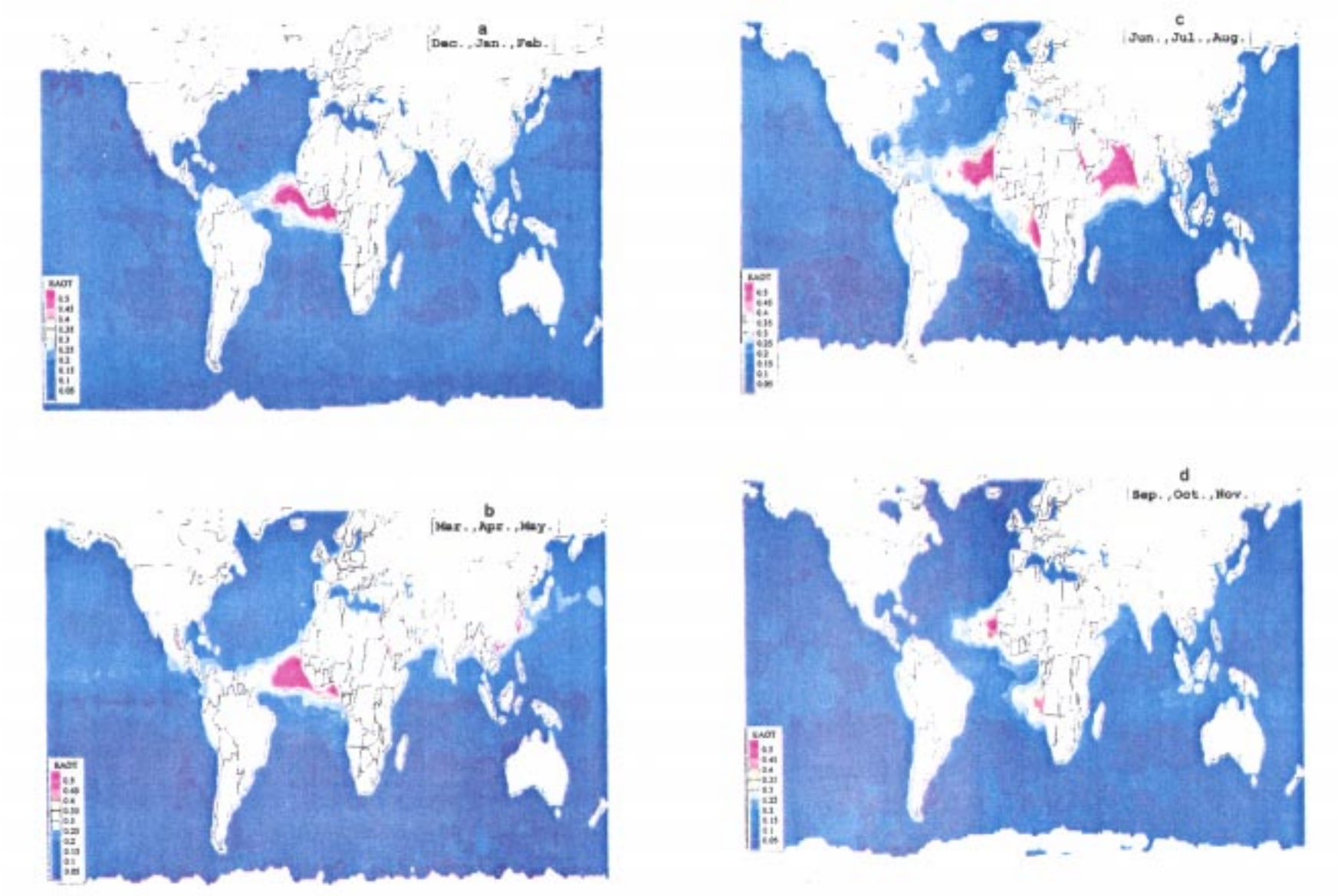


**Figure 20. Radiatively equivalent aerosol optical thickness (EAOT x 1000) over the oceans derived from NOAA AVHRR satellites for the four seasons. The figure incorporates data for the period July 1989 to June 1991** (from *Husar et al., 1997*).

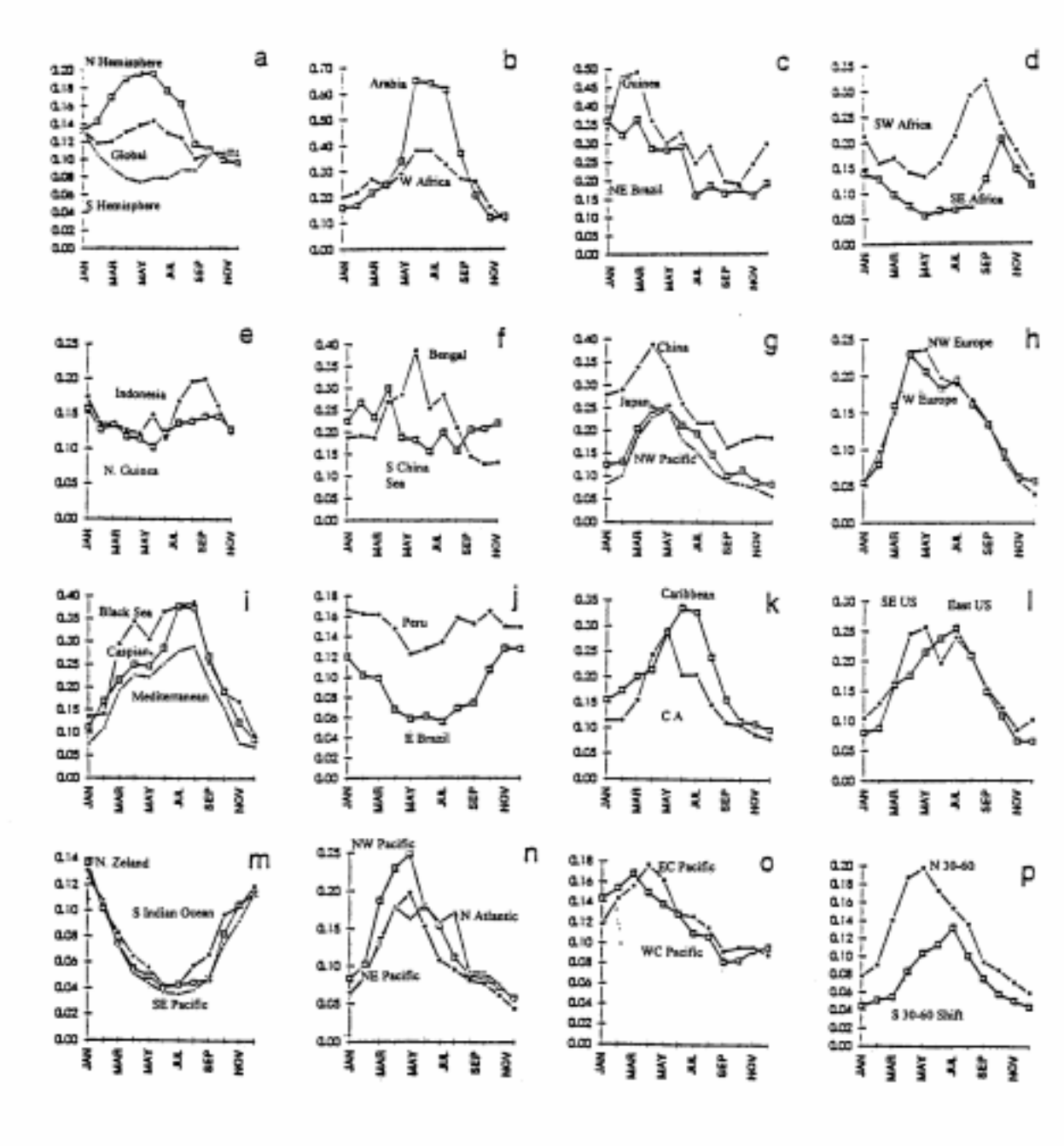


**Figure 21. Seasonal variation of regional optical depth** [from *Husar et al., 1997*].

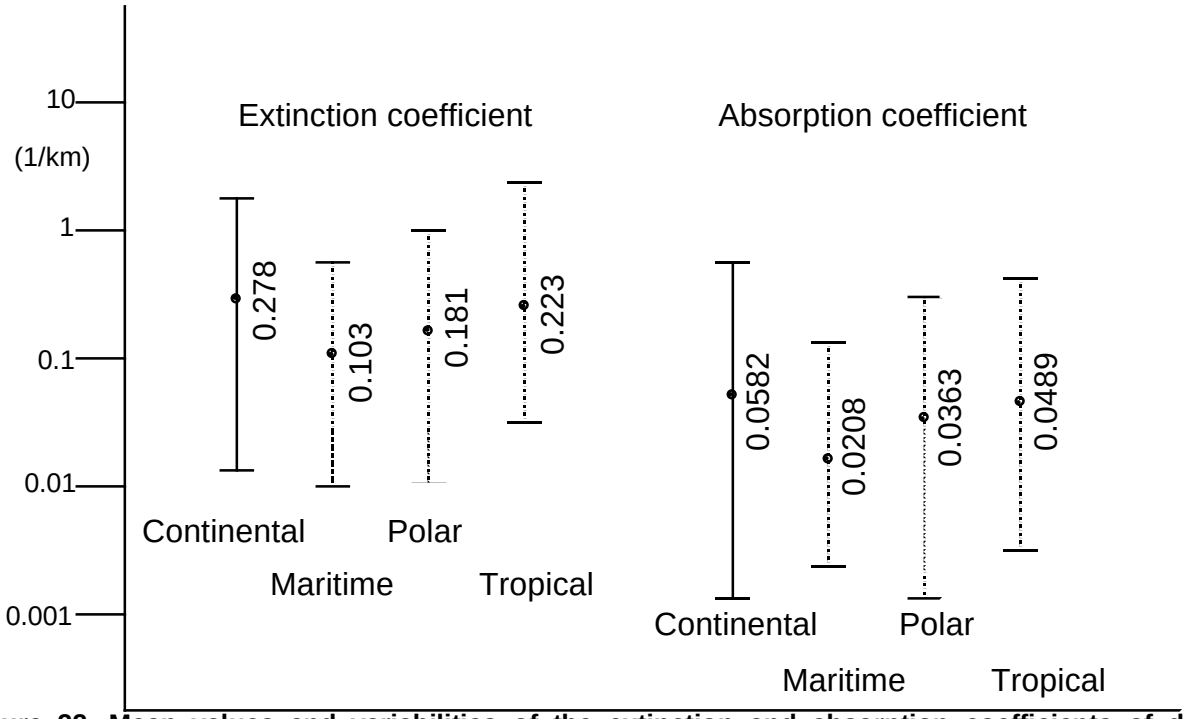


**Figure 22. Mean values and variabilities of the extinction and absorption coefficients of dry atmospheric particles at different air masses.** [From *Hänel, 1994*].

## 3.2 Free Troposphere

### 3.2.1 Vertical Aerosol Distribution

The free troposphere lies above the boundary layer, the top of which is 1–4 km above the earth's surface. The aerosols in this region are influenced by, but no longer principally determined by, the underlying surface characteristics. They are longer lived, of lower concentration than those in the boundary layer and may contain components that have been transported for very long distances. The second of these characteristics is illustrated in Figure 23(a) and (b) which show respectively the vertical distribution of aerosol mass and number concentration through the boundary layer and into the free troposphere. The ranges of the number concentrations are shown for ocean as well as remote continental aerosols. For the sake of a graphically smoothed presentation, the following equation has been used (where $n_o$ is the number concentration at the surface and $n_B$ is the number concentration of the corresponding background aerosols aloft) These figures are taken from Jaenicke *[1993]* and the curves shown are described by the relationship:

$$p = p_0 \left\{ \exp \frac{-z}{|H_p|} + \left( \frac{p_b}{p_0} \right)^{\nu} \right\}^{\nu}$$

$$n = n_0 \left\{ \exp\left( \frac{-z}{|H_n|} \right) + \left( \frac{n_s}{n_0} \right)^{\nu} \right\}^{\nu} \; : \; H_n \neq 0; \; \nu = \frac{H_n}{|H_n|} \qquad [22]$$

$$H_p \neq 0 \; and \; \nu = \frac{H_p}{|H_p|}$$

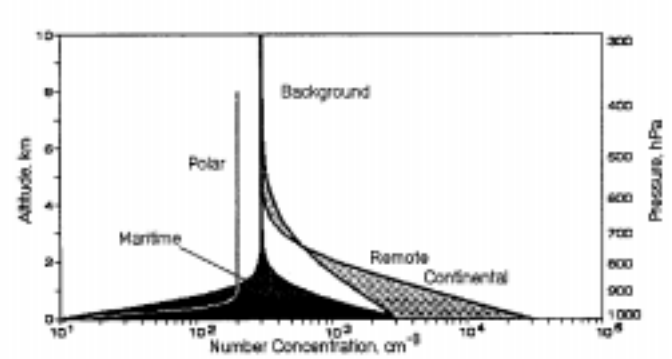


**Figure 23(a). Altitude distributions of particle mass concentration.**

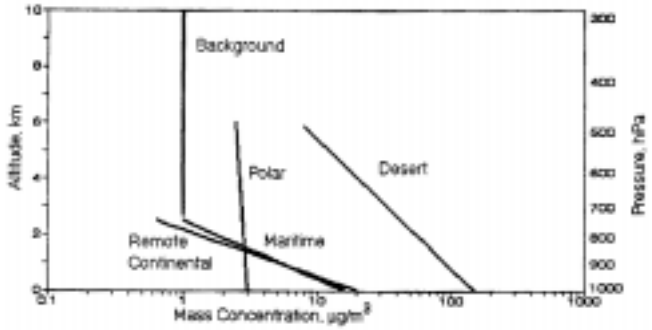


**Figure 23(b). Altitude distribution of aerosol number concentration.** [From *Jaenicke, 1993*].

where $p$ can be either the mass or number concentration at altitude $z$, $p_o$ is the value of $p$ at the earth's surface, and $p_B$ is the corresponding background value, $H_p$ is the scale-height of the aerosol. The aerosols are classified as in Table 5 and the figures show the smooth decrease (mass concentration) or increase/decrease (number concentration) through the boundary layer to the free troposphere. Parameters to be used with the above equations are shown in Table 13. The values here are approximate only, an indication of the likely error is shown by the poor convergence of the boundary layer polar and desert aerosols to the background level. Tables also exist for the altitude variation of aerosol optical properties. That given by D'Almeida et al. *[1991]* for the aerosol extinction at a wavelength of 0.5 µm is shown in Table 14. The atmosphere is here divided into 3–4 layers, of which the third is the free troposphere and the fourth the stratosphere (under background conditions). Surface classification is similar to that given in Table 5 and Table 6. Note that while the extinction values for the free troposphere and stratosphere are absolute, those for the boundary layer are normalized to 1 particle per $cm^3$.

**Table 13. Parameters of Vertical Aerosol Profiles** (Taken from *Jaenicke, 1993*)

| **Aerosol Type** | **Altitude** (m) | **Scale Height** $H_p$ | **Surface Value** $p_o$ | **Background Value** $p_B$ |
|---|---|---|---|---|
| | | *Aerosol Mass Concentration (p=m, in µg $m^{-3}$* | | |
| Ocean | iii. 2400 | 900 | | |
| Remote Continental | iv. 2400 | 730 | | |
| Desert | v. 6000 | 2000 | | |
| Polar | vi. 6000 | 30,000 | | |
| Background | vii. Tropopause | ∞ | | |

*The parameters are explained in Eq. [21]. Replace the general term $p$ by $m$ or $n$ to get mass or number concentration, respectively:

$$p = p_o\left\{\exp\left(\frac{-z}{|H_p|}\right) + \left(\frac{p_a}{p_B}\right)\right\}; \quad H_p \neq 0; y = \frac{H_p}{|H_p|} \qquad [23]$$

** The order of the $H_p$ values corresponds to the order of the $n_o$ values. The minus sign is intended.

**Table 14. Vertical Distribution of Atmospheric Aerosol in 3 or 4 Layers: Aerosol Concentrations Given as Extinction Coefficients for the Wavelength 0.500 μm** (Taken from *D'Almeida et al., 1991*)

| **Aerosol Type** | **1. Layer** | **2. Layer** | **3. Layer (Trop. Backgr.)** | **4. Layer (Stratosph.)** |
|---|---|---|---|---|
| Clean Continental | 0–2 km<br>$\sigma_e(h) = \sigma_{eo}$<br>(1.263E–5)* | | 2–12 km<br><br>(0.0020) | 12–35 km<br><br>(2.174E–4) |
| Average Continental | 0–2 km<br>$\sigma_e(h) = \sigma_{eo}$<br>(1.113E–5)* | | 2–12 km<br><br>(0.0020) | 12–35 km<br><br>(2.174E–4) |
| Desert (Wintertime) | 0–3 km<br>(3.032E–4)* | | 3–12 km<br>(0.0020) | 12–35 km<br>(2.174E–4) |
| Desert (Summertime) | 0–2km<br>(4.904E–4)* | | 3–12 km<br>(0.0020) | 12–35 km<br>(2.174E–4) |
| Urban | 0–2km<br>$\sigma_e(h) = \sigma_{eo}$<br>(7.277E–6)* | | 2–12 km<br><br>(0.0020) | 12–35 km<br><br>(2.174E–4) |
| Clean Maritime | 0–3km<br>$\sigma_e(h) = \sigma_{eo}e^{-h/z}$<br>($\sigma_{eo}$=2.054E–4)*<br>Z=1 km | | 3–12 km<br>(0.0020) | 12–35 km<br>(2.174E–4) |
| Maritime Mineral | 0–3 km<br>$\sigma_e(h) = \sigma_{eo}e^{-h/z}$<br>($\sigma_{eo}(h)$=2.054E–4)*<br>Z=1 km | 3–4.5 km<br>(5.71E–4)* | 4.5–12 km<br>(0.0020 | 12–35 km<br>(2.174E–4) |
| Maritime Polluted | 0–3 km<br>$\sigma_e(h) = \sigma_{eo}e^{-h/z}$<br>($\sigma_{eo}$=4.334E–6)*<br>Z=1.4 km | | 3.5–12 km<br>(0.0020) | 12–35 km<br>(2.174E–4) |
| Arctic Aerosol | 0–3.5 km<br>$\sigma_e(h) = \sigma_{eo}e^{-h/z}$<br>($\sigma_{eo}$ = 3.963E–4)*<br>Z = 1.4 km | | 3.5–12 km<br>(0.0020) | 12–35 km<br>(2.174E–4) |
| Antarctic Aerosol | 0–10 km<br>$\sigma_e(h) = \sigma_{eo}e^{-h/z}$ | | 10–12 km<br>(0.0020) | 12–35 km<br>(2.174E–4) |
| ($\sigma_{eo}$ = 8.809E–5)* Z = 3.5 | | | | |

The data indexed with (*) represent normalized (to N = 1 $cm^{-3}$) values of the aerosol type in question. $\sigma_{eo}$ and $\sigma_e(h)$ give the extinction coefficient in $km^{-1}$ for 10 m above ground and at a height h. The quantity Z means the scale height for an exponential profile type.

### 3.2.2 Continental and Maritime Background

Dust concentrations from the arid regions of the earth have their maximum influence on the free troposphere between latitudes 20°N and 40°N and, to a lesser extent, between 20°S and 40°S. *Tegen and*

*Fung [1994]* have modeled the mean vertical concentration for four size classes of dust aerosol, their modeled distribution are shown as a function of latitude in Figure 24. These plots are significant in showing how the smaller particles (< 1 μm in size) become quite widely distributed in both altitude and latitude, whereas the coarser sand particles do not leave the boundary layer of the source region.

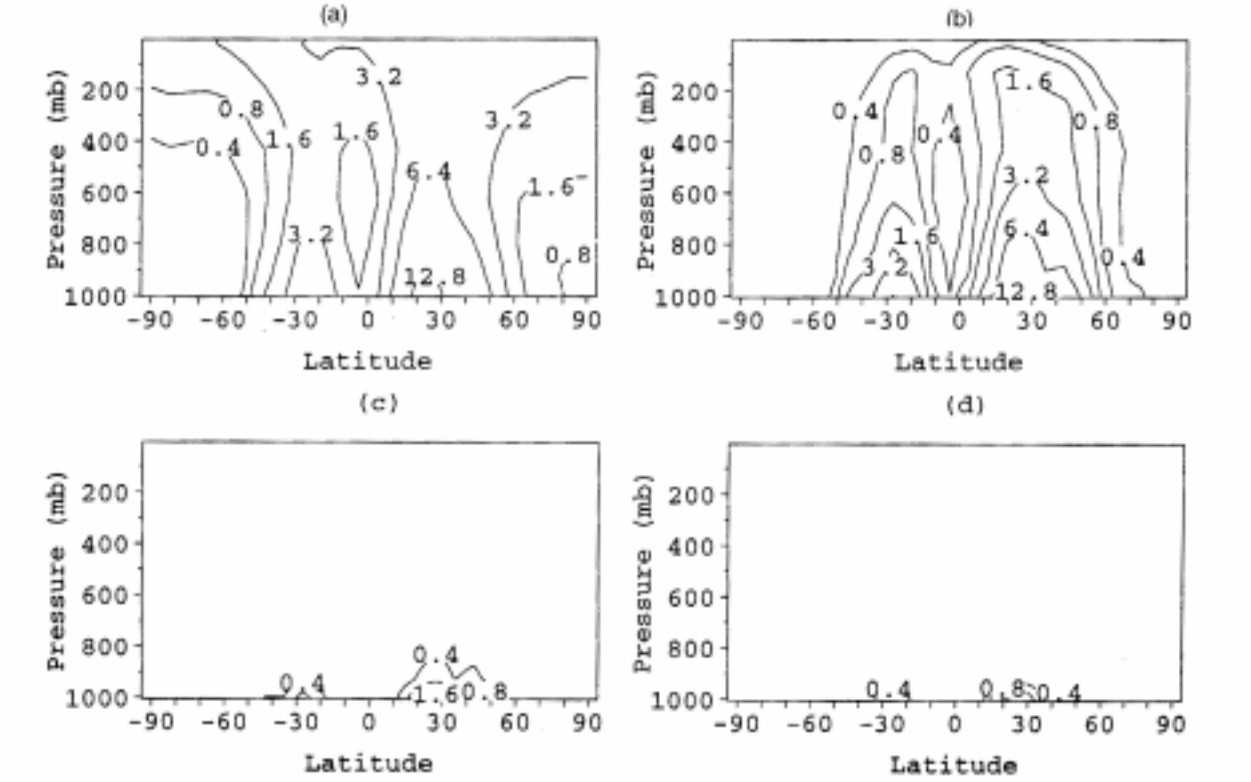


**Figure 24. Vertical distribution of dust concentration for the four different size classes (averaged over all longitudes) in units of microgram dust per kilogram air: (a) Clay [<1 μm], (b) small silt [1–10 μm], (c) large silt [10–25 μm], (d) sand [>25 μm].** [Taken from *Tegun and Fung, 1994*.]

Figure 25 shows examples of *in situ* measured size distributions for a continental aerosol as a function of season, and altitude in the free troposphere. The data, taken by balloon-borne dust sonde, show long-term averages for Laramie, Wyoming (Lat., Long.) from *Hofmann [1993]*. The solid points are the average measured cumulative column size distributions which are used to derive the differential bimodal log-normal distributions (the dashed curves). The latter are then reintegrated to give calculated integral distributions (the full curves) and to calculate the column mass loading and optical depth. Coincidence of the integral curves and the measured points indicates the goodness of fit. Log-normal parameters for each size mode of the distribution and calculated column mass are given in Table 15. Bimodal log-normal size distributions have been fitted to the data, the parameters for the fitted function being given in Table 15. Also listed in this table are the total mass concentrations for these distributions. [Note: (1) Concentrations are expressed in terms of total column content per unit surface area; (2) The higher mass concentrations in summer due to increase convective activity, particularly in the 5–10 km altitude range.]

*In situ* measurements over the remote oceans are uncommon. One such data set for the Pacific basin has been presented by Pueschel et al. (1994). Table 16 shows the parameters for fitted bimodal log normal size distributions. Concentrations in Table 16 are given in terms of volume as opposed to the column content given in Table 15 for continental aerosols. Values given in Table 16 are means over the altitude range. Figure 26 shows the variation in elemental composition of the aerosols for the same data set as in Table 16 as a function of altitude. The lowest altitude range (below 8000 ft ~ 2.4 km) is dominated by sodium and chlorine (as sea-salt). As the altitude increases, these two components become increasingly less significant and aerosols containing sulfur, partially or totally, become dominant.

The liquid nature of the aerosol at these levels and locations indicates that sulfuric acid is the principal constituent.

Solar occultation data from the SAGE II satellite instrument have been used to study the global-scale behavior of the extinction due to upper tropospheric aerosols and to use these as a basis for the calculations of the aerosol mass loading and effective radius. Figure 27 shows the seasonal and latitudinal dependence of the background aerosol determined from this data set for an altitude of 7.5 km [*Kent et al., 1995*]. The main features are (1) strong latitudinal gradients in mass density; (2) maximum concentrations in March–May in the northern hemisphere; (3) hemispheric asymmetric in both aerosol concentrations and effective radius; and (4) seasonal oscillations in both aerosol concentration and effective radius.

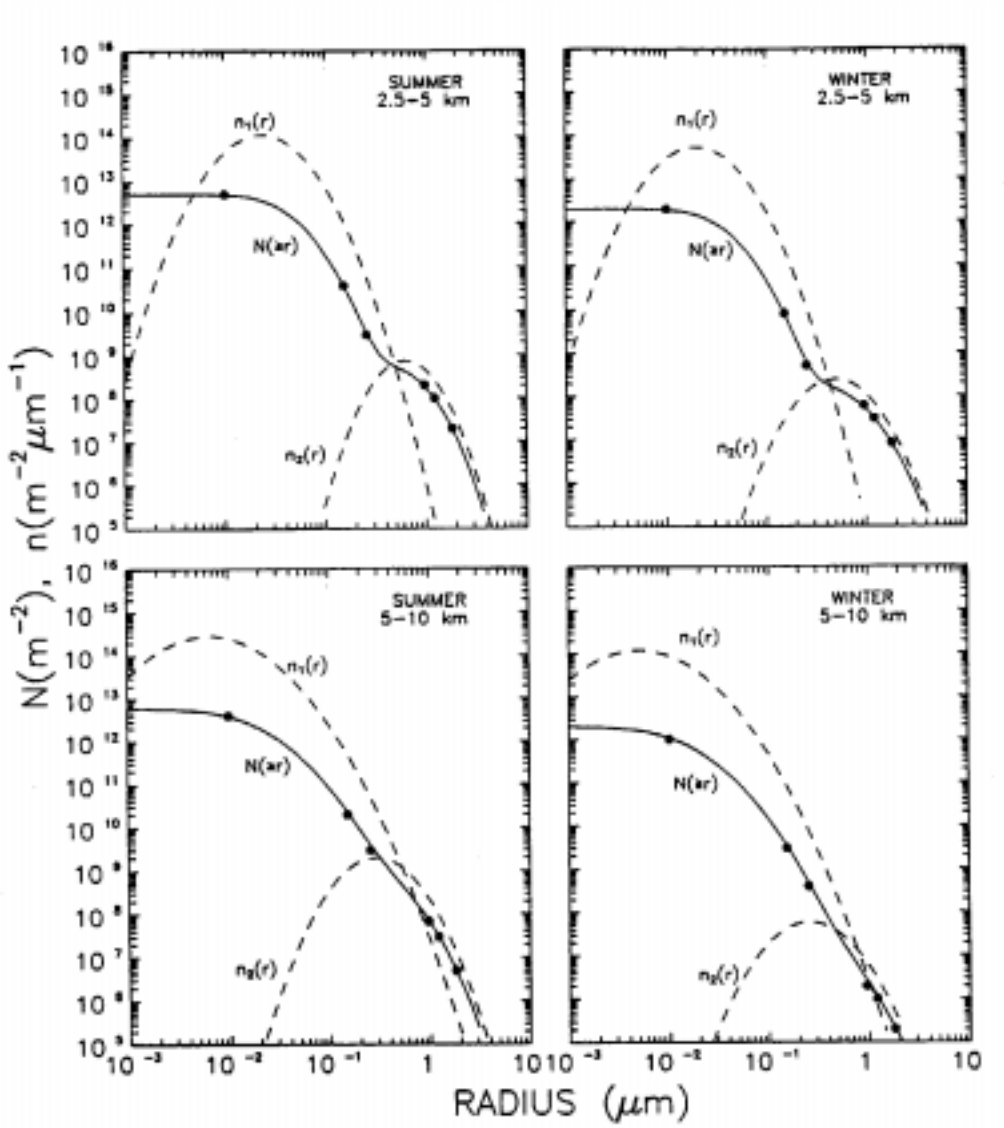


**Figure 25. Long-term average bimodal log normal tropospheric aerosol particle size distributions at Laramie for two altitude intervals during summer (left) and winter (right).** [From *Hofmann, 1993.*]

**Table 15. Tropospheric Aerosol Mean Seasonal Size Distribution and Mass**
(Taken From *Hofmann, 1993*)

| **Altitude** (km) | **Season** | **Mode** | $N_r$ ($m^2$) | $r_r$ (μm) | $\sigma_1$ | $m_r$ (mg $m^{-2}$) | $m_1+m_2$ (mg $m^{-2}$) |
|---|---|---|---|---|---|---|---|
| 2.5–5 | Summer | 1 | 5E12 | 0.033 | 1.85 | 6.5 | |
| | | 2 | 6E8 | 0.76 | 1.60 | 4.0 | 10.5 |
| | Winter | 1 | 2E12 | 0.020 | 2.10 | 1.5 | |
| | | 2 | 2E8 | 0.67 | 1.76 | 1.4 | 2.9 |
| 5–10 | Summer | 1 | 4E12 | 0.020 | 2.10 | 3.0 | |
| | | 2 | 1E9 | 0.40 | 1.79 | 2.0 | 5.0 |
| | Winter | 1 | 2E12 | 0.010 | 2.40 | 0.60 | |
| | | 2 | 3E7 | 0.38 | 1.88 | 0.07 | 0.67 |
| 2.5–10 | Summer | 1 | | | | 9.5 | |
| | | 2 | | | | 6.0 | 15.5 |
| | Winter | 1 | | | | 2.1 | |
| | | 2 | | | | 1.5 | 3.6 |

$N_r$, $r_r$, and $\sigma_1$ are the total column number, mode radius, and mode width, respectively, of a bimodal log normal size distribution: $\rho_\sigma$ = 1.65 g $cm^{-3}$ assumed. Read 5E12 as 5 x $10^{12}$, for example.

**Table 16. Free Tropospheric Size Distribution parameter for the Pacific Basin**
(Taken from *Pueschel et al., 1994*)

| | **Mode 1** | **Mode 2** |
|---|---|---|
| $N_o$ | 19.5 ± 19.9 $cm^{-3}$ | 0.6 ± 0.8 $cm^{-3}$ |
| $r_g$ | 0.06 ± 0.01 μm | 0.2 ± 0.1 μm |
| $\sigma_g$ | 1.5 ± 0.1 | 1.4 ± 0.1 |
| $r_{eff}$ | 0.08 μm | 0.17 μm |

Parameters shown are for a bimodal log-normal size distribution. $r_{eff}$ is the effective radius for each mode.

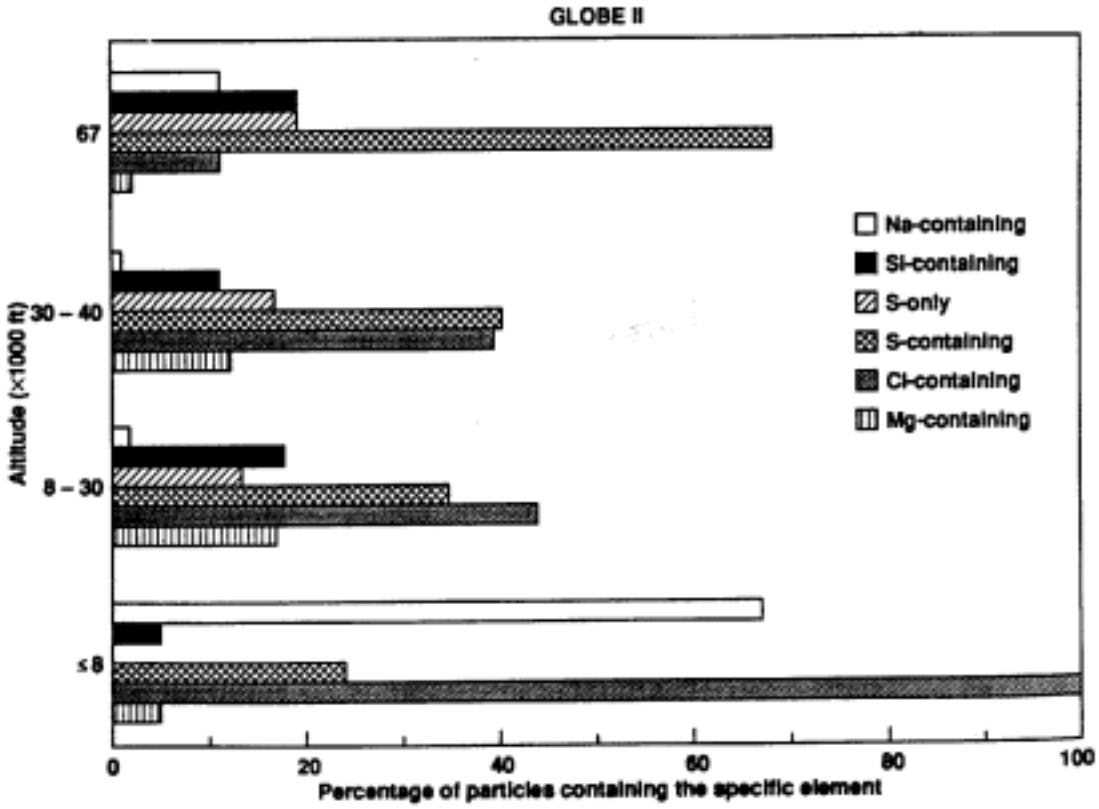


**Figure 26. Elemental composition of aerosols over the Pacific Basin as a function of altitude.** [From *Pueschel et al., 1994.*]

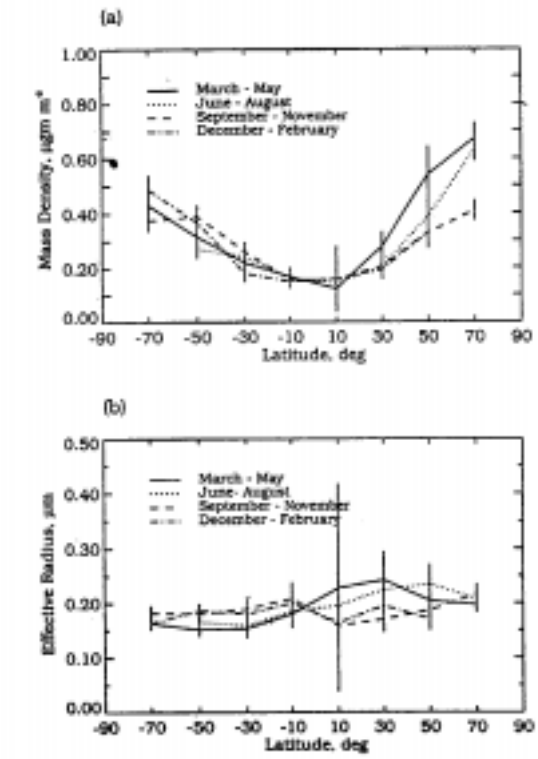


**Figure 27. Seasonal variations in zonally averaged background aerosol characteristics at an altitude of 7.5 km: (a) mass density; (b) effective radius** [from *Kent et al., 1995*].

### 3.2.3 Desert Dust Streams

No tables.

### 3.2.4 Combustion Products

No tables relating to long distance transport, but see Section 3.1.7.

### 3.2.5 Arctic Haze

No tables.

### 3.2.6 Volcanic Contamination, Stratospheric/Tropospheric Exchange

Following volcanic injection of aerosols and aerosol precursor gases into the stratosphere, the aerosol reaches a peak concentration about three months after the volcanic eruption. This is followed by a quasi-exponential decay with a time constant of the order of 12 months *[Yue et al., 1991]*. The aerosol removed from the stratosphere appears in the upper troposphere at latitudes poleward of about 30° latitude. Maximum aerosol concentrations are observed in local Spring down to an altitude of 3 km or 4 km below the tropopause. Table 17 shows a listing of aerosol mass loading estimates obtained from SAGE II for the upper troposphere and stratosphere *[Kent et al., 1995]*. In March 1995, during the decay phase of the 1982 El Chichon eruption, approximately 15% of the total mass of volcanic aerosol remaining lay in the upper troposphere above 6-km altitude. Assuming that the 1985 background was similar to that in 1989–1991, it follows that in March 1995, almost 30% of the aerosol mass loading of the upper free troposphere was volcanic in origin. Further information concerning the base altitude for the volcanic layer and the effective descent rate of the aerosol from the tropopause to its base level is given in Table 18 *[Kent et al., 1995]*.

**Table 17. Annually Smoothed Mass Loading** [From *Kernt et al., 1995*]

| **Aerosol Class** | **Mass Loading, $10^{-3}$ kg** | |
|---|---|---|
| Tropospheric Baseline (1989–1991, 6 km, tropopause) | | |
| Global | 820 | (20) |
| Southern Hemisphere | 390 | (10) |
| Northern Hemisphere | 430 | (10) |
| Stratospheric Baseline (1989–1991) | 1220 | (10) |
| Tropospheric Volcanic (March 1985) | 320 | (10) |
| Stratospheric Volcanic (March 1985) | 1930 | (10) |

Values shown in parentheses are the statistical uncertainties.

**Table 18. Tropospheric Volcanic Data Intercomparisons** [From *Kent et al., 1995*]

| **Quantity** | **SAGE II Value** | **Comparison Data** |
|---|---|---|
| *Volcanic Aerosol Base Altitude* | | |
| 1983–1984: 40°N | 7–8 km | 6 km $CO_2$ lidar *[Post, 1986]* |
| *Upper Tropospheric Aerosol Effective Descent Rate* | | |
| 1983–1984: 40°N | 1.5 km/month (1984–1985) | 3.5–4 km month $CO_2$ lidar *[Post, 1986]* |
| 1991: 40°N | 1.5 km/month (1984–1985) | 1.5 km/month $CO_2$ lidar *[Post et al., 1992]* |
| *Upper Tropospheric Aerosol Effective Residence Time* | | |
| | 2 months | 3 weeks–4 months *[Jaenicke, 1988]* |

## 3.3 Stratosphere and Mesosphere

### 3.3.1 Introduction

The three main categories of stratospheric aerosols are background, volcanic, and PSCs. Table 19 lists the principal characteristics of these, together with those of two other less common categories. Meteoric dust and rocket exhaust can be found throughout the stratosphere and mesosphere.

**Table 19. Characteristics of Stratospheric Aerosols** *[Johnson, 1993; Turco, 1992]*

| Particle Type | Sulfate Aerosol | Type-I PSC | Type-II PSC | Meteoric Dust | Rocket Exhaust |
|---|---|---|---|---|---|
| Physical State | Liquid or Slurry with Crystals | Solid Nitric Acid Trihydrate, Solid Solutions | Solid Crystal, Hexagonal or Cubic Basis | Solid Granular Irregular or Spherical | Solid Spheres or Irregular Surface Ablated Debris |
| Particle Radius (μm) | 0.01–0.5, Amb. 0.01–10, Volc. | 0.3–3 | 1–100 | 1–100, Micro-Meteorites 0.01–0.1, Smoke | 0.1–10 |
| Number (# $cm^{-3}$) | ~1–10 | ~0.1–10 | <<1 | $10^{-6}$, 100 μm $10^{-3}$, 1 μm | $10^{-4}$, 10 μm $10^{-2}$, 1 μm |
| Principal Composition | $H_2SO_4/H_2O$ ~70%/30% | $HNO_3/H_2O$ ~50%/50% | $H_2O$ | $SiO_2$, Fe, Ni, Mg; C | $Al_2O_3$ |
| Trace Composition | $NH_4$+, $NO_3$ | HCl $SO_4^{2-}$ | $HNO_3$, HCl | $SO_4^{2-}$ (Surface) | $Cl^-$, $SO_4^{2-}$ (Surface) |
| Physical Characteristics | Dust Inclusions, in Solution | Equidimensional Crystalline or Droplets | Elongated Crystals w/Polycrystalline Structure | Irregular Mineral Grains, Grain Defects | Homogeneous Composition; Smooth Spheres |
| Distribution | Global, Amb. Region, Volc, 12–35 km alt. | Polar Winter 14–24 km alt. | Polar Winter 14–24 km alt. | ~Global >12 km alt. | Global >12 km alt. |
| Residence Time | ~1–2 yr. Amb. ~1–3 yr. Volc. | ~1 Day to Weeks | ~ Hours | <1 mo. (Micro-Meteorites) 1–10 yr. (Meteoritic Smoke) | <1 yr. |

### 3.3.2 Intervolcanic Background

The aerosol content of the stratosphere has varied by almost as much as two orders of magnitude during the past 20 years (1975–1995). The major cause of the variation has been input from volcanic eruptions whose effect can last for several years in the case of a major eruption. Two such major eruptions were that of El Chichon in April 1982 and Pinatubo in June 1991. Although many other eruptions have occurred, the periods prior to those from large eruptions (1979–1981 and 1988–1990) are generally regarded as more typical of so-called background conditions. Under these conditions, the aerosol should primarily be the result of oxidation and hydrolysis of naturally and anthropogenically produced tropospheric precursor gases, such as $SO_2$, $H_2S$, and COS, which are transported upwards into the stratosphere. Characterization of the background is difficult because of the possibility of contamination by volcanic input *[Thomeson et al., 1997]*; it has also been suggested *[Hofmann, 1990 and 1991]*; that the background may be increasing due to anthropogenic influence.

Figure 28 shows typical measured aerosol size distributions for a background and a volcanic aerosol, measured respectively in July 1981 and February 1983 *[Rosen and Hofmann, 1986]*. The experimental data points have been fitted to a combination of a log normal (for the smaller particles) and a cubic spline (for the larger particles) fit. Each curve was constructed for tensions of 0.1, 3, and 30 as marked. Note that there is very little difference between tensions 0.1 and 3, but at a tension value of 30 the curve has developed more structure than might be considered consistent with the number of data points defining the curve. The formula used and the best-fit parameters are give in Table 20.

SAGE I and SAGE II data have been used to develop altitude dependent models for the 1.0 μm extinction due to the background aerosol *[McCormick and Wang, 1991]*. These are shown as annual mean profiles for 1979 and 1989 in Figure 29 where the altitude is referenced to the tropopause. Data for the two years are similar but not identical and are shown in the form of a third-order polynomial.

$$\log_{10}(\beta) = a + bZ + cZ^2 + dZ^3 \qquad [24]$$

where $\beta$ is the 1.0-micrometer aerosol extinction at altitude $Z$ measured from the tropopause and a, b, c, and d are coefficients to be determined empirically from a fit to the SAGE I/SAGE II data sets.

Values for the coefficients in this expression are shown in Table 21 which also shows those for individual seasons.

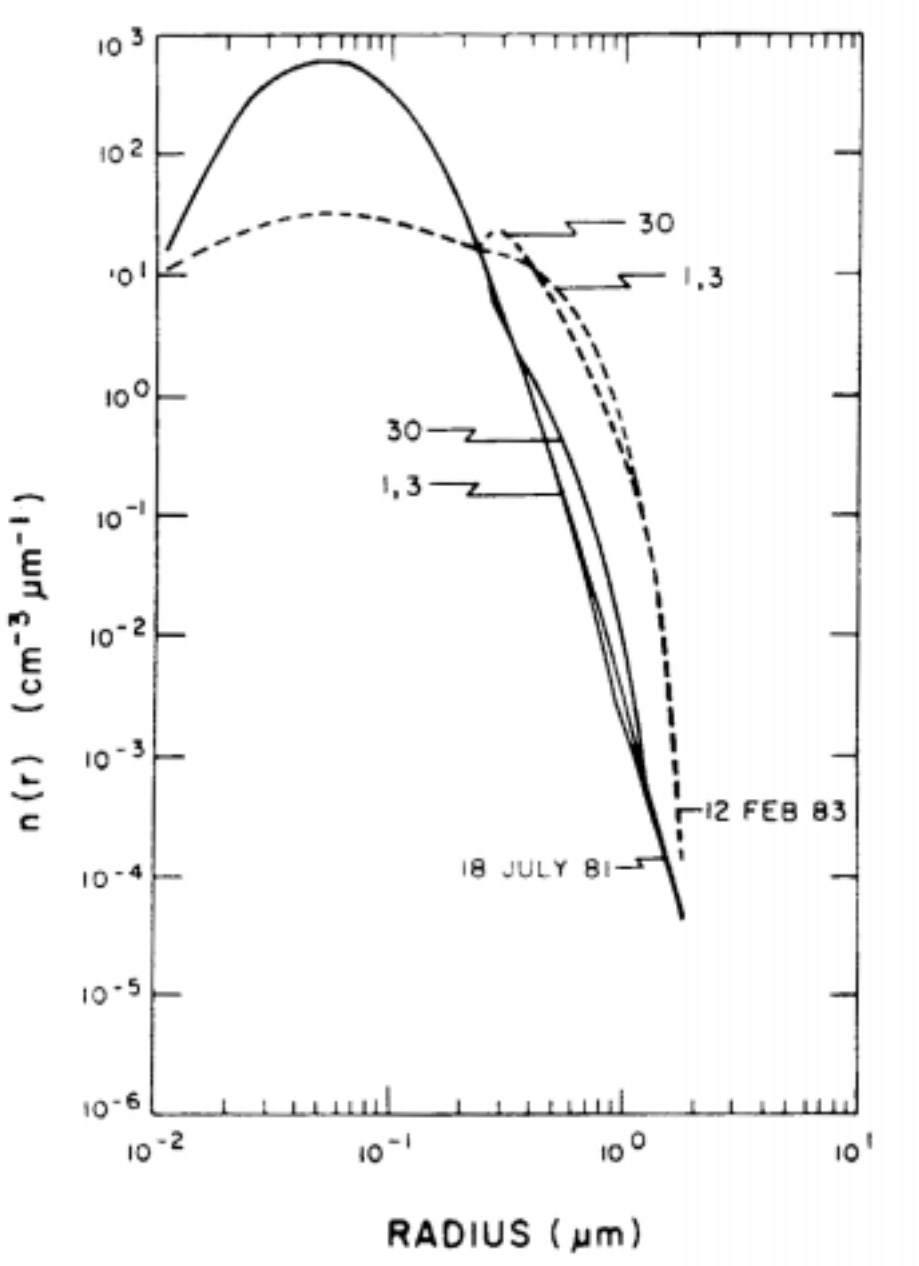


**Figure 28. Log-normal cubic spline model size distribution for two extreme conditions at the peak of the stratospheric aerosol layer.** [From *Rosen and Hofmann, 1986*.]

**Table 20. Parameters for Size Distribution in Figure 28**
(Taken From *Rosen and Hofmann, 1986*)

$$n(r) = N_0(r\sqrt{2\pi}\ \ln\sigma_g)^{-1} \exp[-0.5\ln(r/r_g)^2] \quad r < 0.25$$

$$N(r) = \exp(a + br + cr^2 + dr^3)$$

| Radius Range (μm) | Size Distribution Parameter Type | Parameter Value For | |
|---|---|---|---|
| | | 18 July 1981 | 12 February 1983 |
| 0–0.25 | $N_0$<br>$r_g$<br>$\sigma_g$ | 54.66<br>0.071<br>1.77 | 10.7<br>0.214<br>3.13 |
| 0.25–1.2 | a<br>b<br>c<br>d | 5.215603<br>–26.254624<br>18.345978<br>–5.193810 | 2.145304<br>–1.354558<br>4.095808<br>0.613355 |
| 1.2–1.8 | a<br>b<br>c<br>d | -2.061941 –<br>8.030920<br>3.057170 -<br>.903952 | 19.878082 –<br>45.234379<br>32.234379 –<br>9.339334 |

N(r) is the integral size distribution. n(r) is the differential size distribution

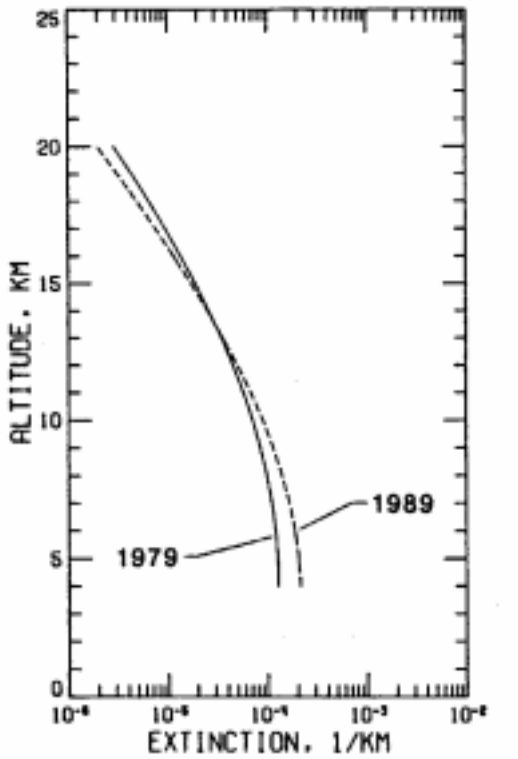


**Figure 29. Global-averaged, annual mean profiles of 1.0-micrometer aerosol extinction from the 1979 and 1989 reference models. Altitudes are referenced to the height above the tropopause.** [From McCormick et al., 1993.]

**Table 21. Coefficients of the Polynomial Derived from SAGE I 1.0-Micrometer Aerosol Extinction**

**(a) (March 1979 to February 1980)**

| Coefficients | | | | |
|---|---|---|---|---|
| **Period*** | **a** | **b** | **c** | **d** |
| MAM | 4.10 | 7.14E-02 | -7.93E-03 | 3.81E-05 |
| JJA | 4.28 | 1.33E-01 | -1.43E-02 | 2.27E-04 |
| SON | 4.12 | 9.90E-02 | -1.18E-02 | 1.69E-04 |
| DJF | 3.71 | -4.38E-04 | -4.43E03 | -1.32E-05 |
| Yearly Mean | -4.05 | 7.58E-02 | -9.61E-03 | 1.05E-04 |

Mean values for the 1.0 μm extinction averaged over a time period of ten years, as opposed to the surface background have been produced by *Hitchman et al., [1994]*. Long term averages of this kind may be regarded as more typical of the behavior of the stratosphere aerosol layer than the background value. These are shown in Table 22 where they are divided by latitude band, and the altitude is given absolutely rather than relative to the tropopause. This time period covers several volcanic eruptions and the extinction values are somewhat higher than those shown in Figure 29. SAGE I/II and SAM II data is shown in the integrated form of stratospheric aerosol optical depth in Figure 30 *[Hitchman et al., 1994]*. The background periods, 1979–1980 and 1988–1990, are clearly visible as are the various volcanic injections. The logarithm of optical depth is shaded for values less than –2.9 to greater than –1.7, with color change at interval 0.1. Letters indicate specific volcanic eruptions (see list below). The dominant phase of the QBO is indicated below the time line, where W (E) indicates westerly (easterly) shear. SAM II data in the northern polar latitudes are unavailable after late 1989 because of gradual orbital precession.

**(b). (March 1989 to February 1990)**

| Coefficients | | | | |
|---|---|---|---|---|
| **Period*** | **a** | **b** | **c** | **d** |
| MAM | -3.80 | 7.32E-02 | -9.85E-03 | 7.56E-05 |
| JJA | -3.97 | 1.30E-01 | -1.60E-02 | 2.55E-04 |
| SON | -3.80 | 9.35E-02 | -1.52E-02 | 2.86E-04 |
| DJF | -3.74 | -5.27E-02 | -1.01E-02 | 1.35E-04 |
| Yearly Mean | -3.83 | 8.73E-02 | -1.28E-02 | 1.88E-04 |

* MAM (March, April, May)
JJA (June, July, August)
SON (September, October, November)
DJF (December, January, February)

**Table 22. Decadal Mean Values of Aerosol Extinction at 1 μm, in Units of $10^{-4}$km$^{-1}$, Given Every 10° From 80°S to 80°N and Every 2 km from 8 km (or the Tropopause) to 34 km Altitude (From *Hitchman et al., 1994*)**

| | 80°S | 70°S | 60°S | 50°S | 40°S | 30°S | 20°S | 10°S | 0° | 10°N | 20°N | 30°N | 40°N | 50°N | 60°N | 70°N | 80°N |
|---|---|---|---|---|---|---|---|---|---|---|---|---|---|---|---|---|---|
| 34 | .01 | .01 | .02 | .02 | .02 | .02 | .03 | .04 | .04 | .03 | .03 | .02 | .02 | .02 | .02 | .01 | .01 |
| 32 | .01 | .02 | .02 | .03 | .03 | .04 | .06 | .09 | .09 | .07 | .06 | .04 | .03 | .03 | .02 | .02 | .02 |
| 30 | .05 | .05 | .04 | .04 | .05 | .08 | .14 | .22 | .24 | .20 | .14 | .08 | .05 | .05 | .03 | .05 | .06 |
| 28 | .05 | .08 | .07 | .07 | .12 | .18 | .34 | .56 | .66 | .57 | .37 | .18 | .11 | .09 | .06 | .08 | .10 |
| 26 | .08 | .13 | .14 | .14 | .29 | .42 | .74 | 1.3 | 1.5 | 1.3 | .80 | .42 | .26 | .21 | .13 | .16 | .16 |
| 24 | .15 | .25 | .28 | .28 | .66 | .87 | 1.5 | 2.6 | 3.1 | 2.5 | 1.5 | .88 | .60 | .47 | .33 | .34 | .28 |
| 22 | .31 | .47 | .56 | .56 | 1.3 | 1.7 | 2.6 | 4.3 | 5.5 | 4.7 | 3.0 | 1.8 | 1.3 | 1.0 | .76 | .70 | .54 |
| 20 | .62 | .91 | 1.1 | 1.1 | 2.5 | 3.1 | 4.0 | 5.5 | 8.1 | 6.7 | 4.4 | 3.2 | 2.6 | 2.1 | 1.7 | 1.6 | 1.2 |
| 18 | 1.0 | 1.7 | 2.0 | 2.0 | 3.7 | 3.9 | 3.3 | 3.2 | 2.9 | 2.8 | 3.2 | 4.1 | 4.1 | 3.6 | 3.1 | 2.6 | 2.4 |
| 16 | 2.1 | 2.8 | 3.1 | 3.1 | 3.8 | 2.8 | 2.1 | 2.1 | 2.7 | 2.5 | 2.3 | 3.0 | 4.4 | 4.8 | 4.1 | 4.4 | 4.1 |
| 14 | 4.8 | 4.5 | 3.9 | 3.9 | 3.3 | 2.5 | | | | | 1.7 | 2.8 | 4.2 | 5.3 | 4.6 | 5.8 | 5.4 |
| 12 | 5.6 | 5.3 | 4.6 | 4.6 | 3.8 | 2.6 | | | | | | 3.0 | 5.0 | 6.0 | 5.7 | 7.1 | 6.6 |
| 10 | 5.3 | 5.6 | 5.7 | 5.7 | 5.1 | 3.4 | | | | | | 4.0 | 7.1 | 7.7 | 8.6 | 7.9 | 7.8 |
| 8 | 3.9 | 5.0 | 5.1 | 5.1 | 6.7 | | | | | | | | 6.0 | 5.8 | 6.6 | 5.9 | 6.1 |

Both remote sensing and *in situ* data have been used to provide information about stratospheric aerosol surface area and mass loading. Figure 31 shows a plot of the aerosol surface density derived from the data in Table 22. The altitude-dependent conversion formula used is

$$S(y, z) = \{0.8\left(\frac{z - z_T(y)}{20}\right) + 0.7\}\, x\, 10^4\, x\, E_o(y, z) \qquad [25]$$

where $Z_T$ is the lowest altitude that is not blank, $Z$ is the actual altitude (in km), $S(y,z)$ is the surface area, and $E_o$ is the 1 μm extinction.

Mass mixing ratios as a function of altitude are shown in Figure 32 *{Hofmann, 1990]*. Aerosol surface areas, as a function of time and latitude, is shown in Figure 33 for four different altitudes. These plots have been derived from SAGE II data using a prescribed component analysis to convert extinction to surface area (*Thomason et al., 1997*). The time period encompassed by these plots included several volcanic eruptions, as well as times of low background level.

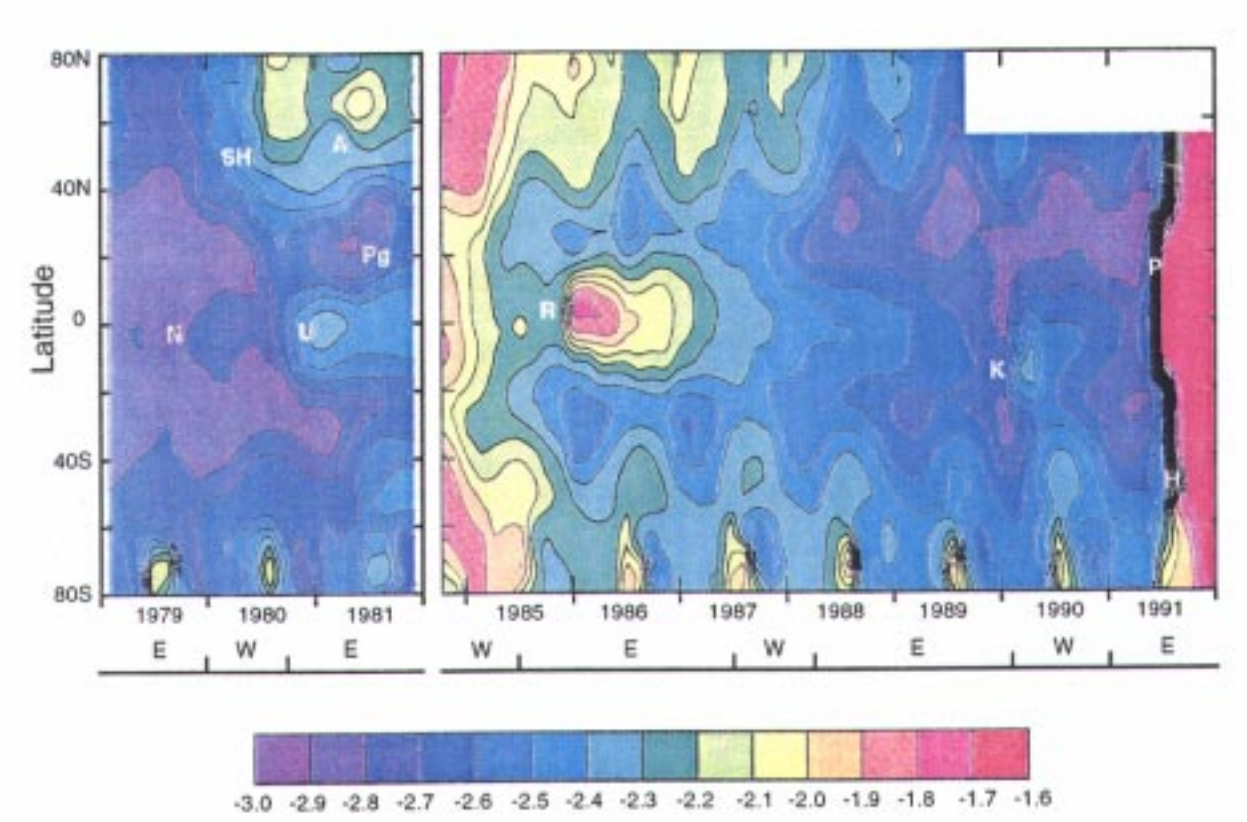


**Figure 30. Time-latitude section of stratospheric aerosol optical depth at 1 μm, blending SAGE I and II and SAM II data.** [From *Hitchman et al., 1994*.]

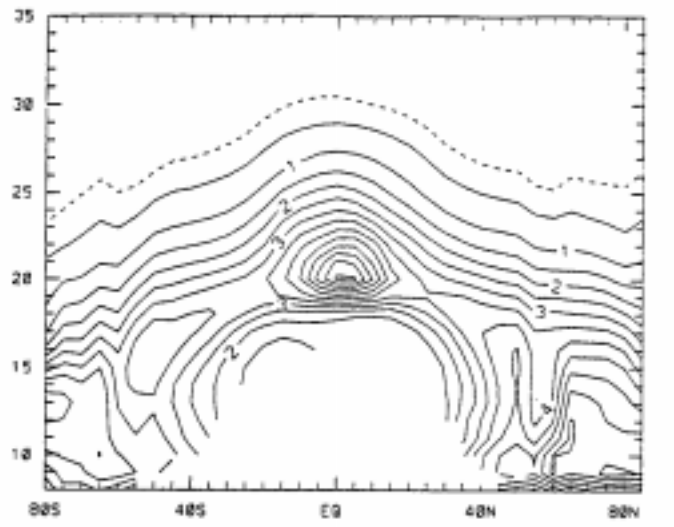


**Figure 31. Aerosol surface area density in square microns per cubic centimeter, using the conversion factor given by Eq. [24] and data in Table 22** [From *Hitchman et al., 1994*].

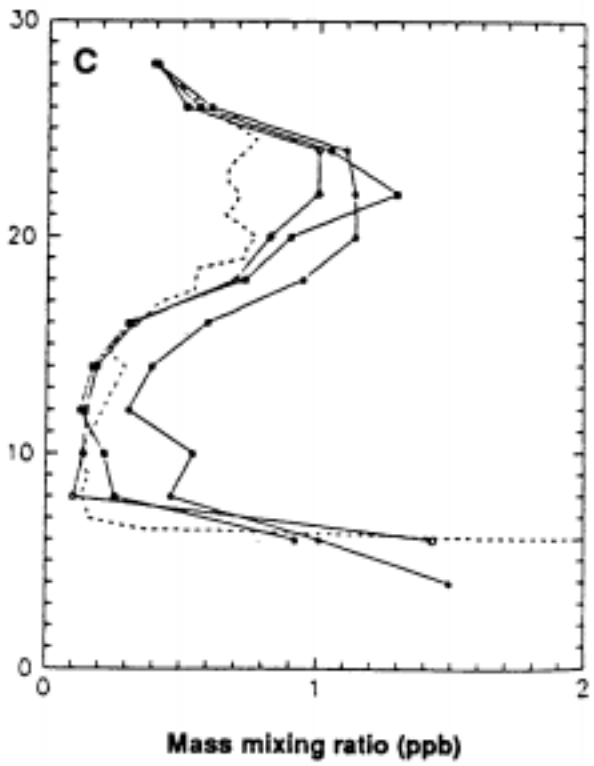


**Figure 32. Background mass mixing ratio as a function of altitude** [From *Hofmann, 1990.*]

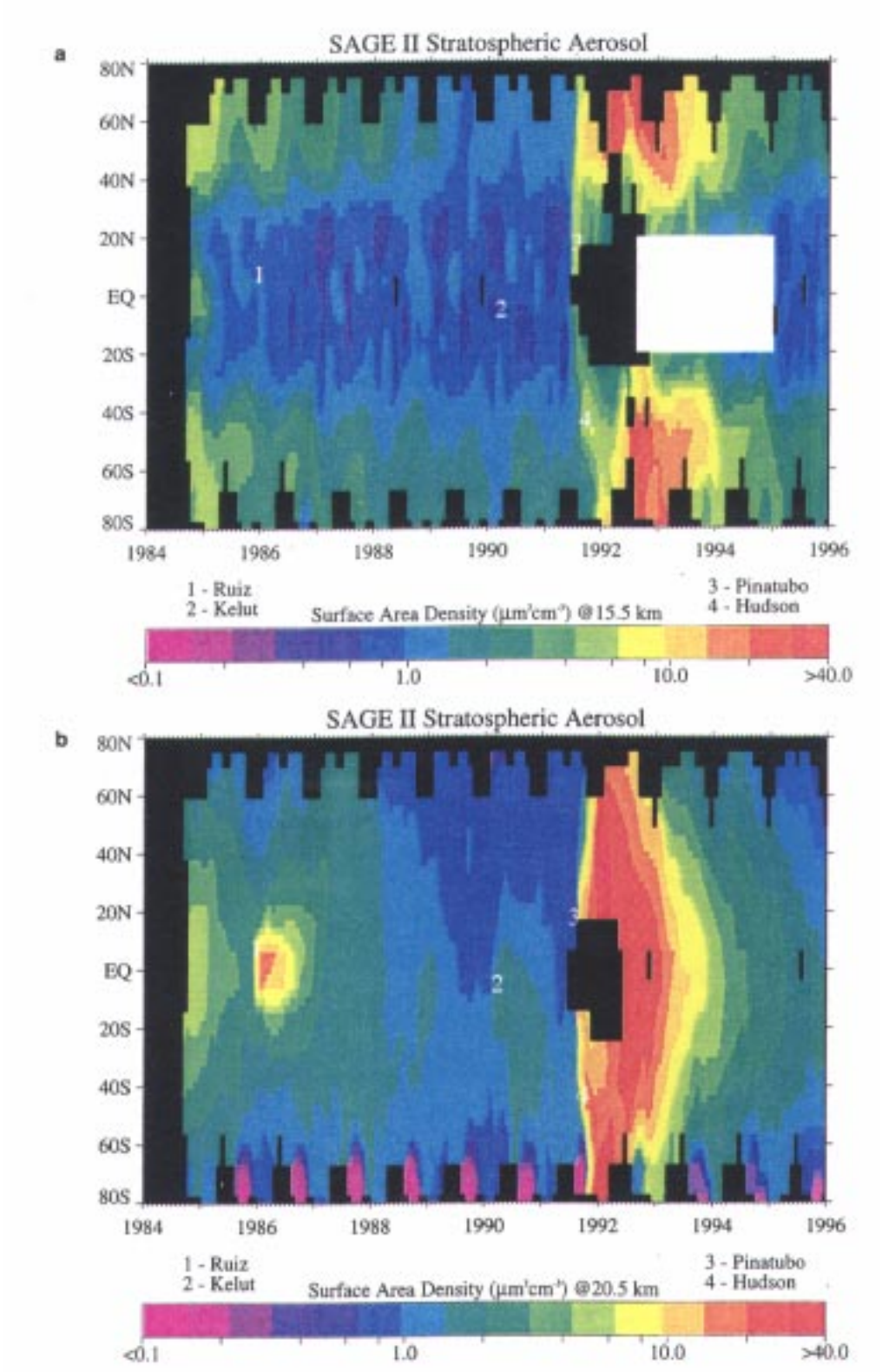


**Figure 33. Aerosol surface area density as a function of time and latitude at the altitudes of (a) 15.5, (b) 20.5, (c) 25.5, (d) 30.5 km.** Black regions denote sections in which no data are available. White regions in Plate 1a denote sections for which cloud clearing is not currently available. The latitude and time of significant volcanic events are noted.

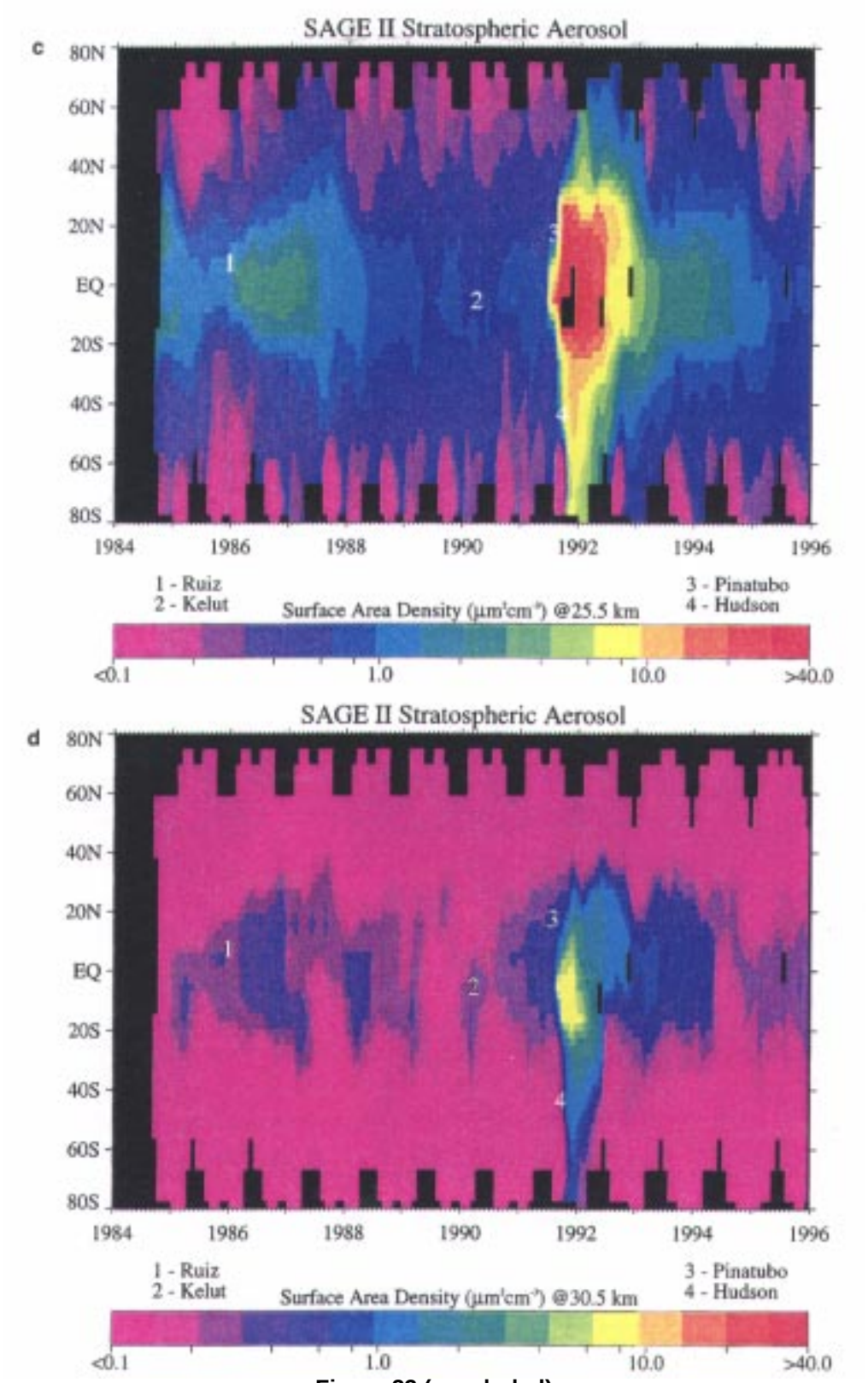


**Figure 33 (concluded)**

### 3.3.3 Volcanic

In Section 3.3.2, the eruption of El Chichon and Pinatubo were described as having the most significant effects on the stratosphere of any eruptions within the past 20 years. Variations of the stratospheric aerosol optical depth (at a wavelength of 0.5 μm) since 1850 are shown in Figure 34 *[Sata et al., 1993]*. The Pinatubo eruption is seen to be exceeded in its affect during this long period of time only by the eruption of Krakatoa in 1885. Table 23 shows the data in tabular form, divided by hemisphere and latitude band. Data for earlier years must be regarded as approximate only.

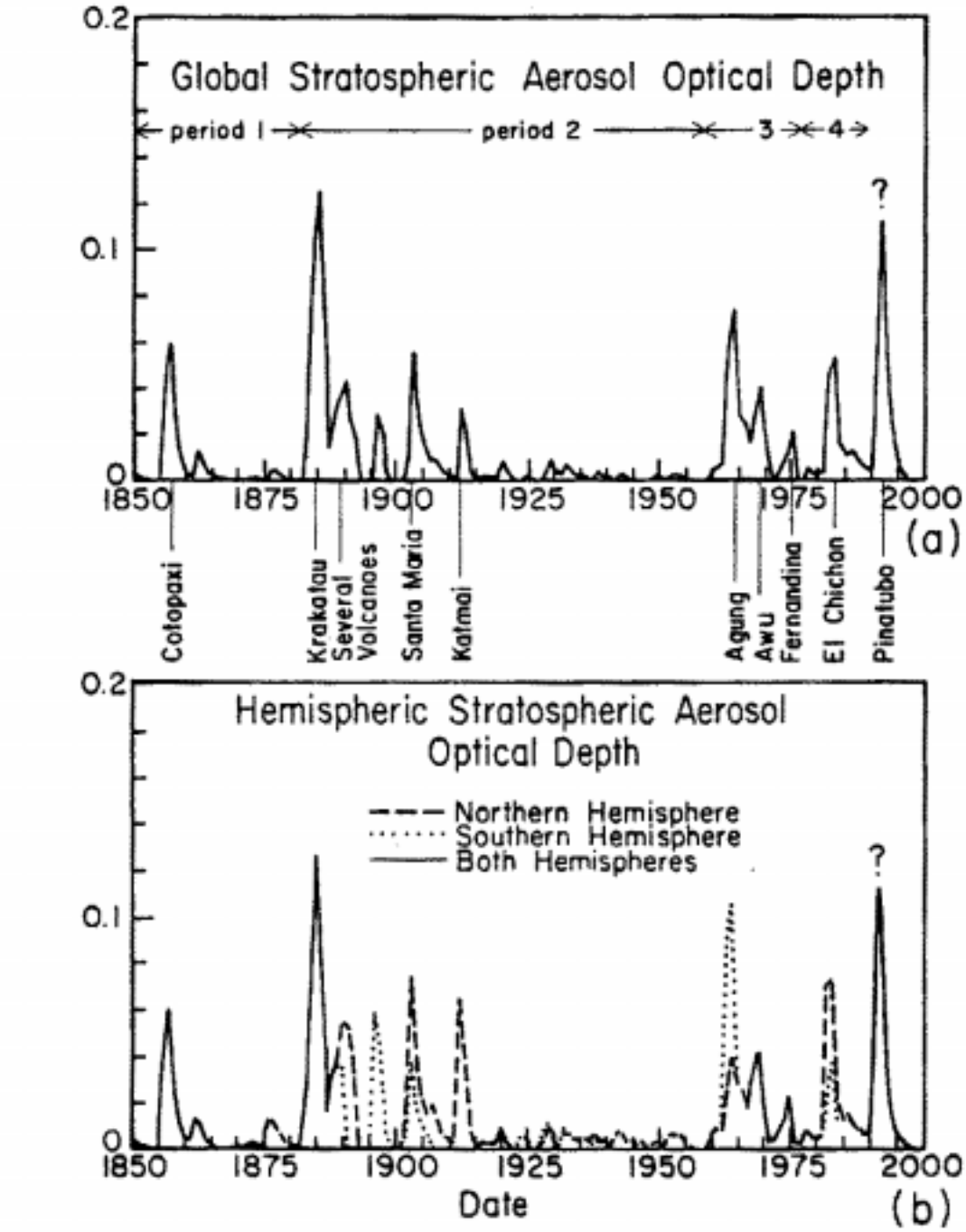


**Figure 34. Estimated stratospheric aerosol optical depth at λ = 0.55 μm: (a) global mean and (b) hemispheric means.** (From *Sato et al., 1993.*)

**Table 23. Estimated Annual Stratospheric Aerosol Optical Depths (Multiplied by 1000) at λ = 0.55 μm.** [From *Sato et al., 1993.*]

| Year | Global | NH | | SH | | Year | Global | NH | | SH | |
|---|---|---|---|---|---|---|---|---|---|---|---|
| | | 90°–30° | 30°–0° | 0°–30° | 30°–90° | | | 90°–30° | 30°–0° | 0°–30° | 30°–90° |
| 1850 | 3 | 3 | 3 | 3 | 3 | 1899 | 0 | 0 | 0 | 0 | 0 |
| 1851 | 2 | 2 | 2 | 2 | 2 | 1900 | 0 | 0 | 0 | 0 | 0 |
| 1852 | 1 | 1 | 1 | 1 | 1 | 1901 | 0 | 0 | 0 | 0 | 0 |
| 1853 | 0 | 0 | 0 | 0 | 0 | 1902 | 12 | 16 | 16 | 8 | 8 |
| 1854 | 0 | 0 | 0 | 0 | 0 | 1903 | 55 | 74 | 74 | 37 | 37 |
| 1855 | 0 | 0 | 0 | 0 | 0 | 1904 | 27 | 36 | 36 | 18 | 18 |
| 1856 | 39 | 39 | 39 | 39 | 39 | 1905 | 15 | 20 | 20 | 10 | 10 |
| 1857 | 60 | 60 | 60 | 60 | 60 | 1906 | 10 | 13 | 13 | 6 | 6 |
| 1858 | 26 | 26 | 26 | 26 | 26 | 1907 | 10 | 39 | 0 | 0 | 0 |
| 1859 | 11 | 11 | 11 | 11 | 11 | 1908 | 6 | 24 | 0 | 0 | 0 |
| 1860 | 4 | 4 | 4 | 4 | 4 | 1909 | 3 | 10 | 0 | 0 | 0 |
| 1861 | 3 | 3 | 3 | 3 | 3 | 1910 | 2 | 9 | 0 | 0 | 0 |
| 1862 | 14 | 14 | 14 | 14 | 14 | 1911 | 1 | 4 | 0 | 0 | 0 |
| 1863 | 10 | 10 | 10 | 10 | 10 | 1912 | 32 | 98 | 30 | 0 | 0 |
| 1864 | 4 | 4 | 4 | 4 | 4 | 1913 | 21 | 50 | 35 | 0 | 0 |
| 1865 | 2 | 2 | 2 | 2 | 2 | 1914 | 4 | 0 | 16 | 0 | 0 |
| 1866 | 1 | 1 | 1 | 1 | 1 | 1915 | 1 | 0 | 2 | 0 | 0 |
| 1867 | 0 | 0 | 0 | 0 | 0 | 1916 | 2 | 2 | 2 | 2 | 2 |
| 1868 | 0 | 0 | 0 | 0 | 0 | 1917 | 2 | 2 | 2 | 2 | 2 |
| 1869 | 0 | 0 | 0 | 0 | 0 | 1918 | 2 | 2 | 2 | 2 | 2 |
| 1870 | 0 | 0 | 0 | 0 | 0 | 1919 | 2 | 2 | 2 | 2 | 2 |
| 1871 | 0 | 0 | 0 | 0 | 0 | 1920 | 9 | 9 | 9 | 9 | 9 |
| 1872 | 1 | 1 | 1 | 1 | 1 | 1921 | 3 | 3 | 3 | 3 | 3 |
| 1873 | 3 | 3 | 3 | 3 | 3 | 1922 | 0 | 0 | 0 | 0 | 0 |
| 1874 | 2 | 2 | 2 | 2 | 2 | 1923 | 0 | 0 | 0 | 0 | 0 |
| 1875 | 0 | 1 | 0 | 0 | 0 | 1924 | 3 | 0 | 0 | 6 | 6 |
| 1876 | 6 | 25 | 0 | 0 | 0 | 1925 | 2 | 0 | 0 | 4 | 4 |
| 1877 | 5 | 21 | 0 | 0 | 0 | 1926 | 1 | 2 | 2 | 0 | 0 |
| 1878 | 3 | 12 | 0 | 0 | 0 | 1927 | 0 | 0 | 0 | 0 | 0 |
| 1879 | 2 | 8 | 0 | 0 | 0 | 1928 | 5 | 2 | 2 | 8 | 8 |
| 1880 | 1 | 4 | 0 | 0 | 0 | 1929 | 10 | 8 | 8 | 11 | 11 |
| 1881 | 0 | 2 | 0 | 0 | 0 | 1930 | 5 | 6 | 6 | 5 | 5 |
| 1882 | 0 | 1 | 0 | 0 | 0 | 1931 | 3 | 6 | 6 | 0 | 0 |
| 1883 | 21 | 21 | 21 | 21 | 21 | 1932 | 8 | 6 | 6 | 10 | 10 |
| 1884 | 81 | 81 | 81 | 81 | 81 | 1933 | 6 | 5 | 5 | 7 | 7 |
| 1885 | 125 | 125 | 125 | 125 | 125 | 1934 | 3 | 3 | 3 | 3 | 3 |
| 1886 | 78 | 78 | 78 | 78 | 78 | 1935 | 4 | 4 | 4 | 3 | 3 |
| 1887 | 16 | 16 | 16 | 16 | 16 | 1936 | 2 | 4 | 4 | 0 | 0 |
| 1888 | 31 | 31 | 31 | 31 | 31 | 1937 | 2 | 3 | 3 | 0 | 0 |
| 1889 | 37 | 37 | 37 | 37 | 37 | 1938 | 5 | 6 | 6 | 3 | 3 |
| 1890 | 43 | 60 | 47 | 33 | 33 | 1939 | 3 | 2 | 2 | 4 | 4 |
| 1891 | 26 | 70 | 35 | 0 | 0 | 1940 | 2 | 1 | 1 | 3 | 3 |
| 1892 | 18 | 47 | 23 | 0 | 0 | 1941 | 0 | 1 | 1 | 0 | 0 |
| 1893 | 0 | 0 | 0 | 0 | 0 | 1942 | 4 | 8 | 8 | 0 | 0 |
| 1894 | 0 | 0 | 0 | 0 | 0 | 1943 | 3 | 7 | 7 | 0 | 0 |
| 1895 | 0 | 0 | 0 | 0 | 0 | 1944 | 1 | 3 | 3 | 0 | 0 |
| 1896 | 29 | 0 | 0 | 39 | 77 | 1945 | 2 | 3 | 3 | 0 | 0 |
| 1897 | 22 | 0 | 0 | 30 | 59 | 1946 | 1 | 1 | 1 | 0 | 0 |
| 1898 | 3 | 0 | 0 | 4 | 7 | 1947 | 1 | 3 | 3 | 0 | 0 |

**Table 23. Estimated Annual Stratospheric Aerosol Optical Depths (Multiplied by 1000) at λ = 0.55 μm.** [From *Sato et al., 1993*.] (Concluded)

| Year | Global | NH | | SH | |
|---|---|---|---|---|---|
| | | 90°–30° | 30°–0° | 0°–30° | 30°–90° |
| 1948 | 0 | 0 | 0 | 0 | 0 |
| 1949 | 3 | 2 | 2 | 3 | 3 |
| 1950 | 1 | 0 | 0 | 3 | 3 |
| 1951 | 1 | 2 | 2 | 0 | 0 |
| 1952 | 3 | 6 | 6 | 0 | 0 |
| 1953 | 3 | 6 | 6 | 0 | 0 |
| 1954 | 3 | 6 | 6 | 0 | 0 |
| 1955 | 1 | 3 | 3 | 01 | 0 |
| 1956 | 0 | 1 | 1 | 0 | 0 |
| 1957 | 0 | 0 | 0 | 0 | 0 |
| 1958 | 0 | 0 | 0 | 0 | 0 |
| 1959 | 0 | 0 | 0 | 0 | 0 |
| 1960 | 5 | 5 | 5 | 5 | 5 |
| 1961 | 7 | 2 | 14 | 10 | 2 |
| 1962 | 8 | 3 | 8 | 17 | 4 |
| 1963 | 53 | 10 | 33 | 92 | 75 |
| 1964 | 72 | 25 | 53 | 132 | 76 |
| 1965 | 27 | 31 | 25 | 24 | 30 |
| 1966 | 25 | 25 | 25 | 25 | 25 |
| 1967 | 17 | 17 | 17 | 17 | 17 |
| 1968 | 32 | 32 | 32 | 32 | 32 |
| 1969 | 41 | 41 | 41 | 41 | 41 |
| 1970 | 19 | 19 | 19 | 19 | 19 |
| 1971 | 2 | 2 | 2 | 2 | 2 |
| 1972 | 3 | 3 | 3 | 3 | 3 |
| 1973 | 8 | 8 | 8 | 8 | 8 |
| 1974 | 13 | 13 | 13 | 13 | 13 |
| 1975 | 22 | 22 | 22 | 22 | 22 |
| 1976 | 2 | 2 | 2 | 2 | 2 |
| 1977 | 1 | 1 | 1 | 1 | 1 |
| 1978 | 7 | 7 | 7 | 7 | 7 |
| 1979 | 4 | 4 | 4 | 4 | 4 |
| 1980 | 4 | 5 | 5 | 3 | 3 |
| 1981 | 5 | 5 | 5 | 4 | 4 |
| 1982 | 46 | 33 | 105 | 29 | 14 |
| 1983 | 55 | 89 | 59 | 35 | 37 |
| 1984 | 16 | 23 | 18 | 10 | 14 |
| 1985 | 13 | 16 | 10 | 10 | 14 |
| 1986 | 13 | 13 | 16 | 13 | 11 |
| 1987 | 10 | 13 | 9 | 8 | 11 |
| 1988 | 7 | 8 | 5 | 6 | 10 |
| 1989 | 6 | 6 | 4 | 5 | 9 |
| 1990 | 6 | 7 | 4 | 5 | 8 |

Figure 35 shows the detailed structure of the optical depth variation (of 1.0 μm) since 1978 as measured by the SAM II satellite instrument over the polar regions (*[McCormick et al., 1993]*. The variation in the Arctic is dominated by the effects of the eruption of El Chichon, but the effects of several smaller eruptions are also visible. In the Antarctic, the volcanic record is modulated by the regular seasonal occurrence of PSCs with a much higher optical density than the background aerosol. To a lesser extent, the effects of PSCs are also visible in the northern hemisphere. Estimates of stratospheric mass loading for the volcanic eruption since 1979, also due to McCormick et al., are shown in Table 24 (this table includes values for the stratospheric background and three earlier eruptions).

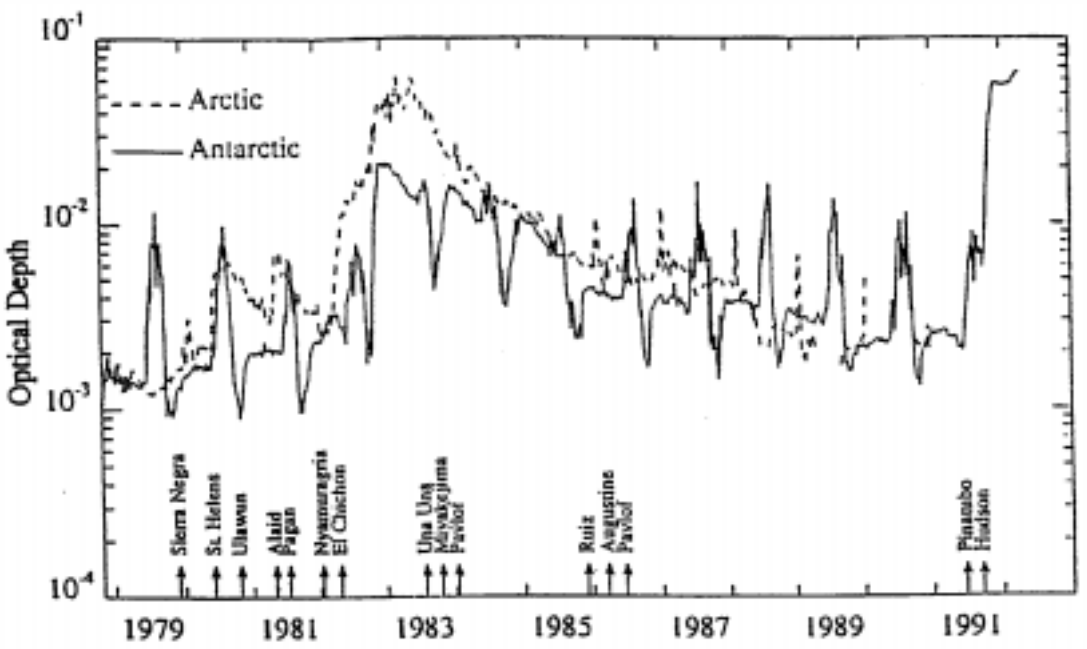


**Figure 35. Time series from SAM II of weekly averaged values of aerosol optical depth (at a wavelength of 1.0 μm) at high latitudes (integrated from 2 km above the tropopause upward).** [From *McCormick et al., 1993*].

**Table 24. Estimate of Aerosol Mass Loading in the Stratosphere** (From *McCormick et al., 1993*)

| Date | Volcano or Background | Location | Mass Loading (in units of $10^5$ tons) | Source |
|---|---|---|---|---|
| 1979 | Background | | 5.7 | *Kent and McCormick [1984]* |
| 1989 | Background | | 7.5 | *Yue and Poole [1992]* |
| 17 Mar 1963 | Agung | 8.4°S, 115.5°E | 160<br>300 | *Deimendjian [1973]*<br>*Cadle et al. [1976, 1977]* |
| 10 Oct 1974 | Fuego | 14.5°N, 90.9°E | 60<br>30 | *Cadle et al. [1976, 1977]*<br>*Lazrus et al. [1979]* |
| 22 Jan 1976 | St. Augustine | 59.4°N, 153.4°4W | 6.0 | *Cadle et al. [1977]* |
| 17 Apr 1979 | La Soutriere | 13.3°N, 61.2°W | 0.023 | *McCormick et al. [1981]* |
| 13 Nov 1979 | Sierra Negra | 0.8°S, 91.2°W | 1.6 | *Kent and McCormick [1984]* |
| 18 May 1980 | St. Helens | 46.2°N, 122.2°W | 5.5 | *Kent and McCormick [1984]* |
| 7 Oct 1980 | Ulawun | 50°S, 151.3°E | 1.8 | *Kent and McCormick [1984]* |
| 27 Apr 1981 | Alaid | 50.8°N, 155.5°E | 3.0 | *Kent and McCormick [1984]* |
| 15 May 1981 | Pagan | 18.1°N, 145.8°E | 2.0 | *Kent and McCormick [1984]* |
| 4 Apr 1982 | El Chichon | 17.3°N, 93.2°W | 200<br>120<br>101 | *Hofmann and Rosen [1983]*<br>*McCormick and Swissler [1983]*<br>*Mioz et al. [1983]* |
| 13 Nov 1985 | Ruiz | 4.9°N, 75.4°W | 5.6 | *Yue et al. [1992]* |
| 10 Feb 1990 | Kelut | 7.9°S, 112.3°E | 1.8 | *Yue et al. [1992]* |
| 15 Jun 1991 | Pinatubo | 15.1°N, 120.4°E | •300–400 | *McCormick and Veiga [1992]* |

The stratospheric aerosol following a major volcanic eruption is characterized by a localized input, post-eruption aerosol growth, global dispersion and finally, decay with a time constant of about 12 months. This is illustrated in Figure 36 which shows the global change in 0.55 μm optical depth following the eruption of Mt. Pinatubo. The departures are computed from the two year weekly mean values observed before the eruption of Mt. Pinatubo. Zones colored gray denote latitudes with departures equal to or less than zero.

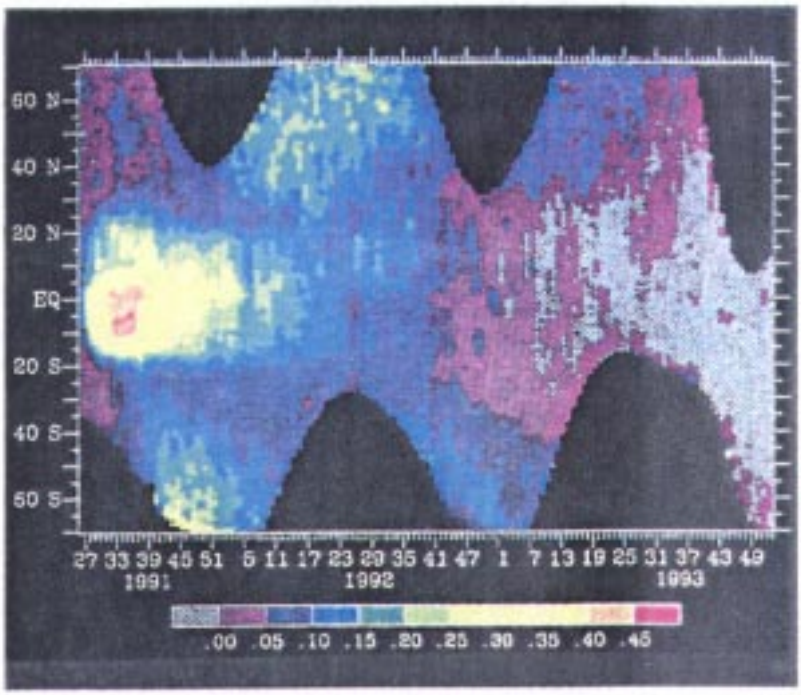


**Figure 36. Time series of one degree zonally averaged optical thickness departures starting at the time just after the Mt. Pinatubo eruption.** (from *Long and Stowe, 1994*).

### 3.3.4 Polar Stratospheric Clouds

PSCs are formed in winter in the Arctic and Antarctic stratospheres when the temperature falls below about 195 K. Type-I PSCs form at temperatures between 195 K and about 200 K and consist of nitric acid trihydrate. Type II PSCs form at lower temperatures and consist principally of water ice. The frequency of PSCs is much greater over the Antarctic than the Arctic region by virtue of the lower temperatures. This is illustrated in Figure 37, which shows the frequency of occurrence as a function of time and altitude. The altitude of PSCs over the Antarctic descends as the season progresses due to subsidence and particle sedimentation. A somewhat smaller change is observed over the Arctic. There are also marked variations in the occurrence frequency with longitude, which are illustrated in Figure 38.

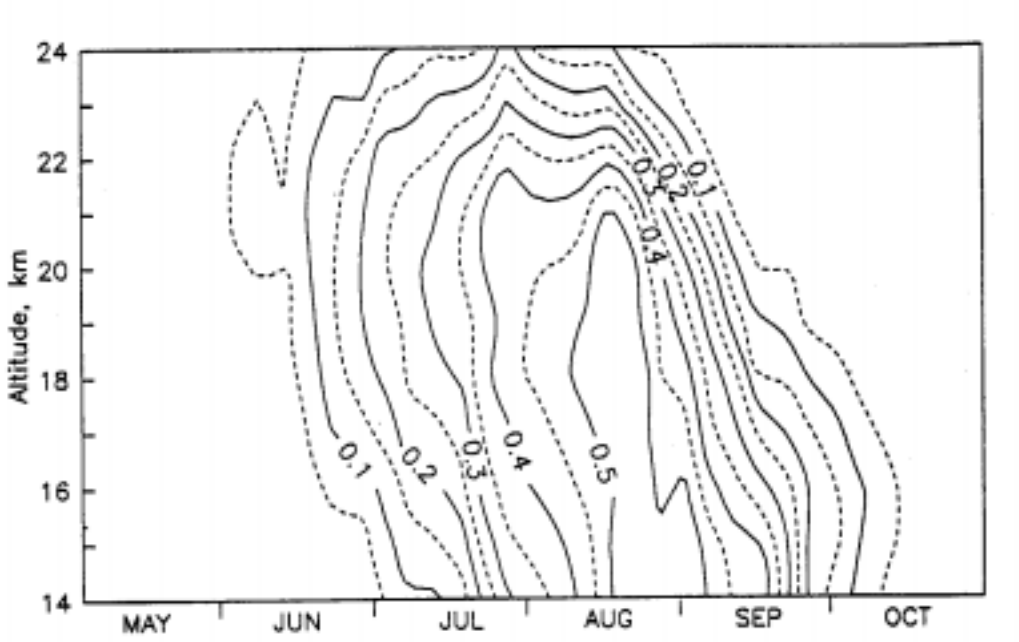


**Figure 37(a). Seasonal variation in the averaged frequency of occurrence of Arctic PSC sightings by SAM II for the period 1978–89. A five-day smoothing window was applied to the data** *[McCormick et al., 1993].*

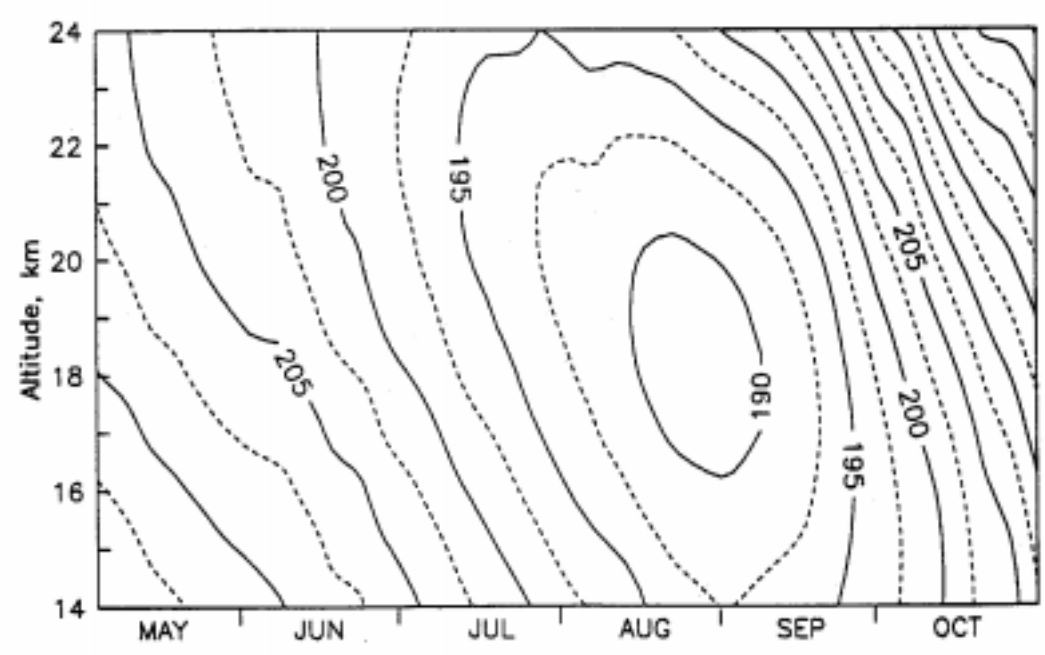


**Figure 37(b). Seasonal variation in the averaged frequency of occurrence of Antarctic PSC sightings by SAM II for the period 1978–89. A five-day smoothing window was applied to the data** *[McCormick et al., 1993].*

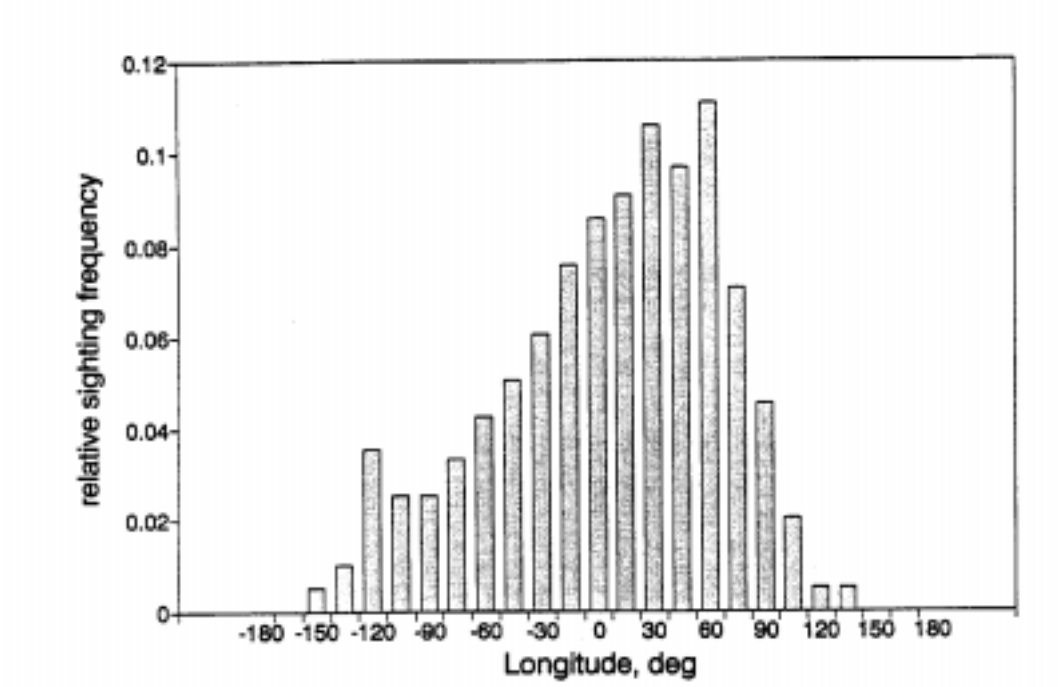


**Figure 38(a). Histogram showing the distribution with longitude of Arctic PSC sightings by SAM II for the period 1978–89** *[McCormick, et al., 1993].*

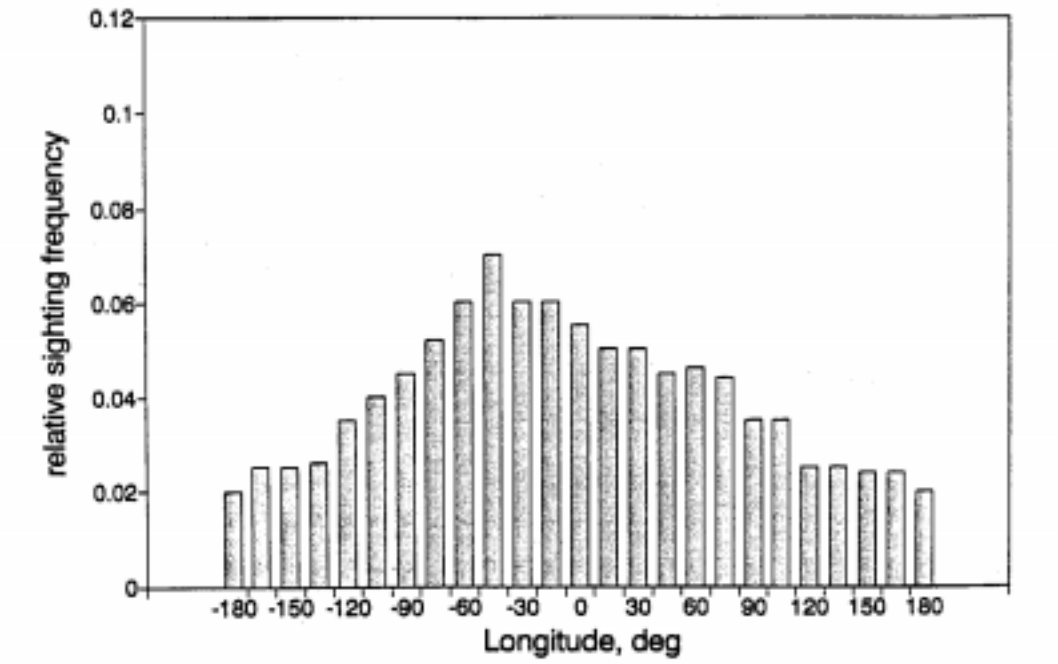


**Figure 38(b). Histogram showing the distribution with longitude of Antarctic PSC sightings by SAM II for the period 1978–89.** *[McCormick et al., 1993].*

### 3.3.5 Mesospheric Clouds

Polar Mesospheric Clouds (PMCs) are believed to consist of small ice particles formed at or below the summer mesopause (near 90 km), at latitudes poleward of about 55°, where the temperatures can go below 140 K (Gadsen & Schröder, 1989). They may be generally observed during an approximately twelve week period centered two weeks after the summer solstice (Thomas & Olivero, 1989). Satellite

observations of PMCs by POAM II (Debrestian et al., 1995) show slant path optical depths ranging from a low of 0.0005 to a maximum of 0.01 (at 442 nm). These measurements show a strong wavelength dependence, consistent with the mean particle radius of less than 100 nm inferred from SME measurements (Rusch et al., 1991).

### 3.3.6 HSST

No recommendations received.

# Annex A. The Altitude-Size Distribution (informative)

This altitude dependence of size distribution is taken into account by the double differential size distribution function $\eta(r,z)$ [$cm^{-3}\mu m^{-1}$], which is defined as the number of particles $cm^{-3}$ having their radii in a unit range r at the altitude $z$ *[Green, Deepak, and Lipofsky, 1970]*.

From $\eta(r,z)$, one may define the altitude-dependent cumulative (undersize) oversize density distribution $\tilde{N}_u(\tilde{N})[cm^{-3}]$ by:

$$E'_u(r,z) = \int_0^r \eta(r',z)\,d'r$$

$$E'_u(r,z) = \int_r^\infty \eta(r',z)\,d'r$$

corresponding to Eq. 2 and Eq. 3, respectively.

If $z$ is the altitude in km, then these distributions represent the altitude dependence of the cumulative undersize (oversize) size distribution. The altitude-dependent number density distribution, $N(r,z)$, is then defined as the total number of particles $cm^{-3}$ having their radii -$r$ at the altitude z (km). The density of particles at $z$ is then $N(0,z)$.

In addition, one may define the *cumulative oversize-overaltitude density distribution,* $\tilde{N}_{r,z}$, [$cm^3$ km] as the total number of particles $cm^{-3}$ having their radii -$r$ above the altitude $z$ (km), namely:

$$\grave{E}_{r,z} = \int_r^\infty \int_z^\infty \eta(r',z')dz'd'r\ [cm^{-3}km]$$

The *cumulative overaltitude size distribution,* $N_z(r,z)$, [$cm^{-3}\mu m^{-1}$ km] represents the number of particles $cm^{-3}$ having their radii in a unit range r and are above the altitude $z$, that is

$$N_z(r) = \int_z^\infty \eta(r,z')dz'\ [cm^{-3}\mu m^{-1}km]$$

## References


1 Bauer, E., 1969: *Applied Optics*, **3**, 197.

2 Cadle, R. D., C. S. Kiang, and J. F. Louis, 1976: The global scale dispersion of the eruption clouds from major volcanic eruptions, *J. Geophys. Res.*, **81**, 3125–3132.

3 Cadle, R. D., F. G. Fernald, and C. L. Frush, 1977: Combined use of lidar and numerical diffusion models to estimate the quantity and dispersion of volcanic eruption clouds in the stratosphere: Volcan Fuego, 1974, and Augustine, 1976, *J. Geophys. Res.*, **82**, 1783–1786.

4 Chandrasekhar, S., 1950: *Radiative Transfer*, Oxford Clarendon Press, London.

5 D'Almeida, P. Koepki, and E. P. Shettle, 1991: *Atmospheric Aerosols, Global Climatology, and Radiative Characteristics*, A. Deepak Publishing, Hampton, VA.

6 Debrestian, D. J., E.P. Shettle, J. Lumpe, R. M. Bevilacqua, J. Hornstein, W. Glacuum, and J. Olivero, 1995: POAM II observations of polar mesospheric clouds: Preliminary analysis, presented at the AGU 1995 Spring Meeting, 30 May–2 June, Baltimore, Md. [Abstract in Supplement to EOS, 25 April 1995, p. S62.]

7 Deepak, A., and H. E. Gerber, 1983: *Report of Experts Meeting on Aerosols and Their Climatic Effects*, Williamsburg, VA., 28–30 March 1983, World Meteorological Organization, WCP-55.

8 Deirmendjian, D., 1969: *Electromagnetic Scattering on Spherical Polydispersions*, Elsevier Press, NY.

9 Deirmendjian, D., 1973: On volcanic and other particulate turbidity anomalies, *Advances In Geophys.*, **16**, 267-296.

10 Gadsen, M., and W. Schöder, *Noctilucent Clouds*, Springer-Verlag, 1989.

11 Green, A.E.S., A. Deepak, and B. J. Lipofsky, 1970: Interpretation of the Sun's Aureole Based on Atmospheric Aerosol Models, *Applied Optics*, **10**, 1263–1279.

12 Hänel, G., 1976: The properties of atmospheric aerosol particles as functions of the relative humidity at thermodynamic equilibrium with the surrounding moist air, *Advances In Geophysics*, **19**, 73–188.

13 Hänel, G., 1997: Private communication.

14 Hänel, G., and K. Bullrich, 1978: Physico-chemical property models of tropospheric aerosol particles, *Contrib. Atmos. Phys.*, **51**, 129–1389.

15 Hänel, G., and M. Lehmann, 1981: Equilibrium size of aerosol particles and relative humidity: New experimental data from various aerosol types and their treatment for cloud physics application, *Contrib. Atmos. Phys.*, **54**, 57–71.

16 Hitchman, M.H., M. McKay, and C. R. Trepte, 1994: A climatology of stratospheric aerosol, *J. Geophys. Res.*, **99**, 20689–20700.

17 Hofmann, D. J., 1990: Increase in the stratospheric background sulfuric acid aerosol mass in the past 10 years, *Science*, **248**, 996–1000.

18 Hofmann, D. J., 1991: Aircraft sulfur emissions, *Nature*, **349**, 659.

19 Hofmann, D. J., 1993: 20 years of balloon borne tropospheric aerosol measurements at Laramie, Wyoming, *J. Geophys. Res.*, **98**, 12753.

20 Hofmann, D. J., and J. M. Rosen, 1981: On the background stratospheric aerosol layer, *J. Atmos. Sci.*, **38**, 168–181.

21 Hofmann, D. J., and J. M. Rosen, 1983: Stratospheric sulfuric acid fraction and mass estimate for the 1982 volcanic eruption of El Chichon, *Geophys. Res. Lett.*, **10**, 313–316.

22 Husar, R. B., J. M. Prospero, and L. L. Stowe, 1997: Characterization of tropospheric aerosols over the oceans with the NOAA advanced very high resolution radiometer optical thickness operational product, *J. Geophys. Res.,* **102**, 16889–16909.

23 Jaenicke, R., 1980: Atmospheric aerosols and global climate, *J. Aerosol Sci.*, **11**, 577–588.

24 Jaenicke, R., 1988: Physical and chemical properties of the air. In *Numerical Data and Functional Relationships in Science and Technology*, edited by G. Fischer, Landolt-Bornstein new Series, V: Geophysics and Space Research 4: Meteorology, Springer, Berlin, 391–457.

25 Jaenicke, R., 1993: *Tropospheric Aerosols in Aerosol-Cloud-Climate Interactions*, edited by P.V. Hobbs, Academic Press.

26 Johnson, D. L., Editor, 1993: *terrestrial Environment (Climatic) Criteria Guidelines for Use in Aerospace Vehicle Development* [1993 revision]. NASA Technical Memorandum 4511, Marshall Space Flight Center, AL.

27 Junge, C. E., 1963: *Air Chemistry and Radioactivity*, Academic Press, NY.

28 Kent, G. S., and M. P. McCormick, 1984: SAGE and SAM II measurement of global stratospheric aerosol optical depth and mass loading, *J. Geophys. Res.*, **89**, 5303–5314.

29 Kent, G. S., P-H. Wang, M. P. McCormick, and K. M. Skeens, 1995: Multiyear Stratospheric Aerosol and Gas Experiment II measurements of upper tropospheric aerosol characteristics, *J. Geophys. Res.*, **100**, 13875–13899.

30 Kerker, M., 1969: *The Scattering of Light*, Academic Press, NY.

31 Lazrus, A. L., R. D. Cadle, B. W. Gandrud, J. P. Greenberg, B. J. Huebert, and W. I. Rose, Jr., 1979: Sulphur and halogen chemistry of the stratosphere and of volcanic eruption plumes, *J. Geophys. Res.*, **84**, 7869–7875.

32 Lenoble, J., 1993: *Atmospheric Radiative Transfer*, A. Deepak Publishing, Hampton, VA.

33 Long, C. S., and L. L. Stowe, 1994: Using the NOAA/AVHRR to study stratospheric aerosol optical thicknesses following the Mt. Pinatubo eruption, *Geophys. Res. Lett.*, **21**, 2215.

34 Longtin, D. R., E. P. Shettle, J. R. Hummel, and J. D. Pryce, 1988: *A Wind Dependent Aerosol Model: Radiative Properties*, Report No. AFGL-TR-88-0112, Air Force Geophysics Laboratory.

35 McCartney, E. J., 1976: *Optics of the Atmosphere*, Wiley, NY.

36 McCormick, M. P., G. S. Kent, G. K. Yue, and D. M. Cunnold, 1981: *SAGE Measurements of the Stratospheric Aerosol Dispersion and Loading from the Soufriere Volcano*, NASA Tech. Paper. 1922.

37 McCormick, M. P., and R. E. Veiga, 1922: SAGE II measurements of early Pinatubo aerosols, *Geophys. Res. Lett.*, **19**, 155–158.

38 McCormick, M. P., P. H. Wang, and M. C. Pitts, 1993: Background stratospheric aerosol and polar stratospheric cloud reference models, *Adv. Space Res.*, **13**, (1)7–(1)29.

39 Mie, G., 1908: *Ann. Physik*, **25**, 377.

40 Palmer, F., B. Kopcewicz, C. Nagamoto, R. Schnell, P. Sheridan, C. Zhu, and J. Harris, 1992: Aerosol particles in the Kuwait oil fire plumes: Their morphology, size distribution, chemical composition, transport, and potential effect on climate, *J. Geophys. Res.*, **97**, 15867–15992.

41 Parungo, F., C. Nagamoto, M-Y Zhou, A. D. A. Hansen, and J. Harris, 1994: Aeolian transport of aerosol black carbon from China to the ocean, *Atmos. Environ.*

42 Porter, J. N., and A. D. Clarke, 1997: Aerosol size distribution models based on *in situ* measurements, *J. Geophys. Res.*, **102**, 6035–6045.

43 Post, M. J., 1986: Atmospheric purging of El Chichon debris, *J. Geophys. Res.*, **91**, 5222–5228.

44 Post, M. J., C. J. Grund, A. O. Langford, and M. H. Proffitt, 1992: Observations of Pinatubo ejecto over Boulder, Colorado by lidars of three different wavelengths, *Geophys. Res. Lett.*, **19**, 195–198.

45 Prospero, J., R. J. Charlson, V. Mohnen, R. Jaenicke, A. C. Delany, J. Moyers, W. Zoller, and K. Ruhn, 1983: The atmospheric aerosol system: An overview, *Rev. Geophys. and Space Physics*, **21**, 1607–1629.

46 Pruppacher, H. R., and J. D. Klett, 1978: *Microphysics of Clouds and Precipitation*, D. Reidel, Boston, MA.

47 Pueschel, R. F., J. M. Livingston, G. V. Ferry, and T. E. DeFelice, 1994: Aerosol abundances and optical characteristics in the Pacific basin free troposphere, *Atmos. Env.*, **28**, 951–960.

48 *Report of the Experts Meeting on Aerosols and Their Climatic Effects*, Eds. A. Deepak and H. E. Gerber, WCP-55, World Meteorological Organization, 1983.

49 Rosen, J. M., and D. J. Hofmann, 1986: Optical modeling of stratospheric aerosols: Present status, *Appl. Opt.*, **25**, 410–419.

50 Rosen, J., and V. A. Ivanov, 1993: Stratospheric aerosols. In *Aerosol Effects on Climate*, edited by S. G. Jennings, University of Arizona, Tucson, AZ.

51 Rusch, D. W., G.E. Thomas, and E. J. Jensen, 1991: Particle size distributions in polar mesospheric clouds derived from Solar Mesospheric Explorer measurements, *J. Geophys. Res.*, **96**, 933–12,939.

52 Sato, M., J. E. Hansen, M. P. McCormick, and J. B. Pollack, 1993: Stratospheric aerosol optical depths, *J. Geophys. Res.*, **98**, 22987–22994.

53 Shettle, E. P., 1989: *Models of Aerosols, Clouds, and Precipitation for Atmospheric Propagation Studies*, AGARD-CP-452.

54 Stowe, L. L., R. Hitzenberger, A. Deepak (1990): Report of the Experts Meeting on Space Observations of Tropospheric Aerosols and Complimentary Measurements, WMO/TD-No. 389 (1990). [Also available from International Global Aerosol Program (IGAP) Plan, Eds. A. Deepak & G. Vali, A. Deepak Publishing, 1991.]

55 Sviridenkov, M. A., D. A. Gillette, A. A. Isakov, I. N. Sokolik, V. V. Smirnov, B. D. Belan, M. V. Pachenko, A. V. Andronova, S. M. Kolomiets, V. M. Zhukov, and D. A. Zhukovsky, 1993: Size distributions of dust aerosol measured during the Soviet-American experiment in Tadzhikistan–1989, *Atmos. Environ.*, **27A** 2481–2486.

56 Tegen, I., and I. Fung, 1994: Modeling of mineral dust in the atmosphere: Sources, transport, and optical thickness, *J. Geophys. Res.*, **99**, 22897–22914.

57 Thomas, G. E., and J. J. Olivero, 1989: Climatology of Polar Mesospheric Clouds, 2. Further analysis of Solar Mesospheric Explorer data, *J. Geophys. Res.*, **94**, 673–14,702.

58 Thomason, L. W., G. S. Kent, C. R. Trepte, and L. R. Poole, 1997: A comparison of the stratospheric aerosol background periods, *J. Geophys. Res.*, **102**, 3611–3626.

59 Thomason, L. W., L. R. Poole, and T. Deshler, 1997: A global climatology of stratospheric aerosol surface area density deduced from Stratospheric Aerosol and Gas Experiment II Measurements: 1984–1994, *J. Geophys. Res.*, **102**, 8967–8976.

60 Van De Hulst, 1957: *Light Scattering by Small Particles*, John Wiley and Sons, Inc., NY.

61 Wefers, M., 1990: *Numerische Simulation der globalen 3-dimensionalen Verteilung arider Aerosol-partikel ohne Berucksichtigung der nassen Deposition*, Masters Thesis, University Mainz.

62 Wefers, M., and R. Jaenicke, 1990: In *Aerosols. Proc. Third International Aerosol Conference Proceedings*, edited by S. Masuda and K. Takahashi, Pergamon Press, 1086–1089.

63 Whitby, K. T., 1975: Aerosol formation in urban plumes, in aerosol: Anthropogenic and natural sources and transport, *Ann. N.Y. Acad. Sci.*, **338** 258–275.

64 Whitby, K. T., and B. Cantrell, 1976: Atmospheric aerosols—Characteristics and measurements. In *Int. Conf. Environ. Sens. Assess. Proc.*, 1975

65 World Meteorological Organization, 1980: *Report of the Meeting of Experts on Aerosols and Climate*, Geneva, 27–31 October 1980. [WCP-12]

66 Yue, G. K., M. P. McCormick, and E. W. Chiou, 1991: Stratospheric aerosol optical depth observed by the Stratospheric Aerosol and Gas Experiment II: Decay of the El Chichon and Ruiz volcanic perturbations, *J. Geophys. Res.*, **96**, 5209–5219.

67 Yue, G. K., and L. R. Poole, 1991: *Comparison of the Impact of Volcanic Eruptions and Aircraft Emissions on the Aerosol Mass Loading and Sulfur Budget in the Stratosphere*, NASA Conference Publication 10087, Part 1, First Annual High-Speed Research Workshop, 1992.

68 Zimmerman, P., J. Feichter, H. K. Rath, P. J. Crutzen, and W. Weiss, 1989: *Atmos Envir.*, **23**, 25–35.

American Institute of
Aeronautics and Astronautics

1801 Alexander Bell Drive, Suite 500
Reston, VA 20191-4344

ISBN 1-56347-369-0